HYDRATE FORMATION IN WAXY OIL SYSTEMS

By

DEEPIKA VENKATARAMANI

Bachelor of Technology in Chemical Engineering
Anna University
Chennai, Tamil Nadu, India
2009

Master of Science in Environmental Engineering
Syracuse University
Syracuse, NY
2011

Submitted to the Faculty of the
Graduate College of the
Oklahoma State University
in partial fulfillment of
the requirements for
the Degree of
DOCTOR OF PHILOSOPHY
December, 2016

HYDRATE FORMATION IN WAXY OIL SYSTEMS

Dissertation Approved:

Dr. Clint P. Aichele

Dissertation Adviser

Dr. Peter E. Clark

Dr. James E. Smay

Dr. Hariprasad J. Subramani

Dr. Jeffery L. White

ACKNOWLEDGEMENTS

I would like to thank my PhD advisor Dr. Clint P. Aichele for giving me the opportunity to work on this project as well as several others, for his guidance and constant encouragement throughout. I have learned a lot on work ethics from Dr. Aichele which has been highly valuable.

I would like to thank my mentor and committee member Dr. Peter E. Clark for his invaluable time and candid discussions both on professional and personal front. I have deeply enjoyed our conversation on politics, government, and general life experiences.

I would also like to express my gratitude to my mentor and committee member Dr. Hariprasad J. Subramani for initiating my research topic, valuable ideas, and guidance. I would also like to thank my committee members Dr. Jefferey L. White, and Dr. James E. Smay for their valuable time and motivating me to develop a professional attitude towards scientific research. I sincerely appreciate my department head Dr. Rob Whiteley for inspiring and guiding me in every step of my career. I'm grateful to Dr. Sayeed Mohammed for his time and efforts in helping me understand fundamentals on a critical issue related to my thesis. I appreciate Dr. Prem Bikkina, Dr. Jindal Shah, and Dr. Ashlee Ford Versypt's time and efforts in my overall development.

I would like to extend special thanks to Dr. Zachary Aman, Dr. Prasad Karanjkar, Dr. Amit Ahuja, Dr. Sriraj Srinivasan, Shane Morrissey and other colleagues in the industry for their guidance and useful discussions. I thank my colleagues from Shell for providing me an amazing internship opportunity.

I would like to thank Gary Thacker for his help in putting together the flow loop. I also thank Shelley Potter and Yvonne Roberts in guiding through laboratory safe operation. I thank the department staff for their help with the administrative work and special note of thanks to Eileen Nelson for her editorial help.

A very special mention to all the vendors and technical team from Canty Inc., McCrone Microscope Inc., Linkam, Dispersion Technology Inc., Tulco Chemicals, VWR, Evonik, Core Labs and many others. Thank you! A heartfelt thank you also goes out to Victor Lifton (Evonik), Jessica Kostraba, Doug Caldwell, Justin Halbach, Todd Canty (Canty), Andrei Dukhin and Sean Parlia (Dispersion Technology), Ruben Nieblas and John Hart (Linkam/ McCrone Microscope), Josh and James (Core Labs) for their technical help with the instruments.

I thank my colleagues and friends especially Adane Nigatu, Anil Jammula,

Sravanti Vupputuri, and Solomon Gebrehoyannes for their valuable inputs in my research and coursework. I thank my friends Ojo, Mesfin, Yehenew, Saba and several others for their support, and making my stay enjoyable. I would like to acknowledge the help of the past and present students in my research group. I also thank fellow students from civil engineering department for letting me share their lab space and providing a friendly work environment.

I thank my parents, Vasanthi and Venkataramani, for their unconditional love, support, and encouragement without, which I would not have achieved much. A special and heartfelt gratitude goes to my husband Gokul for holding me strong and walking with me through this journey, especially during pressing times. I thank him for providing humor, entertainment, abundant love, and a peaceful and happy home. I also thank my father-in-law, Ganapathy, for his love, and encouragement. A special thanks goes to my grandmother, Savithri for her love and cooking tips. I also thank my uncle, Harish, for inspiring and believing in me. I thank my close and extended family for all their support and encouragement. I would like to finally thank the almighty for giving me the best opportunity I could have asked for. I dedicate this thesis to my parents, husband, uncle, and mother-in-law (Late Mrs. Vijayalakshmi).

Name: DEEPIKA VENKATARAMANI

Date of Degree: DECEMBER, 2016

Title of Study: HYDRATE FORMATION IN WAXY OIL SYSTEMS

Major Field: CHEMICAL ENGINEERING

Abstract: Emulsions are of great importance due to their widespread occurrence in industries such as pharmaceutical, cosmetics, food, agricultural, and energy. In the energy industry, emulsions may be encountered in all stages of production, transportation, and extraction. Along with naturally occurring surfactants, solid particles such as asphaltenes, wax, clay, and silica are also present in crude oil. The formation and deposition of precipitated solids such as waxes, hydrates, and asphaltenes cause significant flow assurance problems for the energy industry. The motivation of this thesis was to develop a fundamental understanding of the hydrate formation mechanisms in waxy oil systems. This thesis focuses on the characterization of emulsions and hydrate formation in waxy oil systems in the presence of stabilizing agents such as a surfactant (span 80). A direct visualization and in-situ experimental method was developed for characterizing hydrate formation in waxy oil systems. Single water drop hydrate formation experiments were conducted with and without surfactant to evaluate the effect of wax concentration (1.25 and 5 wt.%), and cooling rates (0.5, 1, and 2 °C/min) on hydrate formation. In surfactant free systems, the presence of wax in the oil phase was observed to enhance the diffusion resistance of cyclopentane transport to the bulk water phase and hence delay hydrate growth rate. Conversely, the presence of surfactant was observed to reduce the diffusion resistance and promote hydrate formation. Faster hydrate growth was observed in surfactant laden systems due to reduced interfacial tension, thereby enhancing the mass transfer of cyclopentane to the water phase. In the absence of surfactant, wax concentration and the cooling rates had a significant impact on the hydrate conversion time. However, such observations were not seen in the presence of a surfactant. A four step hydrate formation mechanism (wax precipitation, hydrate nucleation, lateral growth, and radial growth) in waxy oil systems was proposed based on the experimental data. Wax precipitation and hydrate nucleation were observed to be heat transfer limited processes. Lateral growth was governed by diffusion of cyclopentane to the oil/water interface, while radial growth was goverened by mass transfer of cyclopentane into the water drop. Interfacial tension was observed to play a major role in hydrate conversion rate. An in-situ experimental method was developed by direct visualization of hydrate growth in emulsions. Hydrate formation was observed to affect the emulsion morphology. Irreversible formation of multiple emulsions was observed upon hydrate dissociation.

TABLE OF CONTENTS

Chapter Page

LIST OF TABLES

Table Page

LIST OF FIGURES

Figure Page

CHAPTER I

INTRODUCTION

1.1. Overview

Emulsions are colloidal dispersions of a liquid in another immiscible liquid stabilized using a surfactant and/ or solid particles [1]. Emulsions are of great importance due to their widespread occurrence in industries such as pharmaceutical, cosmetics, food, agricultural, and energy [2]. In the energy industry, emulsions may be encountered in all stages of production, transportation, and operation [3]. Along with naturally occurring surfactants, a wide variety of solid particles such as asphaltenes, waxes, clay, silica, and inorganic particles are also present in the crude oil [4]. The presence of such stabilizers in the crude oil results in production problems that are otherwise known as flow assurance issues. Flow assurance (coined by Petrobras) in the oil and gas industry simply means ensuring successful, continuous, economical, and environmentally safe transport of fluids from production to point of sale. Flow assurance problems encountered in the energy industry include formation and deposition of solids such as wax, asphaltenes, gas hydrates, inorganic solid/ scale deposits, slugging, and corrosion [2, 5]. In the energy industry, emulsions are difficult to treat due to the presence of a wide variety of stabilizers, thereby causing production and operational problems such as gas-liquid separation, high production and treatment costs, productivity loss, and high pressure

losses [6]. Depositions of solids result in deferment (economic and production loss), safety, and environmental concerns [5, 7-9]. This thesis focuses on emulsions, primarily water-in-oil emulsions with applications pertinent to the energy industry. This thesis provides fundamental understanding of hydrate formation mechanism in waxy oil systems, concentrated water-in-oil emulsions, and emulsion characterization of either surfactant or solid particle stabilized systems. The insight gained from this thesis aids in the development of flow assurance mitigating strategies in emulsion forming systems. This chapter includes the motivation for the work presented in this thesis, literature review about emulsions, gas hydrates, and wax, and outline of this thesis.

1.2. Motivation

Hydrate formation, wax deposition, and other flow assurance issues are common in deep-water extraction and production, as these systems are predisposed to extreme operating conditions such as low temperature and high pressures, thereby plugging pipelines. Hence, addressing these flow assurance issues are critical, as they can occur anywhere and in multiple locations, and there are associated operating and maintenance costs involved in managing and mitigating pipeline blockages. Millions of dollars are spent on remediation strategies that include depressurization, chemical inhibitors/ injection method, mechanical, and thermal methods. Though extensive research has been conducted on each of these flow assurance issues independently from both microscopic to macro-scale level, there is very minimal literature available when two or more of these issues occur simultaneously. Though hydrate formation in waxy crudes and emulsified systems have occurred in several instances in the oilfield, there is seldom any modeling or real-time experimental evidence available on understanding the hydrate formation mechanism in such waxy oil systems or waxy oil

emulsions [10-12]. This has provided an impetus to conduct an experimental investigation to understand hydrate formation mechanism in waxy oil systems. The motivation for this work is twofold and includes: 1) characterization of emulsions, hydrate formation in concentrated emulsions using a variety of stabilizing agents 2) hydrate formation mechanism in waxy oil systems a) without surfactant b) in the presence of a surfactant.

Many researchers have established that solid stabilized/ Pickering emulsion is well known to form stable oil-water dispersions. Even though a significant amount of research has been conducted on solid-stabilized emulsions in flowing conditions, their effect on hydrate agglomeration, plugging, and transportability in the presence of wax crystals is unclear and requires further investigation. Figure 1.1 represents the water droplet stabilization mechanism in waxy oil systems, and the interaction of hydrate-forming guest molecules (cyclopentane) on wax stabilized emulsions.

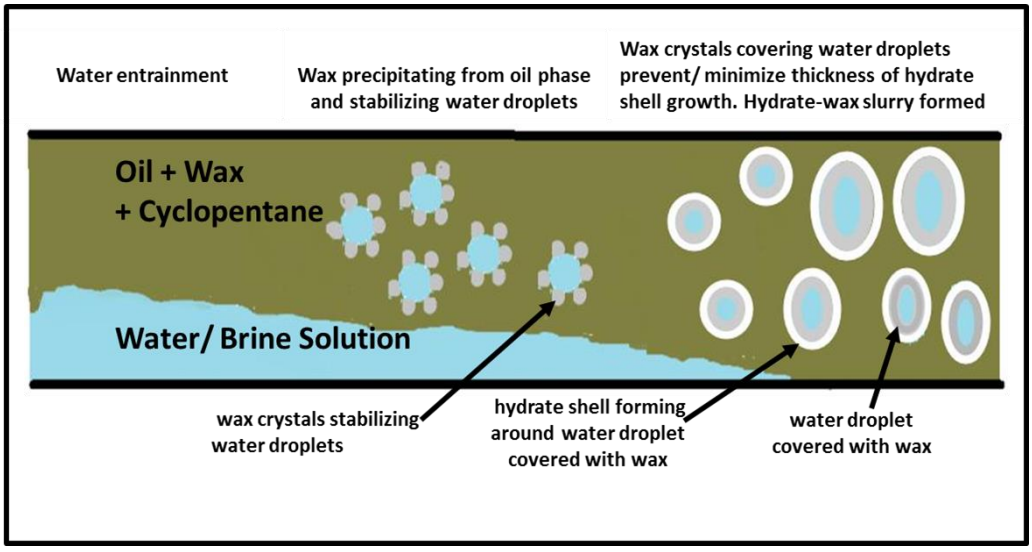

Figure 1.1: Mechanism depicting wax stabilized water-in-oil emulsion preventing/ minimizing hydrate agglomeration and plugging. A hydrate-wax slurry mixture is formed, flows through a pipeline and prevents plugging (adapted from Turner[11])

This thesis provides fundamental understanding of hydrate formation mechanism in waxy oil systems and thereby, pave a way to developing efficient and reliable techniques to resolve aforementioned issues on pipeline plugging. This work involved experimental analysis to investigate the effect of wax on hydrate formation both in the presence and absence of surfactant.

1.3. Literature Review

1.3.1. Emulsions

An emulsion is a heterogeneous mixture of two immiscible liquids (or phases) where one of the liquids, called dispersed phase, is present as droplets in another liquid continuous phase [13]. Emulsions generally consist of polar aqueous and a non-polar phase that are stabilized using a surface active agent called a surfactant. The phase in which the surfactant tends to be soluble is usually the continuous phase as governed by Bancroft's rule [14-18]. Emulsions are classified as oil-in-water (o/w), water-in-oil (w/o), oil-in-water-in-oil (o/w/o), or water-in-oil-water (w/o/w) types, depending on the continuous phase and surfactant type. Oil-in-water emulsions are those in which the oil droplets are dispersed in water continuous phase and contain water-soluble surfactant with typically high hydrophile-lipophile balance (HLB) of >8 [14-18]. Whereas water-in-oil emulsions are that kind where water droplets are suspended in oil continuous phase, and the surfactants are oil-soluble with a HLB ratio of <7. Surfactants consist of a polar head group (hydrophilic) soluble in the aqueous phase, and a non-polar tail group (lipophilic) soluble in the oil phase. Emulsions are made stable in the presence of adequate concentrations of surfactant and emulsification/ mixing conditions. Emulsions are thermodynamically unstable systems due to the high interfacial tension two

immiscible phases, and the free energy of the system is not minimized [19, 20]. The role of a surfactant is to reduce the interfacial tension between the phases, thereby minimizing the free energy of the system. An emulsion is called stable when there is no change in the emulsion droplet size over time, which is generally achieved when the surfactant concentration and emulsification conditions (mixing speed, time) are optimized. The four ways in which an emulsion becomes unstable are: creaming (or sedimentation), flocculation, coalescence, and Ostwald ripening [13]. Changes in temperature, pH etc. also result in changes in emulsion properties. Creaming or sedimentation occurs due to the density difference between the two phases causing movement of the oil droplets (in o/w emulsions) or water droplets (in w/o emulsions). Flocculation occurs due to aggregation of emulsion droplets without rupturing the thin interfacial film, whereas, coalescence results in rupture of the interfacial film. Ostwald ripening occurs due to diffusion of smaller droplets into larger ones.

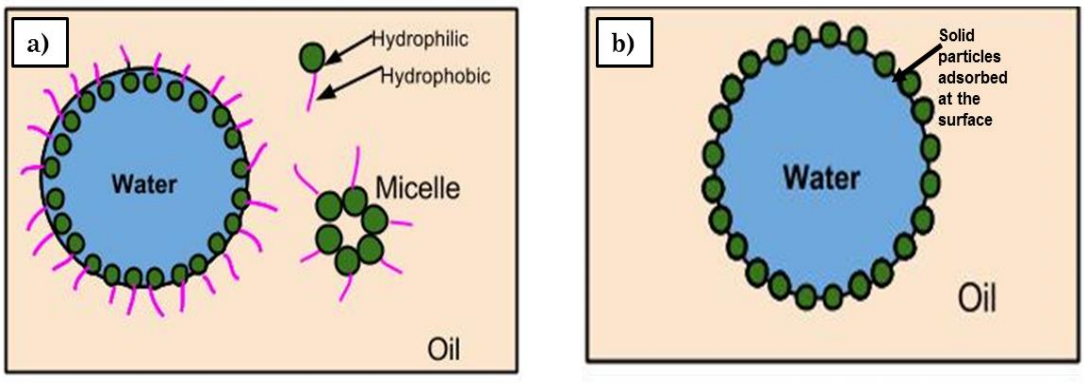

Figure 1.2: Illustration of water-in-oil emulsion stabilized using a) surfactant b) solid particles (Pickering emulsion)

In 1903, Ramsden observed that solid particles were capable of stabilizing emulsions, but it was Pickering who first established through extensive experimental study that solid particles function very similar to surfactant molecules in stabilizing oil-water interface [21,

22]. Figure 1.2 illustrates oil-water interface of an emulsion stabilized using either surfactant or solid particles. Pickering observed that solid particles that are wetted more by the oil phase and have a contact angle > 90°, act as an emulsifying agent for water-in-oil emulsions [23], whereas particles preferably wetted by the water phase and have a contact angle < 90°, produced oil-in-water emulsions [22, 23]. Ramsden and Pickering first quantified that emulsion stabilization by solid particles occurs as a result of strong adsorption at the oil-water interface [21]. Finkle et al established that the stability of emulsion was due to wetting of the particles and the type of emulsion formed [24]. Aveyard and Binks observed that the free energy of adsorption of particles caused emulsion stability [25]. Binks and Lumsdon demonstrated that inversion of emulsions was quantified by the solid particles wettability and contact angle [26]. Since the discovery of solid particle's ability to stabilize emulsions, several studies have been conducted on emulsion characteristics.

Several researchers identified that solid particles impart mechanical rigidity and viscosity to the interfacial film if the solid particles form a tightly packed network around the droplet [25, 27-30]. To this end, Simon et al studied the rheological properties of fumed silica stabilized emulsions [31]. They studied the rheological properties of o/w and w/o emulsions stabilized with particles of different polarity. Hydrophilic Aerosil R7200 and hydrophobic Aerosil R972 were considered as stabilizers for the emulsion systems. Rheological properties of w/o emulsions stabilized by hydrophobic particles were similar to o/w emulsions stabilized by hydrophilic particles. They also investigated the rheological properties of o/w emulsion stabilized by a mixture of particles keeping the total particle concentration constant but varying the mass ratio between particles. They observed that the viscosity and stability of the emulsion decreased with increase in the hydrophobic particle concentration.

Vignati et al examined the droplet interfacial tension of o/w Pickering emulsion using micropipette tensiometry [32]. The authors observed that the particle surface adhesion at the oil-water interface was strong and remained constrained at the droplet interface even upon dilution. The authors demonstrated that the stabilization mechanism in Pickering emulsion was due to steric hindrance or surface rheology effects. Fan and Striolo implemented particle dynamics simulation to study the influence of solid nanoparticles on the oil-water interfacial tension measurements [33]. The authors suggested that the interfacial tension depends directly on the particle coverage and the affinity of nanoparticles to the interface. They observed that increase in the primary particle size significantly increased the nanoparticles desorption energy, leading to larger surface coverage and interfacial tension reduction.

Sullivan and Kilpatrick, Hannisdal, et al were some of the few researchers who investigated the effect of silica nanoparticles on model oil emulsion stability with application to the oil and gas industry [34, 35]. They demonstrated the stabilization mechanism of crude oil components with either only hydrophobic or hydrophilic silica, and the ease of achieving catastrophic phase inversion on emulsions stabilized by particles with intermediate wettability.

This thesis focuses on water-in-oil emulsions stabilized using either surfactant (span 80) or solid particles (such as Aerosil R974, Aerosil R972, Aerosil R816). Different experimental techniques (inflow microscopy, acoustic spectroscopy, optical microscopy and interfacial tensiometer) were used for characterizing emulsion droplet size. All the work discussed in this thesis were conducted using deionized water as the aqueous phase, and either model mineral oil or decalin as the oil continuous phase.

1.3.2. Hydrates

Gas hydrates or clathrates are non-stoichiometric, crystalline like structures formed from host water molecules and low molecular weight hydrocarbons (also known as guest molecules) such as methane, ethane, propane, carbon-dioxide, nitrogen etc. [9]. Gas hydrates are important primarily for two reasons: first, they serve as an energy source, and secondly, they cause plugging of pipelines. In the energy industry, addressing flow assurance issues due to hydrates is of primary importance due to deferred production, severe economic losses, safety, and environmental concerns. On the other hand, however, hydrates are believed to serve as a potential future energy source, as they can entrap large quantities of natural gas (1 m^3 of hydrate can entrain almost 180 m^3 of natural gas at ambient conditions). The thermodynamic conditions required for hydrate formation are low temperature, high pressure, and the presence of hydrate-forming gas molecules, free water or brine. Hydrates are classified as either structure I, II, or H depending on the cage size and fit of the guest molecule into the host molecule [36]. Structure I hydrates are composed of twelve pentagonal (5^{12}) and two hexagonal (6^2) cavities occupied by guest molecules (gases) such as methane, ethane, and carbon-dioxide [36]. Structure II hydrates are the most common type in the oil and gas industry and are composed of $5^{12}6^4$ cavities and occupied by guest molecules such as propane and iso-butane. Structure H hydrates are composed of high molecular gas compounds and are the least common type [36]. This thesis focuses on structure II hydrates, with the only exception being that all the studies would be focused on cyclopentane hydrates which serve the same function as guest molecules in structure II gas hydrates. For the work discussed in this thesis, cyclopentane hydrates are used instead of gas hydrates due to pressure limitations in our laboratory facilities.

Since the discovery of hydrates by Hammerschmidt in early 1930's, plugging due to hydrates has been a serious challenge to the petroleum industry [9]. Hydrate formation may occur during transient and abnormal operations such as start-up, restart, shut in, and in places in the pipeline where there is a change in flow geometry, across valves, risers, and offshore/subsea systems. In most cases, hydrate management is economically feasible and favorable when compared to complete avoidance due to excessive capital and operating costs involved in completely preventing hydrate formation [37]. The four methods used for hydrate management and removing hydrate blockages include pressure reduction/ depressurization, mechanical removal, chemical injection, and thermal application [9].

Hydrate dissociation by reducing pressure (depressurization) is the most widely used technique in regions where the chemical injection is not easily accessible. The mechanical removal method involves the use of coiled tubing which allows jetting of hot water to dissociate hydrate plugs. In the chemical injection method, agents such as methanol, glycols, anti-agglomerants etc. are injected into the pipeline wherever accessible to dissociate the plug. The two different kinds of chemical injection methods include: use of thermodynamic inhibitors or kinetic hydrate inhibitors (KHI). Thermodynamic inhibitors work by simply shifting the phase equilibria/ hydrate equilibrium conditions towards lower temperatures at fixed pressure. The most common thermodynamic inhibitor is methanol or glycol, but the drawback to this method is that large quantities of chemicals are required. The other kind of chemical injection method is called low dosage hydrate inhibitors (LDHI), which works by limiting hydrate growth rate and delaying hydrate formation but has no effect on hydrate phase boundaries. There are two different kinds of LDHI's available: kinetic hydrate inhibitors (KHI) and anti-agglomerants. KHI's delay the hydrate nucleation time and growth of hydrates,

whereas anti-agglomerants such as certain polymeric surfactants, work as an agent that prevent agglomeration/ coalescence of hydrate particles, thereby maintaining a hydrate slurry [38-41]. Certain surfactants such as span 80 perform the same function as an anti-agglomerant. Though chemical injection is one of the most commonly practiced methods in the industry, it is also mostly avoided due to associated costs involved in the separation of chemicals. The last method used for hydrate remediation is the thermal method, where the approach is to increase the temperature of the hydrate plug above the hydrate equilibrium/ dissociation temperature, which is usually performed by heating bundle or electric heating of pipeline. In the energy industry, though emulsions are known to produce production problems, recent studies have shown that stable water-in-oil emulsions promote successful transport of hydrate slurries similar to cold flow technology. The presence of a wide variety of surfactants and solid particles in the crude oil increase stability of emulsions and function similar to anti-agglomerants, thereby minimizing hydrate particle aggregation. Hence, there is an impetus to develop a fundamental understanding of the hydrate formation mechanism in emulsions in the presence of a wide variety of stabilizing agents. This thesis primarily focuses on the hydrate formation mechanism in the presence of solid particles such as wax, and the characterization of such emulsions.

In this thesis, hydrate formation studies are conducted using cyclopentane in the oil continuous phase. Structure II hydrates commonly found in the oilfield are produced at high pressures. Reproducing such conditions in a laboratory scale setup are challenging due to pressure limitations and safety concerns. So, an alternative compound known as cyclopentane is used for hydrate formation. Cyclopentane and tetrahydrofuran (THF) are used as alternatives to conduct laboratory-scale hydrate studies [40, 42-47]. Both cyclopentane and THF are known to form structure II hydrates at atmospheric conditions. However, the literature shows that

cyclopentane is preferred as a hydrate-forming guest molecule over THF, as the latter is miscible in water and also possesses mass transfer limitations between the guest molecule-water that is critical in gas hydrate forming systems [38, 48-50]. Hence, all the work presented in this thesis uses cyclopentane as an atmospheric model for gas hydrates in emulsions.

1.3.3.Wax

Waxes (particularly petroleum wax) are long chain, high molecular weight, saturated hydrocarbons with carbon compounds from C_{18} to C_{75} and melting points ranging from 35-70 °C [51]. Wax present in crude oil consists of paraffin hydrocarbons (C_{18}-C_{36}) and naphthenic hydrocarbons (C_{30}-C_{60}). Petroleum wax consists of a mixture of light paraffinic, intermediate, and naphthenic hydrocarbons along with heavy organic compounds. Cloud point, also known as wax appearance temperature (WAT), is the temperature at which the first wax crystal begins to form [52]. At temperatures below WAT, wax crystals begin to precipitate and aggregate to form a network of crystals. The two main critical challenges that occur due to wax are gel formation and wax deposition [53]. Gel formation occurs typically at static conditions and when the system temperature falls below WAT, thereby resulting in the formation of an intermolecular network of wax particles. Wax deposition occurs when the oil temperature falls below the WAT, and a negative thermal gradient between bulk oil and pipe surface exists.

Measuring WAT is one of the most critical parameters that helps establish a guideline on the temperature ranges to operate in such a manner as to avoid deposition problems. WAT is otherwise known as the highest temperature in which wax crystals are detected in the solid state. WAT is a function of the oil composition, cooling rate, thermal history, pressure, and fluid properties. Some of the most commonly used methods/ techniques for WAT measurement

include viscometry/ rheology, differential scanning calorimetry (DSC), Fourier transform infrared spectroscopy (FTIR), filter plugging, cold finger, cross-polarized microscopy (CPM), and ASTM visual techniques.

Viscometry techniques utilize the rheological behavior of the oil as a function temperature and shear rate. If the sample exhibits Newtonian behavior and is a function of temperature alone, then it is above WAT. Whereas, below WAT, the rheological properties become dependent on the shear rate. WAT is determined as the point at which there is a sudden change in the viscosity-temperature relationship.

DSC is one of the most widely used techniques for WAT measurement, which utilizes the heat of dissociation for detecting WAT. FTIR technique involves the use of infrared wavelengths to measure the increase in energy scattering during wax crystallization. CPM technique is a visual method for detecting wax crystals. This is one of the most widely used techniques for WAT measurement where an optical microscope with temperature controlled stage and an analyzer-polarizer are used, and WAT is measured as a function of cooling rate. Cold finger technique operates by generating a localized cold surface and is used to measure the quantity of kinetics of wax deposition. Except for cold finger, all the other techniques discussed above are used for WAT measurement, whereas, cold finger measures wax deposition [54]. In this thesis, CPM was used for WAT measurement. All the experimental work using waxy oil continuous phase discussed in chapter 5 was carried out using CPM.

Wax deposition is a critical flow assurance issue that can occur at any stage during crude oil extraction, production, transportation, storage, and processing. As exploration and production move into deep-water and offshore drilling, wax deposition problems have been

increasing steadily, as these conditions are subject to low temperatures. Hence, it is essential to have prior knowledge of WAT deposition rate before approaching techniques for complete avoidance. The three remediation methods for addressing flow assurance issues due to wax are: mechanical, thermal, and chemical methods [4, 55].

The mechanical methods involve the use of pigs, plunger lifts, and scrappers to remove wax deposited on pipe surfaces and prevent wax particles from agglomerating and causing gelling of the crude oil. The thermal methods include the use of electric heating of pipelines, circulation of hot water or steam etc. This technique facilitates wax removal by maintaining the fluid temperature above the wax melting point. The chemical method aids in the use of chemicals known as wax inhibitors that modify the pipe wall surface and wax crystal properties. Wax inhibitors are classified into three categories: pour point depressants/ wax crystal modifiers, detergents, and dispersants. Pour point depressants are chemicals that build into wax crystals and modify the surface properties and agglomeration tendency of wax crystals, thereby lowering the pour point.

In the present work, cyclopentane hydrate formation in waxy oil systems with and without surfactant are studied using model oils. This thesis provides fundamental understanding of the effect of wax, wax concentration, the effect of surfactant, and cooling rates on cyclopentane hydrate formation. For this work, CPM technique is used for hydrate and wax crystal characterization. This thesis provides an insight into emulsion properties upon hydrate dissociation in the presence of surfactant and wax.

1.4. Safety

This thesis involved working with model oils such as crystal plus mineral oil, light mineral oil, solvents such as cyclopentane, decalin, surfactants, and solid particles. All the chemicals were stored in a flammable cabinet. Personal protective equipment, safe laboratory practices, and standard operating procedures were followed for all the work presented in this thesis. All the samples were properly labeled, stored in a fume hood when not in use, and properly disposed off according to EHS chemical disposal rules and regulations.

1.5. Thesis Outline

This thesis is arranged in 5 chapters followed by supplementary information and references. Chapter 2 describes transient emulsion properties of surfactant and solid stabilized water-in-oil emulsions. The objective of this work was to elucidate the use of acoustic spectroscopy for characterizing emulsion stabilization/ destabilization mechanism in these emulsions. Acoustic spectroscopy measurements were carried out on these emulsions to determine the initial droplet size distributions and their evolution over a period of one week. A transient stability test was conducted to compare the behavior of surfactant and solid particles at the oil-water interface. Experimental results indicated that a destabilization mechanism, such as coalescence, can be characterized using acoustic spectroscopy. Characteristics prevalent in the coalescing system, such as broad droplet size distribution and polydispersity, were captured by acoustic spectroscopy in terms of change in the raw experimental attenuation.

Chapter 3 describes the characterization of concentrated water-in-oil emulsions under flowing conditions. In this work, an experimental flow loop setup equipped with an inflow

microscope was utilized to quantify emulsion drop size distributions as a function of water concentration, flow rate, temperature, and stabilizing agent type. This work showed that the drop size distribution was a function of temperature, water concentration, and flow rate for surfactant stabilized emulsions. The solid-stabilized emulsions indicated that only water concentration had an overall impact on the drop size distributions. Water concentration, flow rate, and temperature have a significant impact on the emulsion droplet size in surfactant stabilized systems.

Chapter 4 illustrates the effect of hydrate formation on emulsion droplet size captured using optical microscopy. For this work, cyclopentane hydrate forming emulsions were prepared using a surfactant (span 80), solid particles (Aerosil R974, Aerosil R816) and at two different water concentrations of 10 and 40 vol.%. In-situ hydrate formation was observed in concentrated emulsions without dilution. Hydrate formation and ice melting were observed to occur simultaneously. Multiple emulsions formed, and eventually, a change in the emulsion droplet size was observed upon hydrate dissociation.

Chapter 5 outlines single water drop hydrate formation mechanism in waxy oil systems with and without the presence of a surfactant. For this work, an Olympus BX53 temperature controlled and shear stage optical microscope was used for investigating hydrate formation as a function of wax concentration, heating/ cooling rates, and with and without the presence of surfactant (span80). In the absence of surfactant in the waxy oil continuous phase, the time required for visual observation of hydrate formation throughout the entire water droplet was observed to be higher at slower heating/cooling rates, and lower at faster rates irrespective of the wax concentration. However, such observations were not seen in waxy oil systems containing a fixed quantity of surfactant. Hydrate formation throughout the entire water droplet

surface area occurred in less than 20 minutes irrespective of the heating/cooling rates and wax concentration. Such observations were not seen in waxy oil systems without surfactant.

Finally, chapter 6 discusses the preliminary experimental results on hydrate forming emulsions containing wax and surfactant as stabilizing agents. This chapter also discusses the significant modifications made to the flow loop setup described in chapter 3. The modifications made to the flow loop design enables characterizing the pressure drop across the various sections in the flow loop along with visual characterization of emulsions, hydrates, and wax. This chapter enlists significant contributions made in this and for future work.

CHAPTER II

TRANSIENT STABILITY OF SURFACTANT AND SOLID STABILIZED WATER-IN-OIL EMULSIONS

2.1. Introduction

An emulsion is called stable if there is no phase separation against any destabilization phenomenon, such as coagulation and coalescence, phase inversion, creaming, sedimentation and Ostwald ripening, and if the emulsification process is possible [56]. Emulsifiers are additives that stabilize the oil-water interface. Surfactants are the usual choice for this purpose and have been available in the market as an emulsifier for both water-in-oil and oil-in-water emulsions. Surfactants are either ionic, non-ionic or zwitterionic in nature. Surfactants reduce interfacial tension, thereby promoting the creation of water-oil interface, and subsequently stabilizing the interface to resist coalescence [22, 57].

Emulsions stabilized using finely divided particles/ nanoparticles are called solid-stabilized emulsions (also known as Pickering emulsions) [22, 57]. Solid stabilized emulsions have gained importance in the last two decades due to their applicability in many industries (such as food, agriculture, pharmaceutical), their enhanced emulsion stability, and their ability to produce droplets ranging from a few microns to several millimeters

(Levine, Bowen et al. 1989). Pickering identified that solid particles had the ability to produce stable emulsions, and therefore, these are called Pickering emulsions [22, 57]. Solid particles function in a manner similar to surfactants. However, the preferential wetting of solid particles plays a major role in determining whether oil-in-water or water-in-oil emulsions are formed [23]. Solid particles such as pre-treated silica (available in the market as Aerosil) have been widely used in the pharmaceutical and cosmetic industries as a stabilizer, and also in the oil and gas industry for producing stable and large droplet emulsions [58]. Solid particles such as hydrophobic silica are known to be preferentially wetted by the oil phase, and lead to the formation of water-in-oil emulsions; whereas, hydrophilic silica particles, which are preferentially wetted by the water phase, produce stable oil-in-water emulsions [24, 57, 59].

Solid stabilized emulsions can be more stable, depending on surface coverage, as compared to surfactant stabilized emulsions, due to the strong adhesion of solid particles to the oil-water interface. The contact angle, coalescence kinetics, and particle interaction energy contribute to the stability of the emulsions [59]. Stable emulsions are prepared when the particles are neither too hydrophilic nor hydrophobic and if there is complete surface coverage. Particles that form contact angle, $\theta > 90°$ form a water-in-oil emulsion, whereas, $\theta < 90°$ leads to an oil-in-water emulsion [23, 24, 59]. The particle shape, size, and concentration greatly affect the emulsion stability and droplet size [60].

Acoustic and electroacoustic spectroscopy are some of the most reliable techniques for characterizing concentrated dispersions and emulsions in-situ [61]. These ultrasound based methods were chosen over other traditional particle sizing techniques, such as dynamic light scattering, electron microscopy, etc., due to their ability to characterize

polydisperse and concentrated systems without dilution [61, 62]. For this study, we used an Acoustic/Electroacoustic spectrometer DT 1202 (produced by Dispersion Technology Inc.) for characterizing droplet size distribution of both surfactant and solid-stabilized emulsions [61, 62].

The motivation behind this work was to demonstrate how acoustic spectroscopy can be utilized to capture emulsion stabilization/ destabilization phenomena in surfactant and solid-stabilized emulsions and characterize their transient stability over a period of time. For the purpose of this work, emulsions that exhibit two different kinds of stabilization/ destabilization mechanisms were studied using acoustic spectroscopy: one that undergoes coalescence, and a second that exhibits high stability. A surfactant-stabilized emulsion was used for investigating the transient behavior of a highly stable emulsion since it is well known to produce stable and non-coalescing droplets when formed above the critical micelle concentration. Since coalescence in surfactant stabilized systems is well studied and understood, a solid stabilized emulsion was chosen for studying acoustic interrogation of a coalescing system. Another important goal of this work was to investigate how acoustic spectroscopy captures characteristics prevalent in coalescing droplets, such as polydispersity and broad drop size distribution. For the purpose of this study, both coalescing and highly stable emulsions were prepared using similar mixing conditions and composition.

In this chapter, the droplet size distribution of water-in-oil emulsions stabilized using hydrophobic fumed silica (Aerosil R972) and a non-ionic surfactant, sorbitan monooleate (span 80) was studied at different time intervals after emulsification. Bottle

test and optical microscopy measurements were also carried out to validate the results obtained from acoustic spectroscopy.

2.2. Material and Methods

2.2.1. Emulsion Preparation

The water-in-oil emulsions prepared for this study contained decalin with a density of 0.786 g/cm^3, and ultra-pure, deionized water with a resistivity of 18.2 MΩcm. Two different stabilizers used for this study were sorbitan monooleate (span 80) and hydrophobic fumed silica (Aerosil R972). Decalin was supplied by BDH chemicals.

For a surfactant-stabilized emulsion, span 80, $C_{24}H_{44}O_6$ (molecular weight = 428.6 g/mol), supplied by Sigma Aldrich, with a density of 0.99 g/cm^3 was used as an emulsifier. The critical micelle concentration of span 80 in solvents such as decalin (dielectric constant = 2.2) was identified as 1.5-2 wt.%[63]. Hence, the oil phase was composed of 2 wt.% of span 80. Span 80 is used in industries as a surface-active emulsifier. Span 80 is a non-ionic lipophilic emulsifier with a hydrophile-lipophile balance ratio (HLB) of 4.3. The low HLB ratio of Span 80 is well known to produce w/o emulsion.

For Pickering emulsions, hydrophobic fumed silica (Aerosil R972) manufactured by Evonik Industries (Rheinfelden, Germany), with a tamped density of 1.06 g/cm^3 was used as the stabilizing agent. Aerosil R972 is manufactured by flame pyrolysis of silica at 1000 °C and surface treated with dichlorodimethyl silane to impart hydrophobic functionality. The primary particle size of Aerosil R972 is 16 nm, and the material typically exists as a sintered aggregate with size varying in the size range 100-300 nm. To keep the

emulsifier concentration constant for both kinds of emulsions, 2 wt.% aerosil R972 was dispersed in the oil phase.

Both types of emulsions were prepared using an Ultraturrax T25 homogenizer with a maximum operating power of 25,000 rpm. The oil phase of the emulsions was prepared by mixing 81.98 vol.% of Decalin with 2.12 vol.% of the stabilizer using a spatula and homogenizing at 8000 rpm for 1 min to completely homogenize the oil phase. Then, 15.9 vol.% of water was slowly added to the oil phase and the emulsion was mixed using the homogenizer at 8000 rpm for 10 minutes.

2.2.2 Acoustic Spectroscopy

For this work, an acoustic/electroacoustic spectrometer DT-1202 (manufactured by Dispersion Technology, Inc.) was used for characterizing both kinds of emulsions. A detailed description of this device is available in the literature [64] (Figure 2.1). The spectrometer is used for measuring drop size distribution, zeta potential, and conductivity simultaneously. The acoustic technique utilizes acoustic sound waves for measuring particle and drop size distributions. The electroacoustic technique utilizes both electric and acoustic signals for measuring the surface charge and zeta potential.

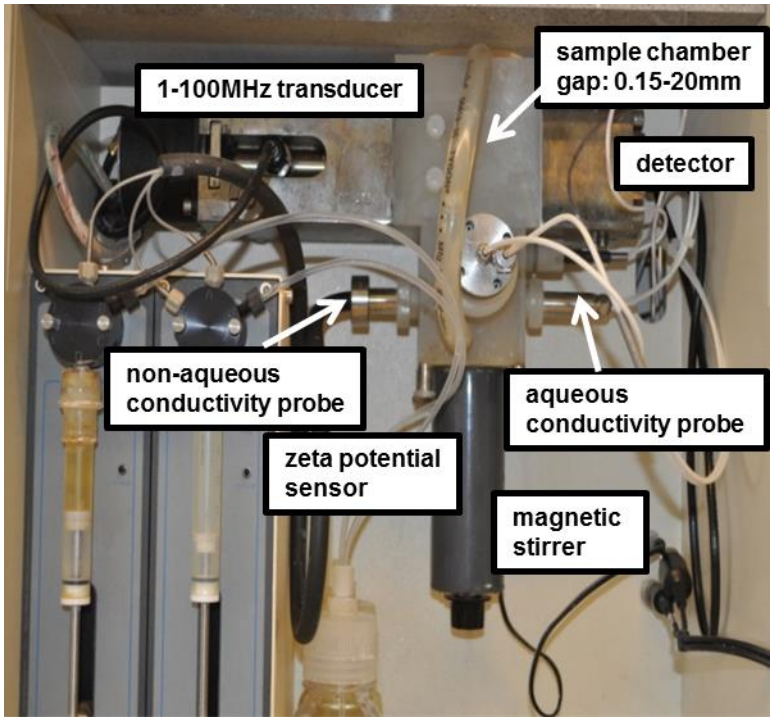

Figure 2.1: Representative image of DT 1202 acoustic and electroacoustic spectrometer. For this work, this instrument was used for measuring the emulsion droplet size, colloidal vibration current (CVI), and aqueous/ non-aqueous conductivity

Acoustic particle sizing is regulated by two International Standards: ISO 20998 Parts 1 and 2 [61, 62, 64]. The two essential features of the acoustic particle sizing technique that make it absolute and keep it from requiring calibration are pulse technique and variable gap method. The acoustic spectrometer works on the principle of generating pulses at 18 different frequencies within the range from 1 to 100 MHz, and 21 gaps between transmitter and receiver from 0.3 mm to 20 mm. A piezoelectric transducer (transmitter) converts these signals to ultrasound pulses of the same frequency. These ultrasound pulses propagate through a liquid sample, interact with the liquid and particles, and consequently attenuate. A second transducer (receiver) converts the received sound pulse into electric signals. The difference in the initial and final electric pulses serves as a measurement of

energy loss within the sample and is measured as attenuation. This energy loss is measured at variable gaps and frequencies between the transmitter and receiver. The variable gap method is coupled with the Beer-Lambert law for calculating attenuation coefficient, α, and per unit length (dB/cm/MHz) [65]. Like density, viscosity, and sound speed, acoustic attenuation is an intrinsic property, and unique to each system. The acoustic spectrometer measures the raw experimental attenuation, which is then fitted into theoretical models to predict the drop size distribution. The theoretical model used to predict the drop size distribution is a function of the experimental attenuation and intrinsic properties of the phases of the system. The software searches for the drop size distribution that provides the best fit to the experimental attenuation spectra and predicts the mean droplet size and distribution.

2.2.3 Optical Microscopy

For this work, a visualization technique was employed to quantify droplet size distributions and transient emulsion behavior through the use of an Olympus BX53 polarized optical microscope with shear cell and temperature control (-50°C to 450°C) stage. The specifications of the microscope are discussed in detail in Chapters 3, 4, and 5.

2.2.4 Experimental Procedure

An emulsion sample of 180 g was prepared as described in the emulsion preparation method. Immediately after emulsification, the sample chamber of DT 1202 was filled with the emulsion, and the particle size, colloidal vibration current, and conductivity were measured and reported as "0^{th} hour". Transient emulsion stability and evolution of droplet size was studied at different time intervals. Measurements were reported as "48^{th} hour" and "after 1 week" of emulsification. During the entire process, the emulsion samples were

constantly stirred on a Thermo Scientific Inc. (Ashville) magnetic stir plate with a 25.4 mm long stir bar at 800 rpm. The DT 1202 spectrometer was set up with a peristaltic pump operating at half of the full speed range to ensure that there was no phase separation within the sample chamber.

Bottle test experiments were conducted to study the emulsion behavior and any de-emulsification phenomena that might occur in these emulsions at different time intervals. Bottle tests simply consisted of placing a known amount of sample into a bottle and subsequently observing the behavior of the sample as a function of time. Optical microscopy was also employed to measure drop size distributions.

2.3.Results and Discussion

2.3.1 Emulsion stability using bottle tests

The stability of emulsions against coalescence and phase separation was monitored and assessed using conventional bottle test methods. Sedimentation of the emulsion and separation of the oil phase was observed in both surfactant and solid particle stabilized emulsions (Figure 2.2). However, separation of the oil phase in the solid-stabilized emulsions was predominant at all-time intervals when compared to surfactant stabilized emulsions. As seen in Figure 2.2, though sedimentation in surfactant-stabilized emulsion is present, the cloudiness seen in the supernatant likely indicates a large amount of stable, small droplets being kept in suspension by Brownian motion. Rapid separation of the oil phase and sedimentation of droplets seen in solid-stabilized emulsions indicate two likely possibilities: a) the droplets are coalescing due to insufficient surface coverage, or b) droplets are experiencing sedimentation due to a density difference, with or without any

change in droplet size. No aqueous phase separation was noticed in either type of emulsion even after 1 week of emulsification.

The evolution of both emulsions over time was followed simultaneously using optical microscopy and acoustic spectroscopy for up to 1 week after emulsification. The results obtained from these techniques are discussed in the following sections.

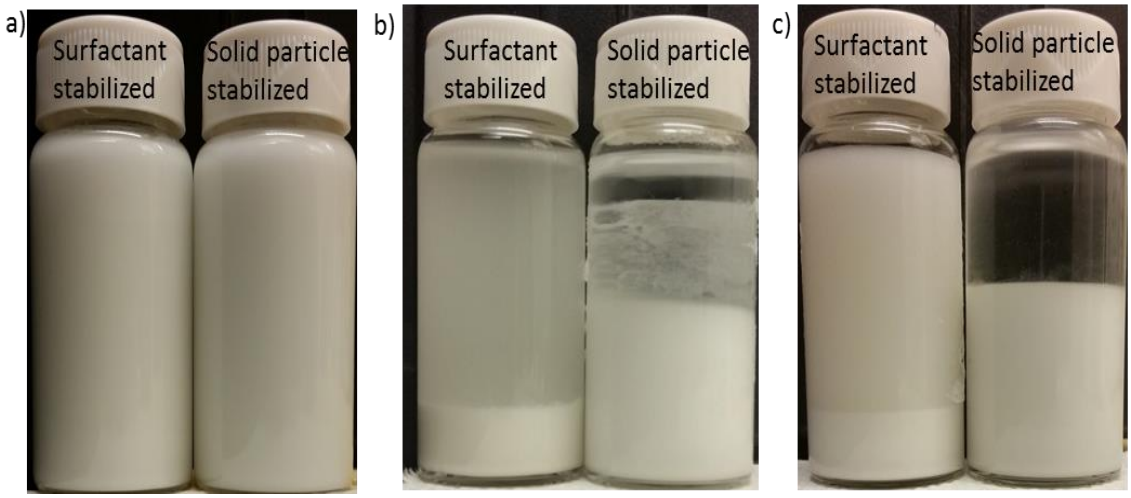

Figure 2.2: Bottle test experiment showing the stability, phase separation and sedimentation of water droplets in surfactant stabilized water-in-oil and solid particle stabilized water-in-oil emulsion at different time intervals of sample preparation: a) 0^{th} hour, b) after 48 hours of emulsion preparation, c) after 1 week of emulsion preparation. The sample was not stirred throughout this experiment.

2.3.2 Emulsion characterization: optical microscopy and acoustic/electroacoustic spectroscopy

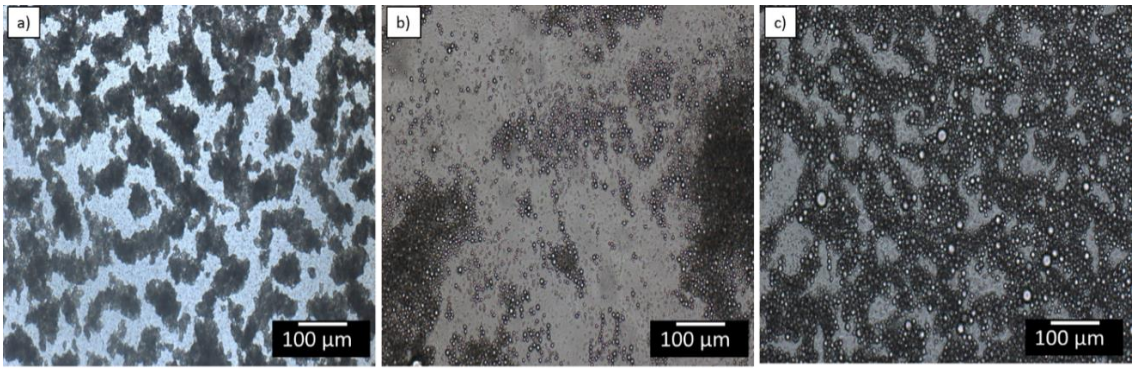

Figure 2.3: Optical microscopy images (20X magnification) of span 80 stabilized water-in-decalin emulsion taken at different time intervals after emulsification a) 0^{th} hour b) 48^{th} hour c) after 1 week.

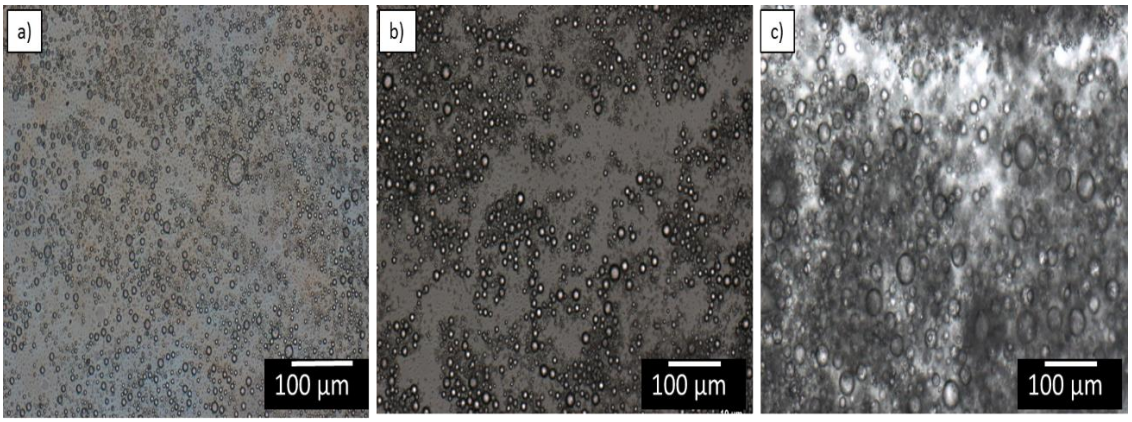

Figure 2.4: Optical microscopy images (20X magnification) of fumed silica stabilized water-in-decalin emulsion taken at different time intervals after emulsification a) 0^{th} hour b) 48^{th} hour c) after 1 week.

Optical microscopy experiments were conducted on the emulsion samples at time intervals at which bottle test experiments were carried out. Images shown in Figure 2.3 a) indicate that the droplet size distribution centered around 2 µm for the span80 stabilized emulsion at the 0^{th} hour measurement. Whereas in the solid stabilized emulsions, the

distribution shifted towards larger droplet size with a mean size around 8 µm (Figure 2.4 a). The solid stabilized emulsion also reveals polydisperse character with droplets in the size range of 2- 20 µm. Images shown in Figure 2.3 indicate that for span80 stabilized emulsions, the morphology of the droplets displays very little change with time. There was only a slight shift in the mean droplet size from 1.5 to 3 µm after 1 week of emulsification. Drelich et al., observed similar behavior in water-in-paraffin oil emulsion stabilized using span80 [66]. The authors observed that up to 7 days after emulsification, there was only a slight shift in the droplet size distribution from 1.5-3 µm [66].

Images in Figure 2.4 indicate the evolution of droplets over time with the distribution shifting towards larger droplet size. Figure 2.4 also reveals that a large number of small droplets coalesce to form bigger droplets, thus resulting in polydisperse behavior.

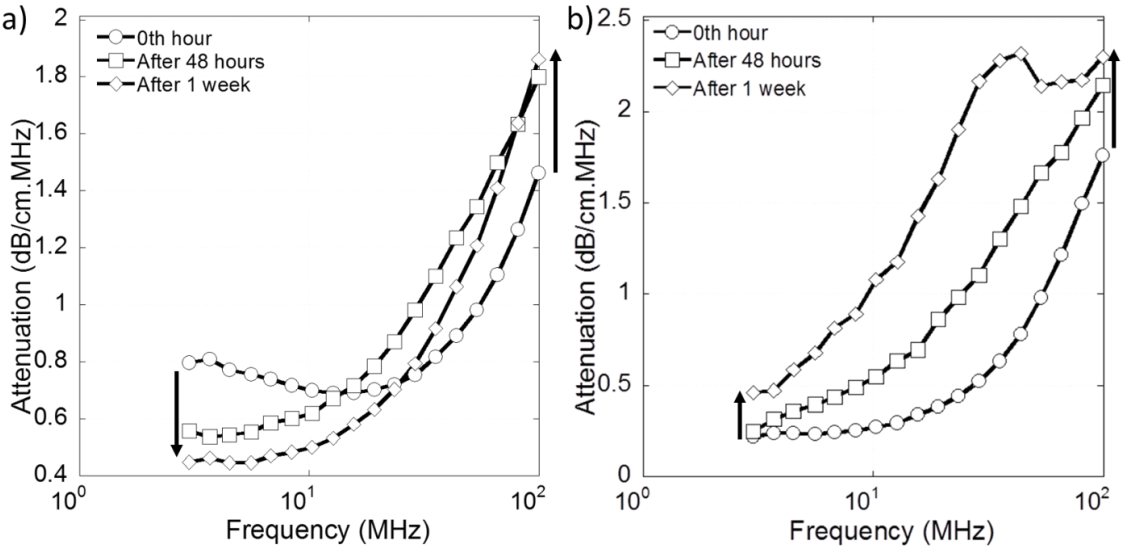

Figure 2.5: Attenuation spectra of a) span 80 stabilized emulsion b) fumed silica stabilized emulsion at various time intervals using the acoustic spectrometer. Arrows show the trend in the attenuation spectra immediately and after 1 week of emulsion preparation at low and high frequency.

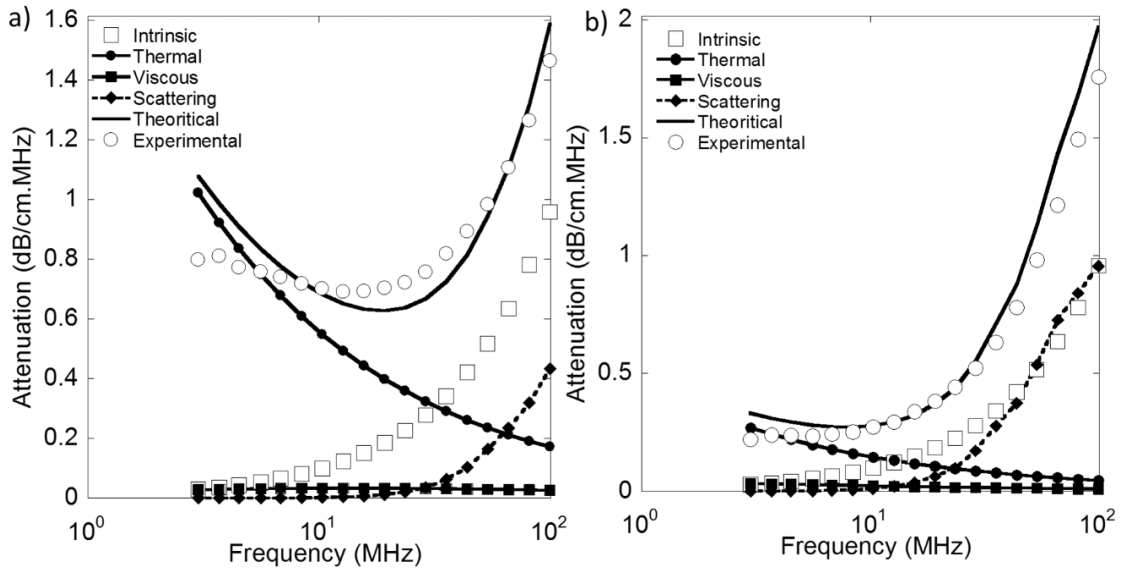

Figure 2.6: Experimental and theoretical attenuation spectra of water-in-oil emulsion measured immediately after sample preparation (0^{th} hour attenuation) a) Attenuation spectra of span80 stabilized emulsion assuming thermal loss mechanism b) Attenuation spectra of fumed silica stabilized emulsion assuming scattering loss mechanism due to the presence of large droplets

Figure 2.5 and Figure 2.6 a) and b) show the attenuation spectra of span80 and fumed silica stabilized emulsion (solid stabilized emulsion) respectively at three different time intervals (0^{th} hour, after 48 hours and after 1 week of emulsification). Figure 2.5 and Figure 2.6 a) and b) show the evolution of attenuation spectra over time at the entire frequency range (1-100 MHz). Figure 2.5 indicates that for span80 stabilized emulsions, the low-frequency attenuation begins to decay with time. Whereas, this trend was not observed for solid-stabilized emulsions Figure 2.6 b). The high-frequency attenuation (>10 MHz) was observed to increase for both kinds of emulsions with time. Dukhin and Goetz also observed a similar trend in the evolution of attenuation spectra for span80 stabilized emulsions [67]. The authors observed that for span80 stabilized water-in-kerosene oil

emulsion, the attenuation at lower frequency decays with time, whereas, at higher frequencies, it increases over time [67]. The measured raw attenuation is a combination of intrinsic, thermal, and scattering loss mechanisms. For this work, the intrinsic loss is the attenuation caused by the continuous oil phase (decalin). As seen in Figure 2.5 a), for the surfactant-stabilized emulsion, the thermal loss mechanism contributes to the overall attenuation. Whereas, for the solid stabilized emulsion, the scattering loss mechanism dominates the attenuation spectra over the entire frequency bandwidth with a decay in the attenuation due to a thermal loss at higher frequencies (Figure 2.6 b)). High-frequency attenuation is caused by scattering loss which is sensitive to large droplet size [64]. For the two emulsion systems studied in this paper, the search routine in the DT-1202 software was modified to take into account only the thermal loss mechanism for surfactant stabilized emulsions and scattering loss for solid-stabilized emulsions. It was seen that the theoretical attenuation fits the experimental data with a fitting error of < 15% for both kinds of emulsions at all the measured time intervals. Thermal loss mechanism is sensitive at lower frequencies up to 10 MHz and small droplet sizes [64, 67]. Whereas, scattering loss mechanism is sensitive to higher frequencies and large droplet sizes [64, 67]. The evolution of attenuation directly indicates variation in the droplet size distribution. An increase in both the low and high-frequency attenuation as seen in Figure 2.6 b) indirectly indicates changes in the physical and morphological properties of the system such as droplet coalescence, polydispersity, and broad droplet size distributions.

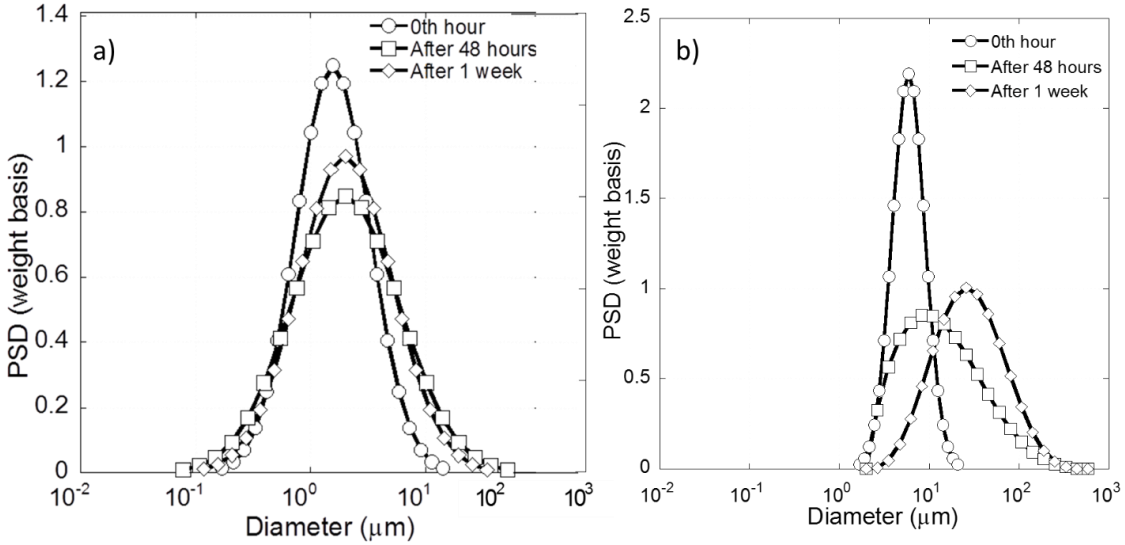

Figure 2.7: Drop size distributions of a) span80 stabilized emulsion b) fumed silica stabilized emulsion at various time intervals using acoustic spectrometer

Table 2.1: Average water droplet size in span80 and fumed silica stabilized emulsion measured at different time intervals after emulsion preparation using acoustic spectrometer

Sample	**Time after emulsion preparation**	**Mean (μm)**
Surfactant-stabilized emulsion	0^{th} hour	2.0±0.32
	48^{th} hour	3.4±0.47
	After 1 week	3.1±0.40
Solid particle stabilized emulsion	0^{th} hour	6.4±0.18
	48^{th} hour	23.9±0.60
	After 1 week	40.0±0.45

The acoustic spectrometer predicts the droplet size distribution based on raw attenuation loss mechanism. Droplet size distribution shown in Figure 2.7 a) and b) are a lognormal distribution that is generated as a result of the automatic calculation performed

by the DT 1202 software [64]. Figure 2.7 a) and Table 2.1 indicate that for the surfactant-stabilized emulsion, no further increase in the mean droplet size is seen after 1 week of emulsification and ceases after reaching 3 μm. This could be attributed to the fact that there is leveling of attenuation at both low and high frequencies, as seen in Figure 2.5 a). This behavior indicates that the emulsion is stable against de-stabilization mechanisms such as coalescence. Table 2.1and Figure 2.7 b) indicates that droplet size evolves with time and leads to broad and polydisperse droplet size distributions for solid-stabilized emulsions. Figure 2.7 b) shows that with time, attenuation at both the low and high-frequency regions increases, thereby indicating the generation of small and large micron-sized, polydisperse droplets. This directly indicates that the Pickering emulsion is not stable against coalescence. Bottle test results shown in Figure 2.2 also support this observation. Images shown in Figure 2.4 illustrate that for solid-stabilized emulsions over time, a large number of small droplets coalesce to form bigger droplets. This behavior results in a shift in the distribution towards larger droplets.

Though solid particles are well known to produce stable emulsions, a lack of particles at the interface can also result in poor emulsion stability [27, 60]. Emulsions are stable against coalescence when the droplets are completely covered by a monolayer of solid particles [27, 68]. Several studies have shown that emulsion stability increases with increase in the concentration of particles [27, 69],[70],[71]. It has been previously found that as particle concentration increases, the average drop size of solid-stabilized emulsions decreases as more solid particles are available to stabilize small droplets [60, 72]. Depending on the amount of particles available and adsorbed on the droplet interface, the droplets that have insufficient surface coverage will continue to coalesce [60, 71, 73]. This

results in a decrease in the total surface area until there is a sufficient amount of solid surfactant available to stabilize the droplets against coalescence [27, 69].

Binks and others have observed that solid particles adsorb at the droplet interface forming a hexagonal closed packed monolayer of particles [28, 68, 70, 71]. The amount of solid particles required to completely cover the droplets versus the amount of solid particles available would indicate whether the emulsion would be stable against coalescence [69]. Several studies have been conducted to understand the effect of particle concentration on emulsion stability [27, 60, 69, 74]. It has been observed that the emulsion droplet size and ratio of the amount of particles available to that required for complete coverage is a function of particle concentration [28, 69, 74, 75]. Studies have also shown that excess particles result in smaller droplet size emulsions and remain suspended in the continuous phase, causing an increase in the viscosity and producing emulsions stable against coalescence by forming a network of particles entrapping the water droplets [60, 69].

By knowing the oil concentration, droplet diameter, and interfacial area per unit mass of silica particles, we can predict the amount of silica needed to achieve monolayer coverage by hexagonal close packing [28, 69, 74, 75]. For this work, the interfacial area per unit mass of silica particles was calculated using the relationship predicted by Wiley and Aridity et al. [70, 71]. For the purpose of this work, we calculated that the amount of silica needed to achieve dense monolayer coverage was 4.08g. The amount of silica available (the mass of silica particles in the emulsion was 2 g) was found to be less than the amount required to achieve monolayer coverage (4.08 g). This suggests that the droplets initially formed had incomplete surface coverage and showed the tendency of the droplets to coalesce. The results shown in Table 2.2 and Figure 2.7 b) agree with this findings.

Table 2.2: Colloidal vibration current (CVI) and conductivity of decalin, decalin with span80, decalin and fumed silica, span80 and fumed silica stabilized emulsion measured at various time intervals using acoustic spectrometer

Sample		**CVI**	**Conductivity (S/m)**
Decalin		30456	4.70E-12
Decalin+ 2wt% Span80		30970	5.50E-08
Decalin+ 2wt% Fumed Silica		30878	4.00E-12
Span80 stabilized emulsion	0^{th} hour	19234	4.49E-08
	48^{th} hour	4858	5.25E-08
	After 1 week	3970	3.70E-08
Solid stabilize emulsion	0^{th} hour	7021	3.00E-12
	48^{th} hour	5966	1.10E-11
	After 1 week	2193	8.90E-11

For non-aqueous systems, electroacoustic/ zeta potential measurement involves a two-step process: 1. measurement of the background continuous phase colloidal vibrational signal (CVI) and 2. measurement of CVI signal of the emulsion [64]. As seen in Table 2.2 the presence of a stabilizing agent had no significant impact on the continuous phase “decalin” CVI. The CVI of the emulsion was calculated by subtracting the CVI contributed from the continuous oil phase “decalin”. It was observed that the addition of dispersed phase to the continuous oil phase resulted in a decrease in the decalin CVI (Table 2.2). CVI for both types of emulsions was observed to decrease with evolution in time.

Table 2.2 illustrates that immediately after emulsification, the CVI of surfactant and solid-stabilized emulsions decreased by 37% and 77%, respectively. This indicates that solid particles dramatically decrease the CVI magnitude of the emulsion. It was observed that for surfactant-stabilized emulsion, within 48 hours of emulsification, there was a 75% decrease in the emulsion CVI. For solid-stabilized emulsions, the CVI gradually decreases with time.

CVI signal is a magnitude of the zeta potential and is used for calculating the surface charge of water droplets [64]. CVI is an intrinsic property of the sample and is a function of the fluid properties, droplet size, and dielectric constant of the liquid phase [64]. The magnitude of CVI has no direct correlation to emulsion stability but corresponds to the magnitude of zeta potential and changes in emulsion behavior and morphology [64]. CVI indicates the dynamic mobility of the droplets and is found to be proportional to the surface charge and droplet diameter [64]. The CVI values of solid-stabilized emulsions were found to be lower than surfactant stabilized emulsions at all-time intervals except after 48 hours of emulsification. The decrease in the magnitude of CVI indicates changes in the sample properties and emulsion behavior.

A correlation between decay in surface charge and conductivity increase was established by Dukhin [67]. During coalescence, the droplets release ions into the continuous phase thereby decreasing their surface charge and increasing conductivity [67]. As seen in Table 2.2, the addition of a stabilizer to the continuous oil phase resulted in an increase in the conductivity. The conductivity of the initial emulsion (both span80 and fumed silica stabilized emulsion) was greater than the continuous phase as a result of adsorption of the stabilizing agent to the oil-water interface. As described by Dukhin,

increases in the conductivity of an emulsion with time indicate changes in the chemistry of the system, such as coalescence [67].

A sharp increase in the conductivity was seen in solid stabilized emulsion (Table 2.2). The conductivity of the emulsion increases during droplet coalescence .Coalescence causes the release of counter-ions from water droplets to the continuous phase and in turn results in an increase in the conductivity [67]. As seen in Figure 2.4 and Figure 2.7 b), the solid stabilized emulsion undergoes coalescence and a shift in the distribution towards larger droplet sizes. This causes an increase in the conductivity of the emulsion with time.

2.4 Conclusions and Future Work

In this chapter, the drop size distribution, surface properties, and transient stability of water-in-oil emulsion stabilized using a non-ionic surfactant (Span80) and hydrophobic fumed silica was measured using acoustic spectroscopy. Differences in terms of the evolution of drop size distribution and weakening of the surface charge of droplets were observed. Increases in the attenuation at low and high frequencies for solid-stabilized emulsions illustrate that droplet coalescence occurred, thereby leading to polydisperse morphologies and large droplet size emulsions. Optical microscopy results validate the droplet size distribution results obtained by acoustic spectroscopy. The acoustic spectroscopy technique can be used to characterize the transient behavior of emulsions, as it captures both morphological and physical changes in the emulsions through raw attenuation, surface charge, and conductivity measurements. Changes in the experimental attenuation and the colloidal vibration current can be used to illustrate changes in the physical properties of the emulsions.

Further experiments and evaluation of the droplet size distribution and transient stability for mixed surfactant and solid-stabilized emulsions as a function of water concentration and emulsifier concentration would provide more insight into emulsion stabilization mechanism and interfacial properties. To better understand the emulsion stabilization and destabilization mechanisms, further work will be performed on specific interfacial and rheological interactions between surfactant molecules and solid particles.

CHAPTER III

CONCENTRATED EMULSION CHARACTERIZATION IN FLOWING CONDITIONS

3.1. Introduction

Characterizing concentrated dispersions is of importance, as the formation and stabilization mechanisms of crude oil emulsions are challenging and require continuous development. Several studies have demonstrated that fundamental understanding of emulsion stability is imperative to predict strategies to address flow assurance related issues and the associated economic costs [10, 11, 76]. Hence, characterizing concentrated systems stabilized using both surfactants as well as solid particles is imperative to predict the dynamic behavior of such complex emulsions under flowing conditions.

The objective of this chapter was to evaluate the effect of flow rate, water fraction, and temperature on the emulsion morphology and stability of both surfactant and solid particle stabilized emulsions. For this work, an experimental flow loop setup equipped with an inflow microscope was utilized to quantify the behavior of concentrated emulsions in flowing conditions.

3.2. Materials and Methods

3.2.1. Experimental Setup

An experimental flow loop setup equipped with an inflow microscope (Canty Inc.) was used for characterizing emulsion droplet size and distribution, the morphology of the droplets, and behavior of solid particles at the interface. The 8 ft X 8 ft flow loop consists of jacketed 1" stainless steel tubing with fluid circulated using a 5 hp progressive cavity pump. The flow loop can achieve temperatures in the range -30℃ to 125℃ and pressures up to 150 psig. The experimental setup is outlined in Figure 3.1.

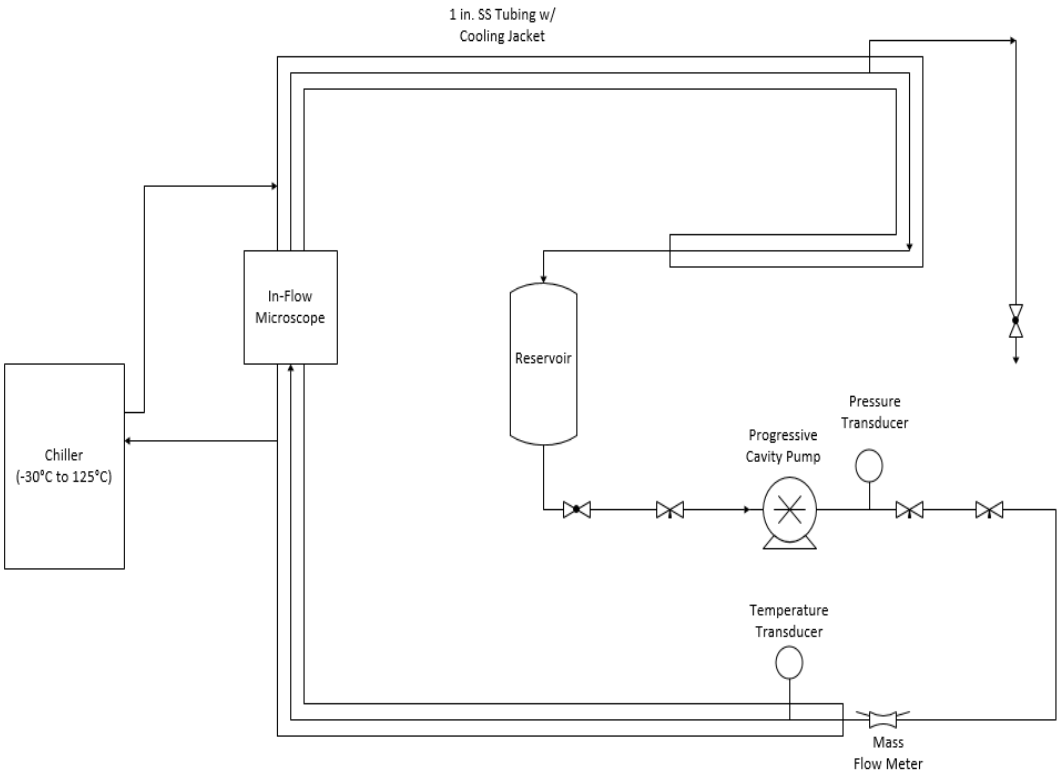

Figure 3.1: Schematic of experimental flow loop setup to characterize concentrated emulsions in flowing conditions.

3.2.2. Materials and Experimental Procedure

To confirm the performance of the inflow microscope, the particle size distribution of glass beads was measured in the flow loop. For this work, glass beads were purchased from Polysciences Inc. with a vendor specified mean size in the range of 30-50 μm. A deionized (DI) water suspension containing 0.5 wt. % glass beads were prepared by dispersing the particles directly in the reservoir (shown in Figure 3.1). The glass beads suspension was circulated at 3.3 gpm using a progressive cavity pump. The flow loop was operated at room temperature during the entire experiment. Real-time images and videos of the glass beads suspension obtained from the inflow microscope were utilized for measuring particle size distributions. A similar experiment was conducted using a DT 1201 acoustic spectrometer (purchased from Dispersion Technology Inc.) to validate the results obtained from the inflow microscope. For the acoustic spectrometer measurements, a 10 wt. % glass beads sample was used instead of 0.5 wt. % suspension due to signal noise constraints of the acoustic spectrometer. Glass beads were suspended in DI water and circulated using the peristaltic pump attached to the acoustic spectrometer.

Water-in-oil emulsions were prepared using non-paraffinic Crystal Plus 70T Mineral Oil. The mineral oil with a density of 0.85 g/cc and viscosity of 40 cP at 25°C was purchased from STE Oils. For surfactant stabilized emulsions, a non-ionic surfactant, Span80 (sorbitan mono-oleate) was used as the emulsifier. Span 80 has a density of 0.99 g/cc, and hydrophile-lipophile balance (HLB) of 4.3. For solid-stabilized emulsions, solid nanoparticles were used as the stabilizing agent. For this work, hydrophobic fumed silica nanoparticles, Aerosil R972 (purchased from Evonik Inc.) was used as the solid stabilizer. Aerosil R972 is made up of sintered aggregates of nanoparticles with a primary particle

size of 16 nm and aggregate size varying in the range 100 nm – 1 μm. Aerosil R972 is extremely hydrophobic and is known to form water-in-oil emulsions. Deionized water (DI-Water) with a resistivity of 18.1 mΩ was used as the dispersed phase. Emulsions were investigated with water fractions equal to 5, 10, and 20 vol. %. The surfactant/solids concentration was held constant at 1 vol. % for all samples. All samples were prepared gravimetrically, but concentrations are reported as vol. % to facilitate comparisons with other applications.

For the flow loop experiments, 4 gallons of emulsion were prepared using an Ultraturrax homogenizer at 3000 rpm for 5 mins. The emulsions were initially prepared outside the flow loop and transferred to the reservoir immediately after preparation and the temperature was maintained constant at 25°C using the recirculating chiller. The emulsion sample was circulated at three different flow rates (3.3 gpm, 6.6 gpm and 8.3 gpm) at 25°C and the corresponding images and videos were captured using the inflow microscope. The emulsion sample was cooled from 25°C to 15°C while the sample still remained in the flow loop. The flow loop operating temperature was decreased by circulating the chiller fluid to a set point of 15°C. This temperature ensured that the upper pressure limit of the flow loop would not be exceeded at the high water concentrations. Images and videos of the emulsion were captured at 15°C at the three different flow rates (3 gpm, 6.6 gpm and 8.3 gpm).

A small quantity (25 mL) of the emulsion sample from the flow loop operating at 25°C was used for conductivity measurements. A non-aqueous conductivity probe purchased from Dispersion Technology, Inc. was used in this work. Emulsion conductivity measurements were performed at 25°C.

3.3. Results and Discussion

Figure 3.2 a) illustrates the particle size distribution of a glass beads suspension in DI water obtained from the inflow microscope and acoustic spectrometer. Optical microscopy and scanning electron microscopy (SEM) were also employed to validate the results obtained from the inflow microscope. The mean particle diameter obtained from inflow microscopy and acoustic spectroscopy techniques were 37.7 and 33.8 µm, respectively. Though the mean particle diameters from the two techniques were not identical, both mean values were within the vendor specified range. Acoustic spectroscopy assumes a spherical morphology and predicts the hydrodynamic particle size [64], whereas the inflow optical microscopy technique is a direct visual interrogation of the system, and takes into account the particle aspect ratio. Images shown in Figure 3.2 b) and d) indicate that glass beads contain irregularly shaped debris (confirmed by discussions with the vendor), and contribute toward predicting a larger mean size, as seen by the inflow microscopy technique.

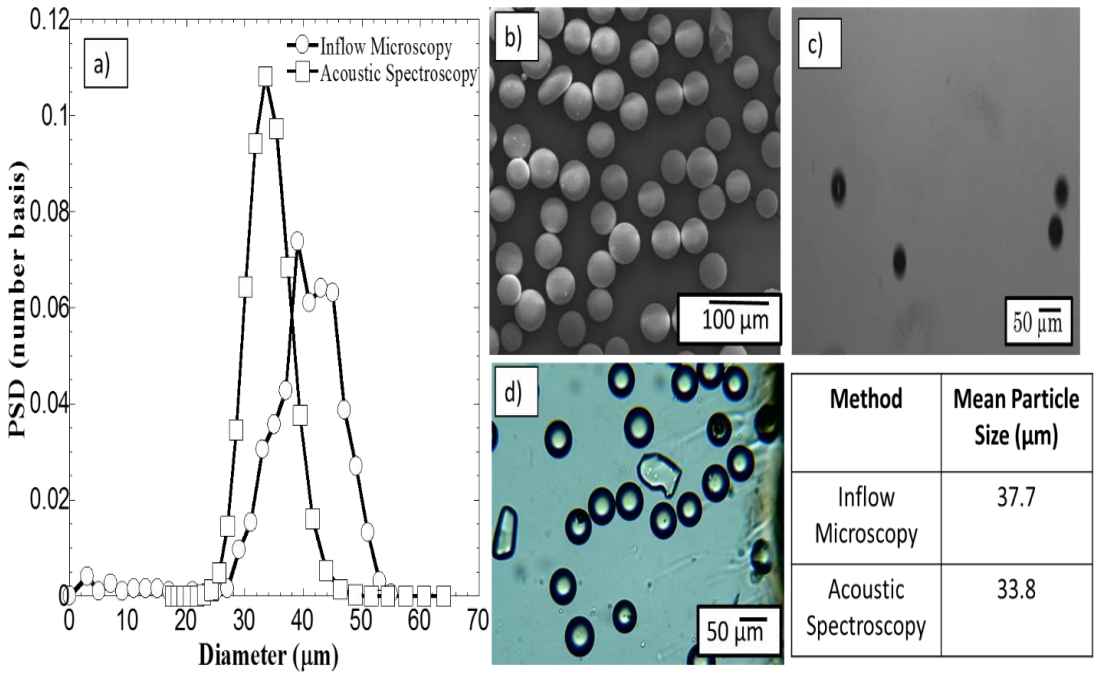

Method	Mean Particle Size (µm)
Inflow Microscopy	37.7
Acoustic Spectroscopy	33.8

Figure 3.2: Glass beads particle size distribution (psd). a) Comparison of glass beads psd measured using inflow microscopy (0.5 wt. % glass beads) and acoustic spectroscopy (10 wt. % glass beads b) Scanning electron microscopy image of 0.1 wt.% glass beads suspension c) Image captured by inflow microscope d) Optical microscope image of 0.5 wt. % glass beads taken at 10X magnification.

Figures 3.3 and 3.4 represent droplet size distributions of solid stabilized 20 vol. % water-in-oil emulsion at three different flow rates at 25°C and 15°C, respectively. Inflow microscopy images seen in Figures 3 and 4 illustrate the presence of polydisperse and large water droplets in addition to small droplets. As seen in the distributions, as well as in images in Figures 3.3, the fluid flow rate was observed to have minimal effect on the droplet size and distributions. Results observed in Figures 3.3 and 3.4 indicate that solid particles impart mechanical rigidity to droplets and prevent droplet breakup and interfacial film rupture. The images shown in Figure 3.4 were captured when the process fluid

temperature was maintained at 15°C. Figure 3.3 a) and 4 a) illustrate that with a decrease in process fluid temperature, the distribution shifted slightly to the left.

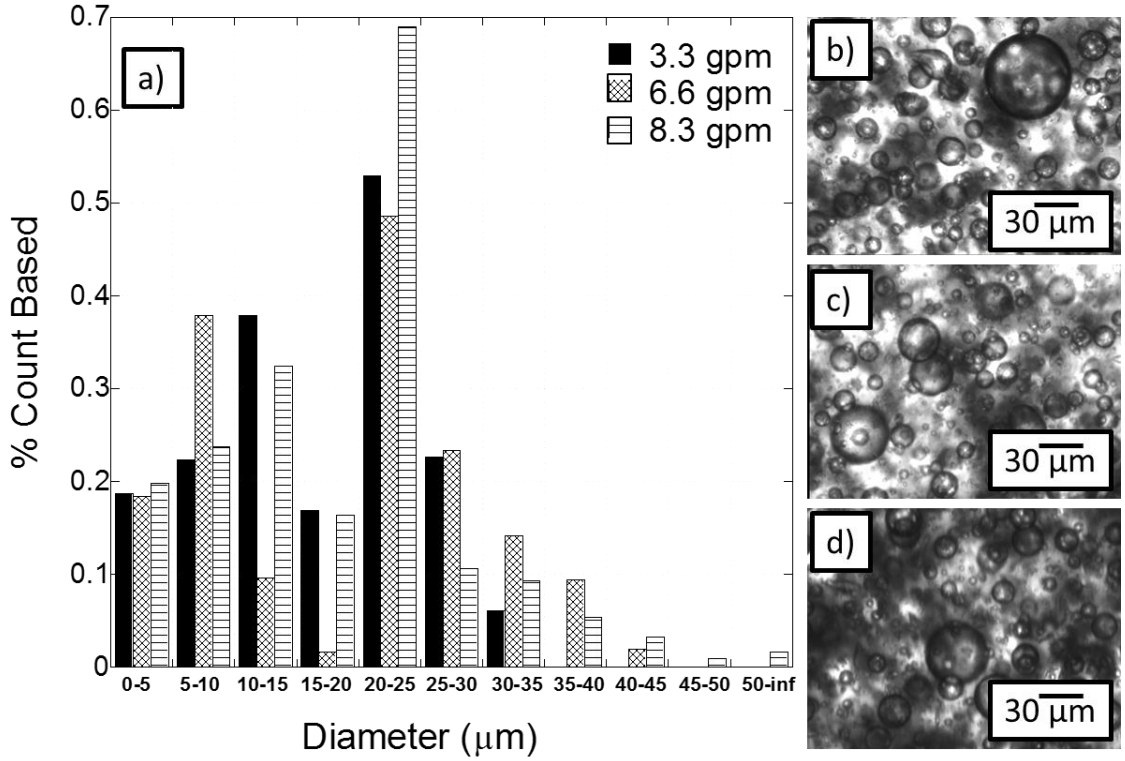

Figure 3.3: Droplet size distribution of solid stabilized 20 vol. % water-in-oil emulsion and the corresponding images of the emulsion captured by an inflow microscope at different operating flow rates at 25°C. In the figure, a) comparison of the psd obtained from the inflow microscope of the emulsion at three different flow rates, and the images of emulsion captured at b) 3.3 gpm, c) 6.6 gpm, and d) 8.3 gpm.

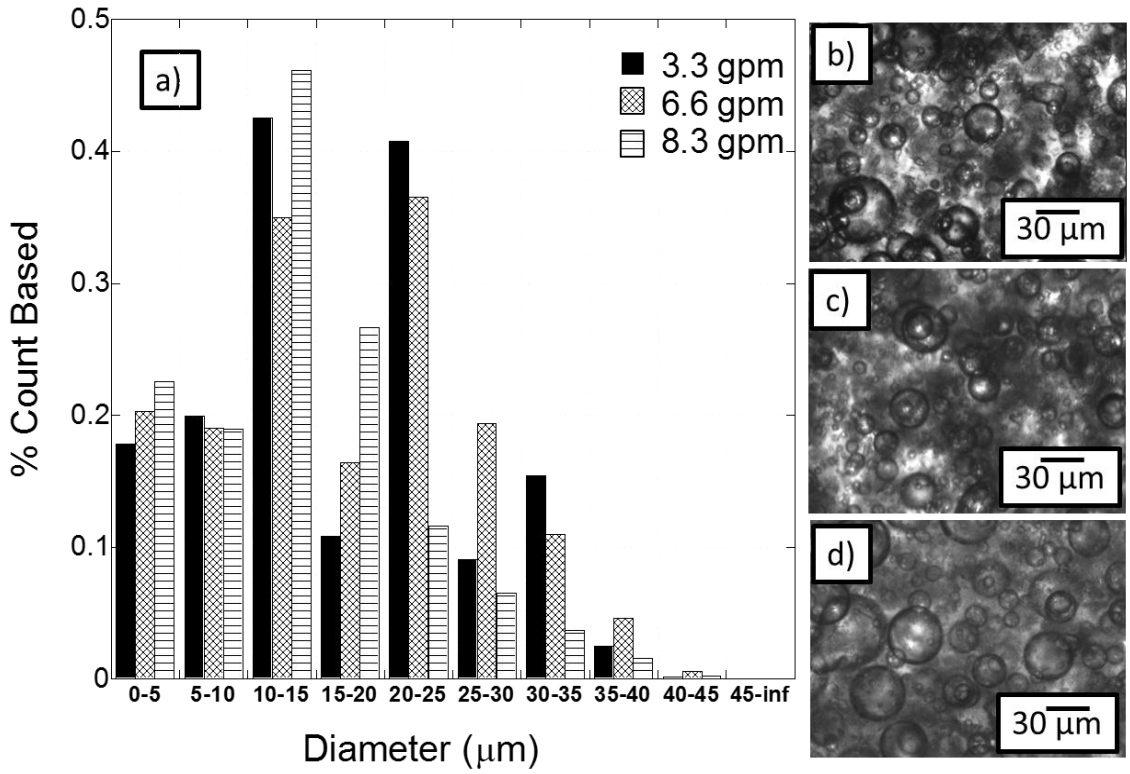

Figure 3.4: Droplet size distribution of solid stabilized 20 vol. % water-in-oil emulsion and the corresponding images of the emulsion captured by an inflow microscope at different operating flow rates at 15°C. In the figure, a) comparison of the psd obtained from the inflow microscope of the emulsion at three different flow rates, and the images of emulsion captured at b) 3.3 gpm, c) 6.6 gpm, and d) 8.3 gpm.

A similar trend was observed for solid stabilized 5 vol. % and 10 vol. % water-in-oil emulsions at both the operating temperatures. Droplet size distribution and their corresponding inflow microscopy images are not shown for every water concentration and emulsion type, as no drastic difference in the droplet behavior was observed as a function of flow rate and operating temperature. This work suggests that for solid-stabilized emulsions, the operating temperature has a negligible effect on the average droplet size, but it appears to influence the shape of the distributions.

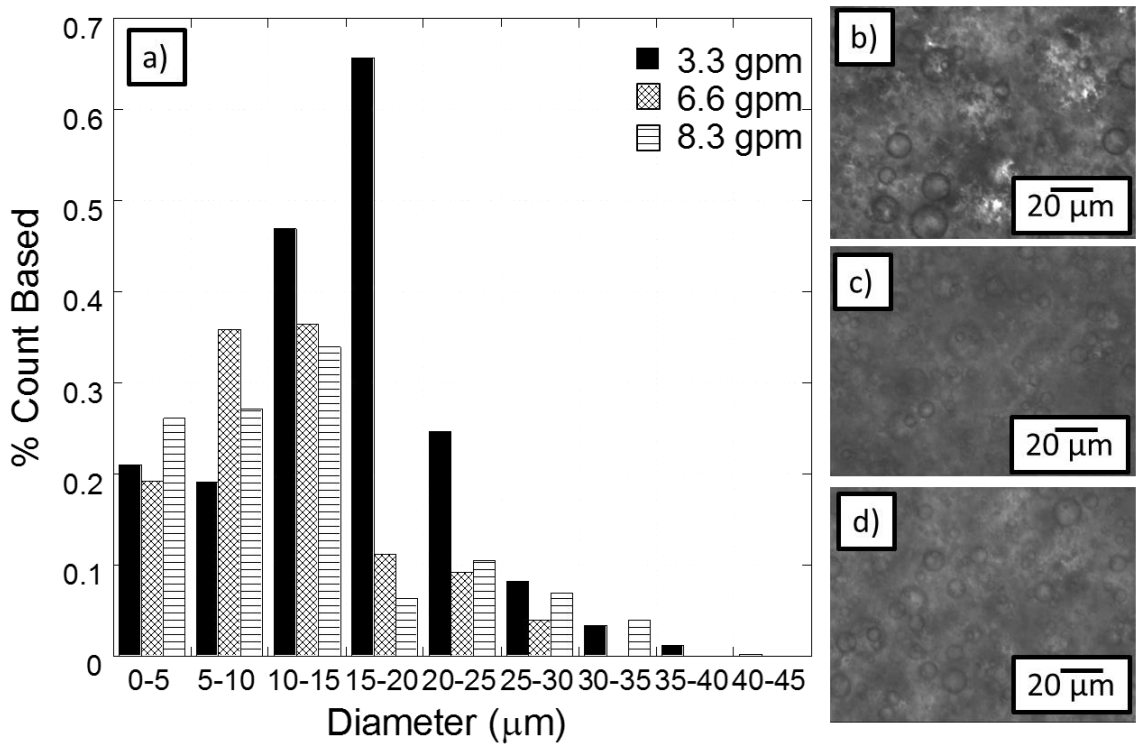

Figure 3.5: Droplet size distribution of surfactant stabilized 20 vol. % water-in-oil emulsion and the corresponding images of the emulsion captured by the inflow microscope at different operating flow rates at 25°C. Figure a) shows a comparison of the psd obtained from the inflow microscope of the emulsion at three different flow rates, and the images of emulsion captured at b) 3.3 gpm, c) 6.6 gpm, and d) 8.3 gpm.

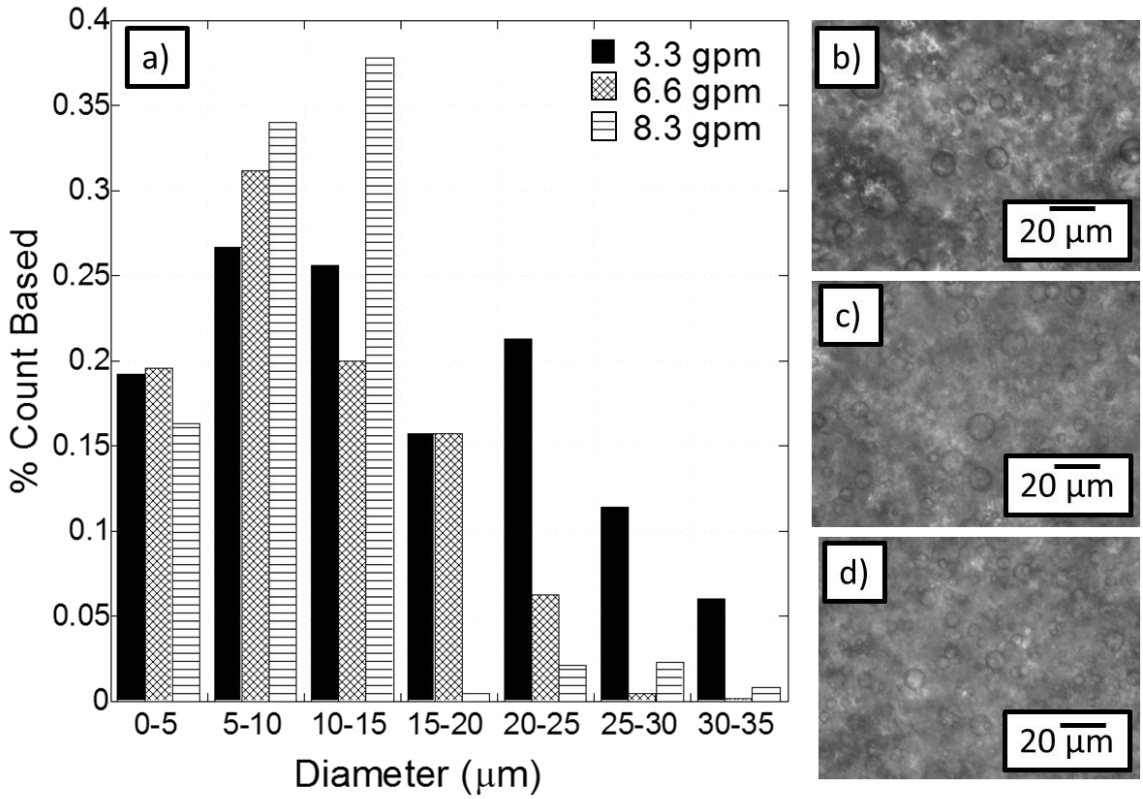

Figure 3.6: Droplet size distribution of surfactant stabilized 20 vol. % water-in-oil emulsion and the corresponding images of the emulsion captured by the inflow microscope at different operating flow rates at 15°C. Figure, a) shows a comparison of the psd obtained from the inflow microscope of the emulsion at three different flow rates, and the images of emulsion captured at b) 3.3 gpm, c) 6.6 gpm, and d) 8.3 gpm

Figures 3.5 and 3.6 represent the drop size distributions of surfactant stabilized 20 vol. % water-in-oil emulsions at three different flow rates at 25°C and 15°C, respectively. The mean droplet size of the emulsion appeared to decrease with an increase in the flow rate (Figure 3.5). This indicates that the droplets are likely deformable and the operating flow rate can have an effect on the drop size distribution. With a decrease in the process fluid temperature from 25°C to 15°C, the average droplet size decreased (Table 1 and Figures 3.5 and 3.6). A decrease in the average droplet size that was observed at higher

flow rates and lower temperatures was possibly due to changes in the structure of the surfactant layer at the interface. Drelich et al observed that span 80 emulsions showed several destabilization processes due to change in the structure of the surfactant molecules at the oil-water interface [66].

Several studies have identified that solid particles impart mechanical rigidity to the interfacial film as the solid particles form a tightly packed network around the droplets [77]. As the solid silica particles used for this work consisted of nanometer-sized particles sintered to form a fractal-like network, we observed that the emulsion droplets in solid-stabilized emulsions were mechanically rigid and didn't show droplet breakup at high flow rates (Figures 3.3 and 3.4). In addition, it has been shown that solid particles increase the viscosity of emulsions by facilitating the production of large emulsion droplets [66]. As the emulsion droplet size increases, the hydrodynamic distance between droplets decreases; thereby, increasing the emulsion viscosity [78].

Though the emulsion stress-strain relationship was not investigated in the present work, visual observations suggest that solid particles acted as viscosity adjusters and produced more viscous emulsions even at low water fractions in contrast to surfactant stabilized emulsions. It was observed that the back-pressure on the pump while handling solid-stabilized emulsions was consistently 2-3 times higher than that of surfactant stabilized emulsions at all water fractions. Drelich et al performed rheological measurements on span 80 and Aerosil R711 solid particle stabilized water-in-paraffin oil emulsions to better understand the role of each of these systems on the emulsion stabilization and formation mechanism [66]. They observed that span 80 stabilized emulsions displayed a little change in the fluid flow behavior when compared to the

continuous paraffin oil phase (Newtonian behavior). The authors found that solid-stabilized emulsions yielded non-Newtonian behavior likely due to the effect of the fractal network formed by silica particles in the continuous oil phase. Similar observations were made by other studies [78].

Conductivity measurements indicate that hydrophobic Aerosil R972 solid particles produce highly non-aqueous emulsions with conductivity in the range of 10^{-11} S/m at all water concentrations investigated in this work; whereas the conductivity of surfactant stabilized emulsions increased from 10^{-9} S/m for the 5 vol. % water-in-oil emulsion to 10^{-4} S/m for the 20 vol. % water-in-oil emulsion.

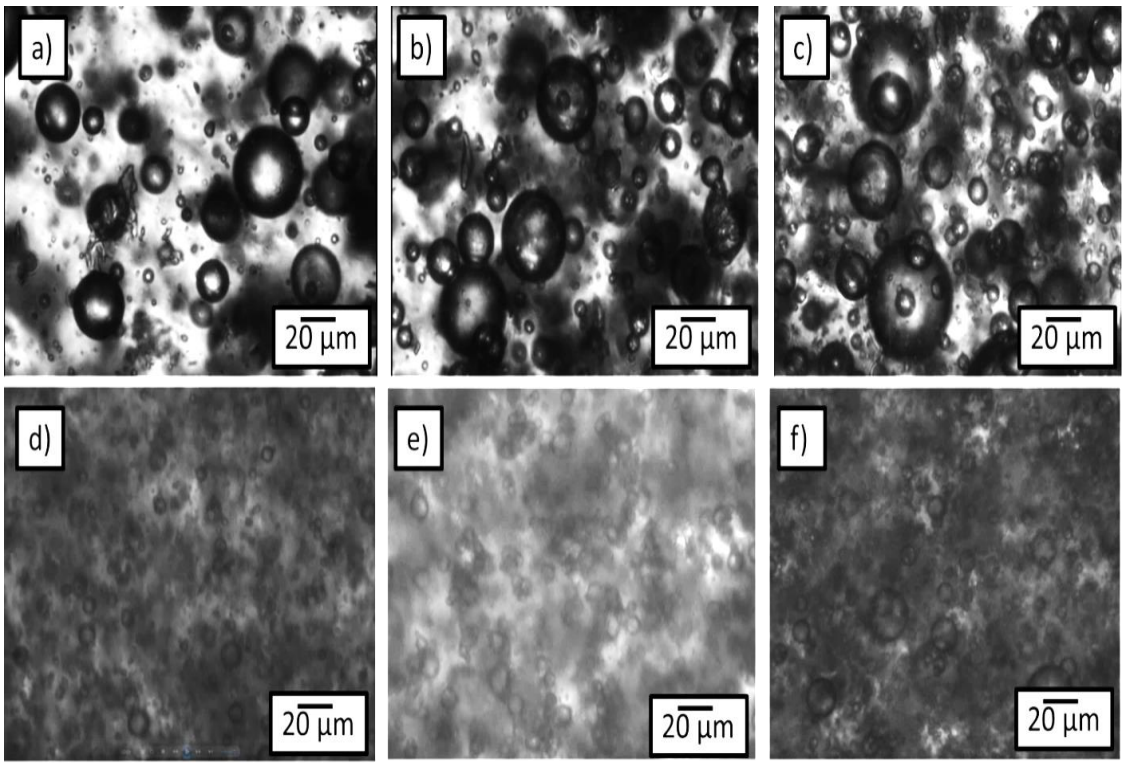

Figure 3.7: Images of emulsions captured by the inflow microscope at different water concentrations at 25°C and a flow rate of 3.3 gpm. a), b) and c) represent images of solid-stabilized emulsions at 5, 10, and 20 vol. % water concentration respectively. d), e) and f)

represent images of surfactant-stabilized emulsion at 5, 10, and 20 vol. % water concentration respectively.

Figure 3.7 provides inflow optical microscopy images captured at varying water concentrations at a fixed fluid flow rate of 3.3 gpm and 25°C. As observed in Figures 3.3-3.7 and Table 3.1, emulsion droplet size is a function of the dispersed phase concentration for both surfactant and solid-stabilized emulsions. The visual evidence shown in Figure 3.7 illustrates the polydispersity of solid-stabilized emulsions, whereas, such polydispersity in the droplet size distribution was not well pronounced in surfactant stabilized emulsions. Figure 3.7 also illustrates the tendency of span 80 emulsions to flocculate.

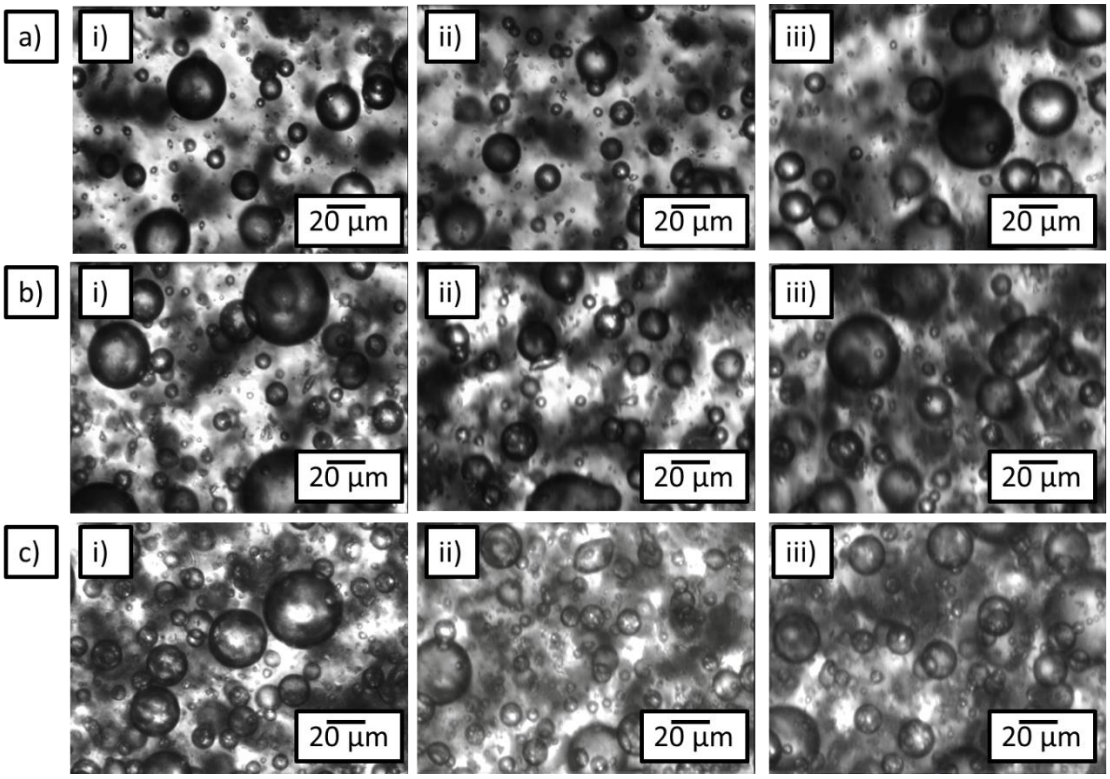

Figure 3.8: Images of solid-stabilized emulsions captured by the inflow microscope at different water concentrations and flow rates at 25°C. In the figure, a), b) and c) represent

images of the emulsion at 5, 10, and 20 vol. % water concentration respectively. i), ii) and iii) represent images of the emulsion at 3.3 gpm, 6.6 gpm and 8.3 gpm, respectively.

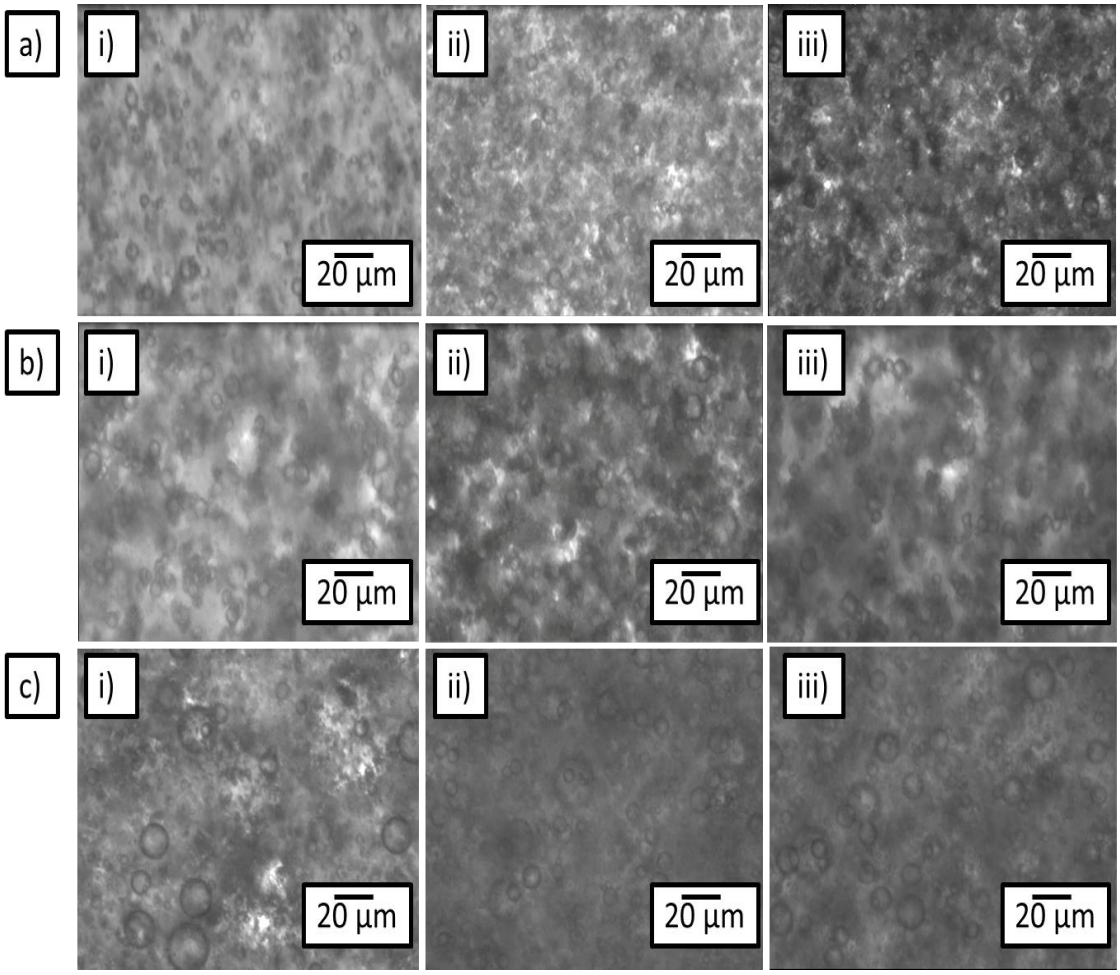

Figure 3.9: Images of surfactant-stabilized emulsion captured by the inflow microscope at different water concentrations and flow rates at 25°C. Figures a), b) and c) represent images of the emulsion at 5, 10, and 20 vol. % water concentration respectively. i), ii) and iii) represent images of the emulsion at 3.3 gpm, 6.6 gpm and 8.3 gpm respectively.

Figures 3.8 and 3.9 correspond to the images captured by the inflow microscope to delineate the effect of water fraction and flow rate on the emulsion drop size distribution and morphology. As noticed in Figure 3.8, there appeared to be a negligible effect of flow

rate on the emulsion drop size and morphology. Figure 3.9 further illustrates the flocculation tendency of span 80 emulsions, even in flowing conditions. Figure 3.9 also illustrates the impact of water fraction and operating flow rate on the resulting drop size distributions.

Several studies have previously shown that there is a significant contrast in the interfacial properties between these two kinds of emulsions. Binks demonstrated that solid particles function in similar ways to surfactant molecules except that they don't reduce the interfacial tension between the two immiscible phases [78]. Drelich et. al conducted interfacial tension measurements on Aerosil R711 and span 80 stabilized emulsions using a drop shape analysis system [66]. The results indicated that the presence of solid particles had no effect on the oil-water interfacial tension, whereas, for surfactant-stabilized emulsion, the oil-water interfacial tension decreased in the presence of surfactant molecules. This insight coupled with the visual observations made in the present work underscore the complexities that can arise in these systems.

Table 3.1: Mean emulsion droplet size of solid particle and surfactant stabilized water-in-oil emulsions at different water concentrations, flow rates, and temperatures. The average droplet size was determined from the real-time images and videos captured from the inflow microscope.

Water Concentration (Vol. %)	Flow rate (gpm)	Solid stabilized emulsions (µm)		Surfactant-stabilized emulsions (µm)	
		25°C	15°C	25°C	15°C
5	3.3	9.5	10.3	5.4	3.8
	6.6	9.1	10.7	4.3	3.2
	8.3	9.2	9.9	3.8	3.0
10	3.3	14.1	14.5	8.7	5.9
	6.6	13.9	13.6	6.7	4.4
	8.3	14.2	13.5	6.2	4.2
20	3.3	16.2	16.3	14.5	8.5
	6.6	16.8	16.2	11.3	7.8
	8.3	16.6	16.7	10.6	7.2

3.4. Conclusion

The experimental flow loop setup equipped with an inflow microscope was successful in characterizing emulsion drop size distribution and morphology over a range of operating conditions. Inflow microscopy images and the drop size distributions of solid-stabilized emulsions exhibited polydispersity. Surfactant-stabilized emulsions exhibited a comparatively smaller droplet size distribution. For solid-stabilized emulsions, temperature and fluid flow rate had a negligible effect on the drop size distributions (Table

3.1). Water concentration was identified as the primary variable that impacted the droplet size distributions. For surfactant stabilized emulsions, flow rate, operating temperature, and water concentration appeared to influence the droplet size distributions. Evolution of multimodal distributions with a decrease in temperature and increase in flow rate was observed in surfactant stabilized emulsions. These observations indicate that solid particles formed a steric barrier around the water droplets imparting rigidity and preventing droplet coalescence even in flowing conditions (Table 3.1). Surfactant-stabilized emulsions were observed to form mechanically deformable droplets (Table 3.1). Further experimental investigation on the rheological and interfacial properties will be performed to evaluate the competitive effect of solid particles and surfactants on emulsion formation and stabilization mechanisms. The experimental results coupled with future investigations on the combined effect of solid particles and surfactants will provide new insights for developing strategies for handling complex emulsions that are prevalent in the energy industry.

CHAPTER IV

IMPACT OF HYDRATE FORMATION ON EMULSION MORPHOLOGY IN SURFACTANT AND SOLID STABILIZED EMULSIONS

4.1. Introduction

Palermo et al and Turner proposed hydrate agglomeration and nucleation mechanism in w/o emulsion[79],[80]. To this end, Høiland et al explored the interaction between hydrates and emulsions at high water fraction[10]. Høiland et al also investigated the effect of hydrate particles on emulsion phase inversion. The authors observed that increase in water fraction resulted in emulsion inversion from water-in-oil (w/o) to oil-in-water (o/w) type in the presence of Freon hydrates. Høiland et al developed and tested a method for evaluating the wettability of hydrate particles in crude oil systems. The authors assumed the solid particles present in the crude oil, such as silica, adsorb to hydrate the acting as colloidal stabilizers resulting in Pickering emulsions. The authors observed that hydrophobic solid particles adsorbed on the hydrate surface prevent hydrate agglomeration.

Linares et al conducted experiments on gas hydrate formation in a water-in-model oil emulsions system[81]. The authors prepared emulsions that are common in crude oil

systems by varying the surfactant concentration and water content to demonstrate the stability of emulsions upon ice and hydrate formation. The model oil (Crystal plus 70T mineral oil) used by Linares et al is similar to the model isoparaffinic oil system that will be used in this proposed work. Stable water-in-oil emulsions were prepared using span 80 and AOT surfactant mixture. Stable emulsions were formed at varying water fractions (10-70 vol. %) and surfactant concentrations (1 and 5 wt. %). The authors observed that emulsion viscosity increased with increase in the water fraction.

Sjöblom et al conducted experiments to investigate the properties of oils that contribute to hydrate plugging and non-plugging of pipelines[12]. Rheological, interfacial, micromechanical force, and droplet size measurements were examined for three different surface treated crude oil-water systems. The authors concluded that capillary attractive forces between hydrate particles contribute to hydrate agglomeration and plugging. Adsorption of solid particles on the oil-water interface, emulsion stability, high shear rate, low interfacial tension, and anti-agglomerants prevent hydrate particle adhesion and agglomeration.

Lachance et al conducted several experiments on the formation of hydrate slurries in a once-through flow loop and field trial test [82]. Once through flow loop tests were conducted to simulate and provide insight into the evolution of hydrate formation in crude oil emulsions using span 80 as a surfactant. A Canty inflow microscope was utilized to obtain droplet size and distribution to study the effect of water cut on dispersion characterization and hydrate slurry formation. The emulsion droplet images and distribution captured by the inflow microscope were similar to the results we obtained for 5 and 20 vol. % water-in-model oil emulsion stabilized using span 80 as a surfactant. The

authors concluded that water dispersion characteristics (water cut, fluid velocity, emulsion composition, and stability) showed the most effect on hydrate formation and aggregation. They observed that emulsions with high water cut aided in increasing droplet coalescence promoting hydrate formation. Increased emulsion stability aided in reducing hydrate aggregation tendencies.

Several studies have been conducted to investigate hydrate nucleation, crystal growth, and their morphology using cyclopentane [45-47, 83-86]. Hence, for this study, cyclopentane is used as a guest molecule in the hydrate forming emulsion. The focus of this work was to investigate hydrate formation in oil-dominated systems in the presence of different stabilizers such as surfactants and solid particles. Water-in-oil emulsions (water dispersed in continuous oil phase) is one of the most predominant multiphase flow situations encountered in the petroleum industry. In such oil dominated systems, hydrate blockages have been proposed to occur in a four-step mechanism [80, 87, 88]. Studies have shown that as the emulsion enters into a hydrate formation region (low temperature and high-pressure conditions favorable to hydrate formation), hydrate grows on water droplets similar to a shrinking core model, agglomerate, or plug flow line. As the hydrate shell grows around the water droplet, diffusion of gas through water droplets occurs as a function of droplet size. Hydrate agglomeration is prevented in the presence of small water droplets as the hydrates grow inward and result in a fully converted hydrate particle that remains suspended. Whereas, large droplets result in capillary attraction between hydrate particles due to water bridging, and cause agglomeration and eventually plugging [37]. Hence, it is imperative to determine the emulsion droplet size, hydrate crystal size, and hydrate morphology.

Hydrate formation is an interfacial phenomenon, so understanding and quantifying interfacial behavior, such as surfactant type and distribution at the interface, is critical in order to develop hydrate management strategies [37]. As crude oil contains several naturally occurring surfactants, solid particles, and surface active materials, it is imperative to investigate hydrate crystal growth and interfacial characterization in the presence of surfactant and solid particles. Furthermore, hydrate characterization would provide an insight into processing efficiency and transportation of hydrate crystals and slurries. To this end, Karanjkar studied the effect of surfactant (Span 80) on hydrate formation and crystal morphology in cyclopentane hydrate forming systems using a visualization technique [44]. Single water drop microscopy experiments showed conical hydrate crystals with hairy or mushy hydrate morphology in a surfactant laden system. Such morphology was observed due to excess Laplace pressure generated by reduced interfacial tension in the presence of surfactant which resulted in inward growth of hydrate crystals. In the absence of surfactant, lateral growth of a faceted plate-like structure was observed. Similar work was conducted by Zylyftari et al. and Ahuja on hydrate formation in emulsions [46, 85]. A porous, hairy, or mushy hydrate structure was formed in the surfactant stabilized emulsions. To this end, Cha et al conducted visualization experiments to evaluate the effect of solid particle loading on hydrate formation[89]. Conical hydrate crystals with a hairy or mushy like structure were observed at solids loading < 1 wt. % of the oil phase, whereas, hydrate formation was greatly reduced or prevented in emulsions containing >2 wt. % solid concentration. Nakajima et al studied the effect of surfactants on energy storage in cyclopentane hydrate formation and observed hydrate morphology similar to that seen by Karanjkar [44, 50]. Several studies have shown that hydrate

formation leads to an abrupt increase in emulsion viscosity, and mechanical properties, thus leading to a sudden rise in system pressure and plugging of flow lines[43, 46, 56, 84, 86, 90-92]. Peixinho et al. studied the effect of nucleation time and crystal growth time in cyclopentane hydrate forming emulsions [83].

Though several studies have been carried out on cyclopentane hydrate forming systems, limited laboratory scale experimental work has been conducted on hydrate characterization and emulsion properties after hydrate dissociation in concentrated emulsions [43-46, 85, 89]. Moreover, the effect of stabilizer type, and the water fraction on hydrate formation in emulsions is not comprehensively understood, and hence requires further investigation. This study probes the effect of stabilizer type and water fraction on emulsion droplet size before hydrate formation and upon hydrate dissociation in cyclopentane hydrate forming water-in-oil emulsions. In this study, emulsion droplet size and hydrate crystal formation are studied using visualization technique, and interfacial properties are characterized using IFT measurements. For this work, cyclopentane hydrate forming emulsions were prepared at two different water fractions (10 and 40 vol. %) and three different stabilizers, such as a non-ionic surfactant (span 80) and solid particles of different wettability (Aerosil R974 and Aerosil R816). Solid particles with different wettability were chosen to investigate the effect on hydrate formation and emulsion properties upon hydrate dissociation. In addition to visualization, a statistical analysis was performed to compare emulsion properties before and after hydrate dissociation. What follows is a detailed description of experimental procedure adopted to accomplish the objectives of this work.

4.2.Materials and Methods

The experiments carried out in this work consist of several steps such as preparation of emulsion samples, cooling and heating process of the samples to study hydrate growth and dissociation and visualization of the samples during this process. Following is a brief description of the materials and methodology used to perform proposed experiments.

4.2.1. Materials

Water-in-oil emulsions were prepared using Crystal Plus 70T mineral oil, cyclopentane, and stabilizers such as non-ionic surfactant (span 80) and solid particles (Aerosil R974 and Aerosil R816). Crystal Plus 70T (purchased from STE Oils) is a technical grade white mineral oil with a density of 825 kg/m^3 at 25 ^{o}C and viscosity of 20 cP at 25 ^{o}C. As discussed earlier, since Cyclopentane forms structure II hydrates at nearly atmospheric conditions, it was considered as an appropriate guest molecule for this work. Cyclopentane used for the experiments were of 99 wt.% purity, density of 750 kg/m^3 purchased from BDH chemicals. The continuous oil phase used in this work was prepared using a 50:50 equal volume mixture of crystal plus 70T mineral oil and cyclopentane. An equal volume mixture of mineral oil and cyclopentane ensured that cyclopentane was in stoichiometric excess (1 mol of cyclopentane:17 mol of water). This emulsion composition is similar to the study conducted by Karanjakar et al. [43]. For the control sample, the oil phase consisted of mineral oil and stabilizer. Deionized water obtained from a Millipore Direct Q3 system was used as the internal/aqueous phase. Two different water concentrations (10 and 40 vol.%) were used in this study to evaluate the effect of

low (10 vol.%) and high (40 vol.%) water cut on hydrate formation and emulsion morphology in water-in-oil emulsions.

The three kinds of stabilizers used for this study were span 80, Aerosil R974, and Aerosil R816. Span 80 (sorbitan monooeleate) was used for this study, as it is well known to form stable water-in-oil emulsions due to its low hydrophilic-lipophilic balance (HLB) of 4.3. Span 80 is a non-ionic surfactant with a density equal to 990 kg/m^3 and was purchased from Sigma-Aldrich. The two kinds of solid particles (Aerosil R974 and Aerosil R816) used as stabilizers in this study were provided by Evonik Inc. Aerosil R974 and Aerosil R816 are fumed silica particles synthesized by flame pyrolysis. The primary particle size of these fumed silica particles are around 10-20 nm with an agglomerate size < 1 μm. The two kinds of fumed silica particles used in this study have a tamped density of 50-60 g/L and a specific surface area of 200 m^2/g. These two types of solid particles were used due to their difference in particle hydrophobicity/wettability. Aerosil R974 is highly hydrophobic and is always known to form water-in-oil emulsions at all water concentrations as compared to Aerosil R816. Aerosil R816 is synthesized with intermittent wettability and hydrophobicity and hence produces both water-in-oil and oil-in-water emulsions depending on the aqueous phase concentration. These two types of solid particles were chosen to evaluate the effect of particle hydrophobicity on emulsion stability and hydrate formation. For both surfactant and solid particle stabilized emulsions, based on the oil concentration, the stabilizer concentration was kept constant at 0.1 vol. %. Karanjkar identified the critical micelle concentration (CMC) for span 80 to be equal to 0.03 vol. % for the oil mixture used in this study. Since our work is based on the

previous studies by Karanjkar and Ahuja, we decided to use 0.1 vol. % span 80 for surfactant stabilized emulsions [44, 85]. As one of our objectives was to probe the similarities/differences in hydrate formation in surfactant and solid-stabilized emulsions, we decided to keep the stabilizer concentration constant (0.1 vol. % of the oil phase) in both kinds of emulsions. The emulsion sample (50 g) used in this work was prepared by adding the stabilizer to the mixture containing equal volume fraction of mineral oil and cyclopentane. The stabilizer was dispersed well in the oil mixture by stirring it using a spatula. The aqueous phase was added to the oil mixture dropwise and mixed well using an IKA Ultraturrax T25 homogenizer at 2800 rpm for 5 min. Similar experiments were performed with a control sample. The control sample, however, did not show any sign of hydrate formation throughout the experiment in the hydrate formation zone. The control samples were prepared similarly except that the oil phase was composed of mineral oil and stabilizer instead of equal volume mixture of mineral oil and cyclopentane.

4.2.2. Methods

To accomplish the objectives of this research, a step by step procedure consisting of measurements of interfacial tension, visualization, and image analysis/measurement was followed.

4.2.2.1.Visualization technique

In this work, an Olympus BX53 polarized optical microscope equipped with a Linkam CSS 450 temperature controlled shear stage and a high-speed camera was used for visualization. The microscope was equipped with a Peltier stage that could operate in the temperature range of -45 °C to 450 °C and a maximum shear rate equal to 10 rad/s. It

should be noted that the samples under visualization were not subjected to shear throughout the course of the experiment. The temperature controlled stage consisted of a circular well mounted on a quartz window with a sample diameter of 30 mm and viewing diameter of 2.8 mm as shown in Figure 4.1.

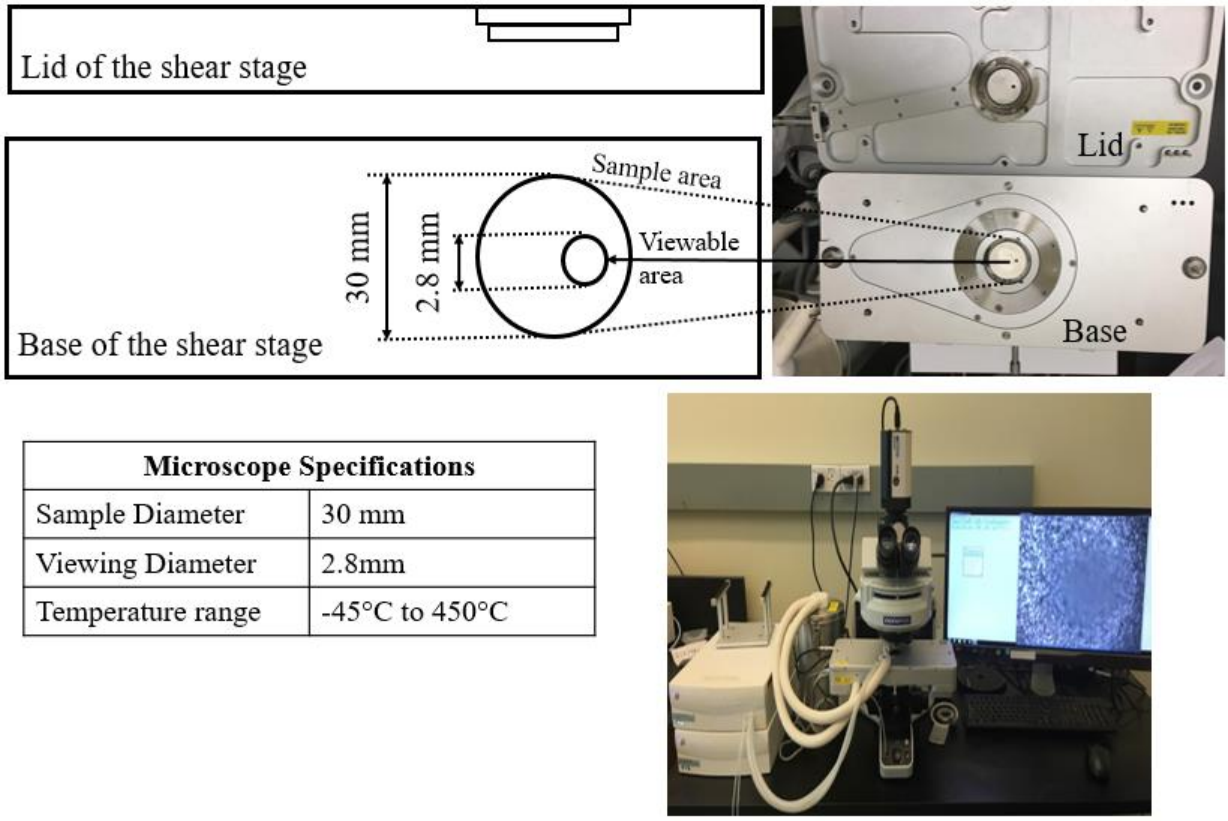

Microscope Specifications	
Sample Diameter	30 mm
Viewing Diameter	2.8mm
Temperature range	-45°C to 450°C

Figure 4.1: Schematic of the temperature controlled stage and the visualization setup used for experiments.

The emulsion sample of volume 0.5 mL at room temperature was loaded on the microscope stage. The experimental procedure followed in this work is similar to the work conducted by Ahuja [45] and Karanjkar [93]. However, the experimental conditions differ in terms of the oil composition, sample volume used for visualization, mixing conditions,

and the temperatures used for the quenching and reheating process. For this work, the temperature profile used in the microscope is described below:

a) The temperature stage was initially set to 25^{o}C followed by the quenching process. Quenching of emulsion to form ice was identified to induce faster hydrate formation by overcoming long induction times during hydrate nucleation [93]. Hence, the temperature was lowered to -25 °C (T_{ice}) at a rate of 10 °C/min to induce ice crystallization of the emulsion droplets.

b) The sample was held at that temperature (T_{ice}) until more than 50% of the water droplets were converted to ice. Visual observation was used to confirm that at least 50% of the water droplets were converted to ice. Our experimental observations showed that at least 30 minutes of hold time was required to convert more than 50% of the droplets to ice. The appearance of white spots on the water droplets indicates ice formation, as seen in Figure 4.2(e).

c) Next, the temperature was increased from T_{ice} to 0.1 °C (T_{hyd}) at a rate of 2 °C/min and held at this temperature for 60 mins to allow the hydrate crystals to grow. A slower heating rate was chosen in this step to ensure melting of ice before hydrate formation.

d) The temperature was increased back to 25 °C at a rate of 5 °C/min rate to study the effect of hydrate dissociation on emulsion droplet size.

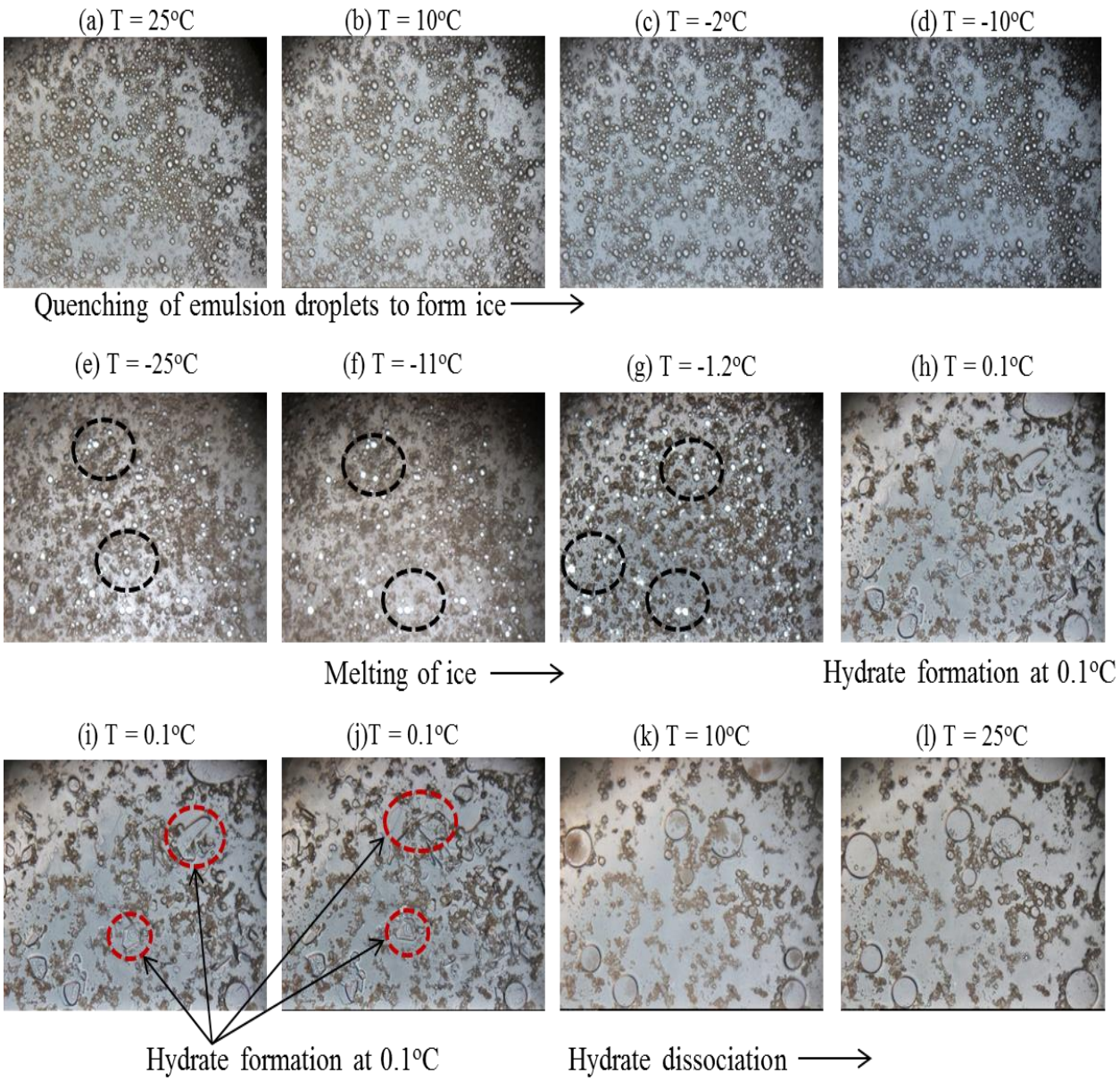

Figure 4.2: Images captured (10x magnification) at various temperatures during hydrate characterization experiment for 0.1 vol. % surfactant stabilized 10 vol. % water emulsion.

Transient emulsion stability tests were conducted on hydrate forming emulsions by measuring the emulsion drop size distribution of a representative sample that was used for hydrate studies. The hydrates experiments were carried out within 5 mins of emulsion preparation, and the transient stability test was conducted after two hours on the same

sample. The drop size distribution for the emulsion before hydrate formation and after hydrate dissociation was determined using Image J software. For each sample, the algorithm illustrated in Figure 4.3 was followed to determine the size of each droplet and statistical parameters, such as mean droplet size and standard deviation of the droplets' size.

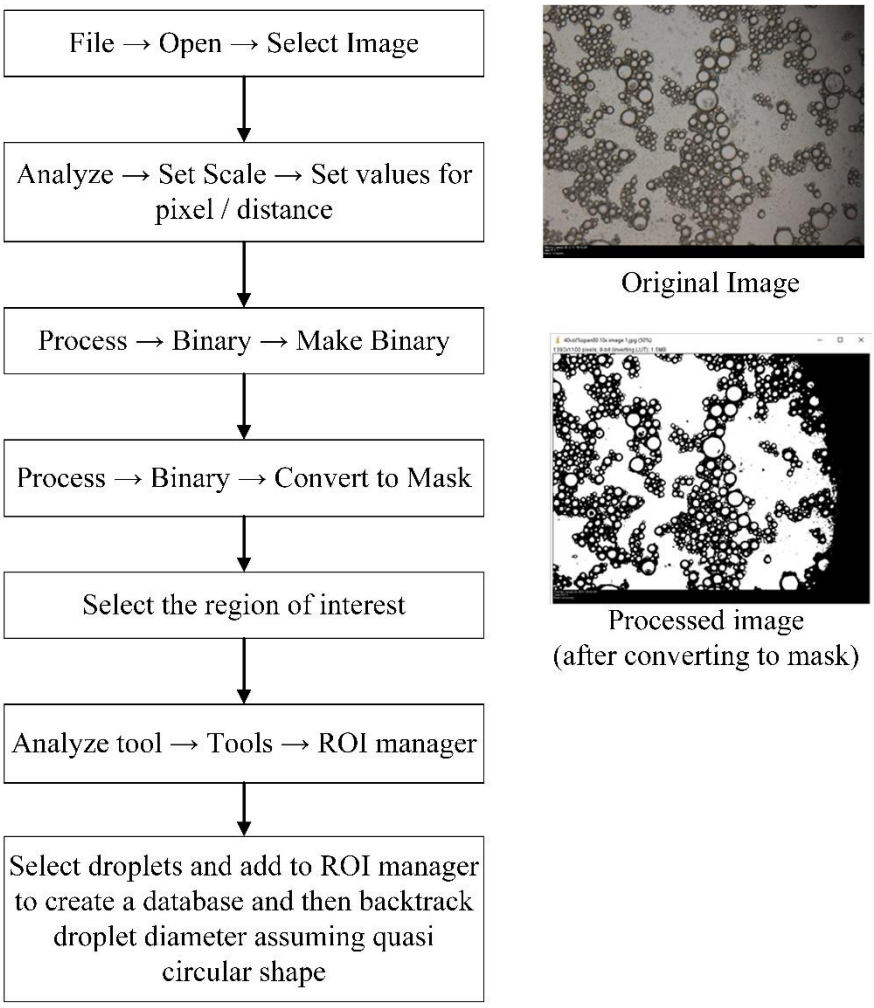

Figure 4.3: Image J algorithm to determine droplets' size and distribution for different emulsion samples.

4.2.2.2.Interfacial tension

A high pressure, interfacial tensiometer (IFT) model # IFT-10-OS purchased from Core Lab Instruments (Tulsa, OK) was used for conducting dynamic interfacial tension measurements. The pendant drop method was used for measuring the interfacial tension of pure water-cyclopentane, 50:50 equal volume mixture of mineral oil-cyclopentane, and water in the absence of stabilizer and at 0.1 vol. % stabilizer (either surfactant or solid particles) concentration at ambient conditions. The measurements were conducted for a minimum of 5 min until steady state was reached as shown in Figure 4.4. The steady state was identified when the IFT measurements showed a variation less than 0.05 mN/m. The experiments were performed at least three times to quantify the precision of the technique. A summary of interfacial tension measurement of the different systems of interest for this study is given in Table 4.1. The interfacial tension of the oil-water system in the presence of 0.1 vol.% solid particles (50 mN/m) was observed to be the same as pure (oil+cyclopentane) - water (48.2 mN/m). This observation is congruent with Drelich et al, who observed that solid particles did not reduce the interfacial tension [56]. The plausible explanation for such behavior by solid particles on the oil-water interfacial tension could be attributed to the high amount of energy required by solid particles to desorb from the interface, whereas in the presence of a surfactant, the interfacial tension was reduced to 3 mN/m [22].

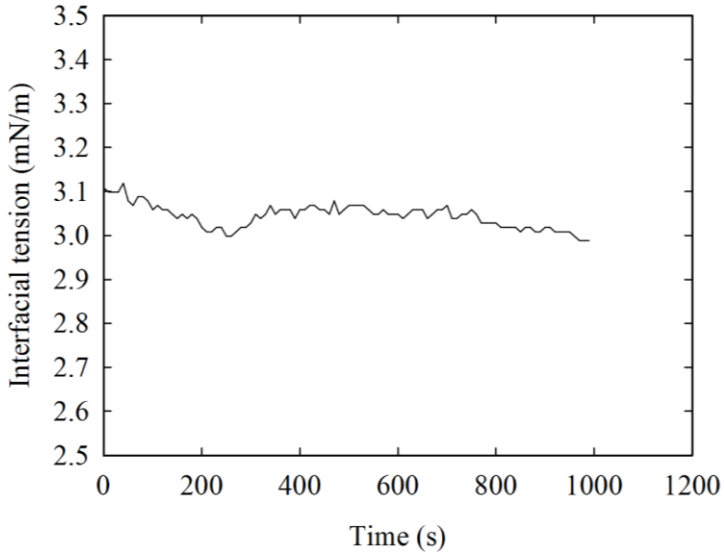

Figure 4.4: Dynamic interfacial tension of 50:50 equal volume mixture of cyclopentane and crystal plus 70T mineral oil containing 0.1 vol.% span 80 measured using pendant drop technique

Table 4.1: Summary of interfacial tension of oil-water interface in the absence and presence of a stabilizer. Oil here represents an equal volume mixture of crystal plus 70T mineral oil and cyclopentane.

System	Dynamic Interfacial Tension (mN/m)
Oil -water	48.36 ±0.06
Oil+ 0.1 vol% Span 80 - water	3.04 ±0.02
Oil+ 0.1 vol% Aerosil R816 - water	50.3 ±0.03
Oil+ 0.1 vol% Aerosil R974 - water	50.16±0.05

4.3. Results and Discussion

The images captured along the temperature variation for surfactant stabilized 10 vol. % water emulsion are presented in Figure 4.2 (a)-(l). Figure 4.2 (a) is a representative image of the emulsion at 25 ^{o}C during the start of the experiment. Figures 4.1 (b) to (d) are images captured during quenching of emulsion droplets to form ice. White spots

highlighted in Figures 4.1 (e) to (g) represent water droplets that are converted to ice. Water droplets that were converted to ice were found to melt around -0.4 ^{o}C. The sample was set to 0.1°C to observe hydrate formation in emulsions. A crystalline like structure was observed to grow at the interface of water droplets that were converted to ice and subsequently melted. Irregularly shaped crystals were observed and are highlighted in red in Figures 4.1 (i) and (j). Figures 4.1 (k) and (l) are representative images of the emulsion after hydrate dissociation. As seen in the images in Figure 4.1, after hydrate dissociation, the mean emulsion droplet size was greater when compared to droplet size at the start of the experiment. Similar observations were reported by Karanjkar [44].

Representative images of hydrate crystals and emulsion morphology at the hydrate formation zone (at 0.1°C) for surfactant stabilized 10 and 40 vol. % water emulsions are reported in Figure 4.5. Figure 4.6 represents images of hydrate crystals captured at higher magnification for surfactant stabilized 40 vol. % water-in-oil emulsion. A similar experimental procedure was carried out in the control sample which is devoid of hydrate forming compound (cyclopentane). Though conversion of water droplets into ice was observed in both control and hydrate forming emulsions, hydrate crystals were not observed in the control sample in the hydrate formation zone.

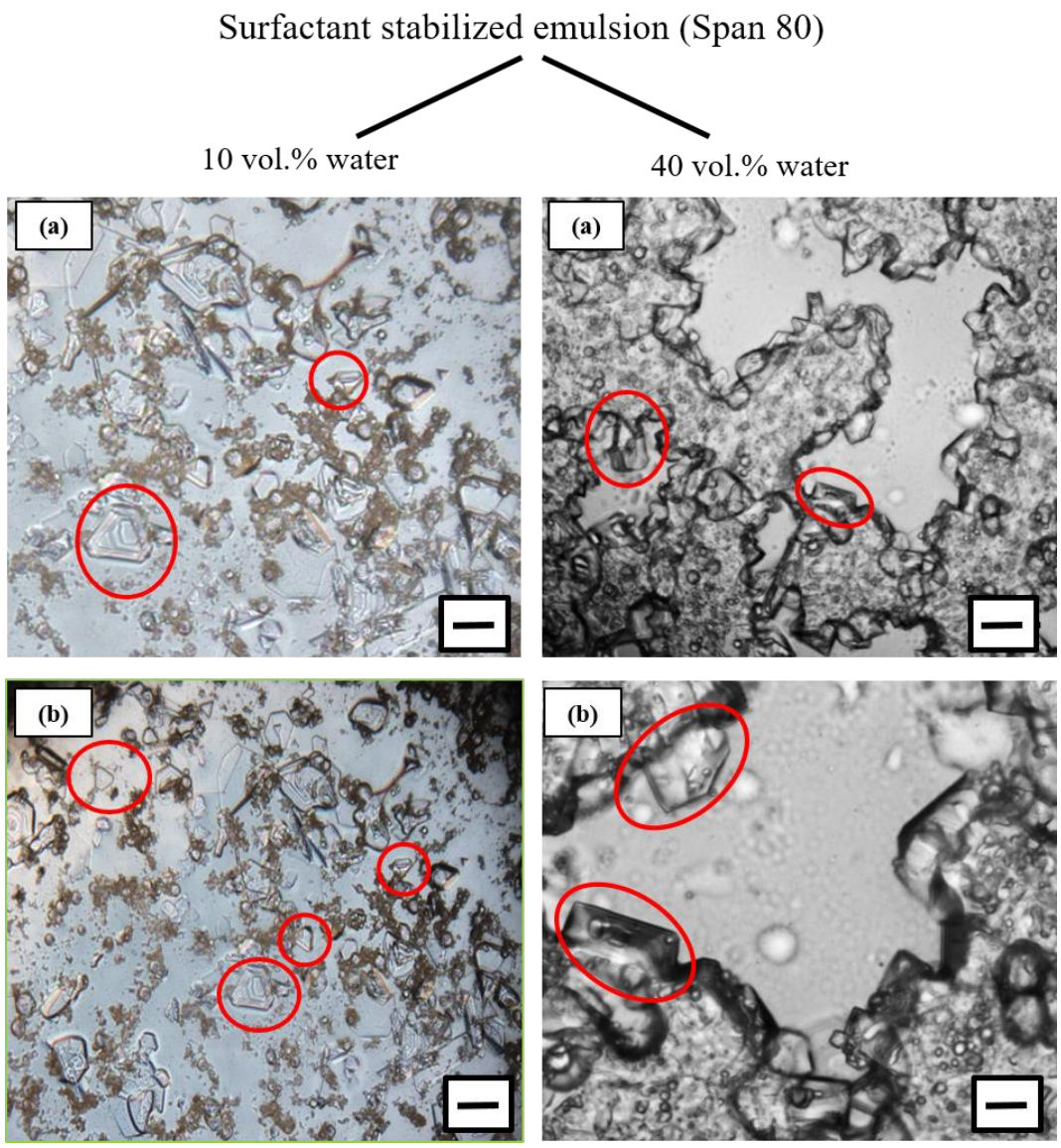

Figure 4.5: Images of hydrate crystals (at 10x magnification for 10 vol% and 20x magnification for 40 vol%) captured in the hydrate formation zone of 0.1 °C for surfactant stabilized emulsions with water concentrations equal to 10 and 40 vol% (scale bar = 100 μm).

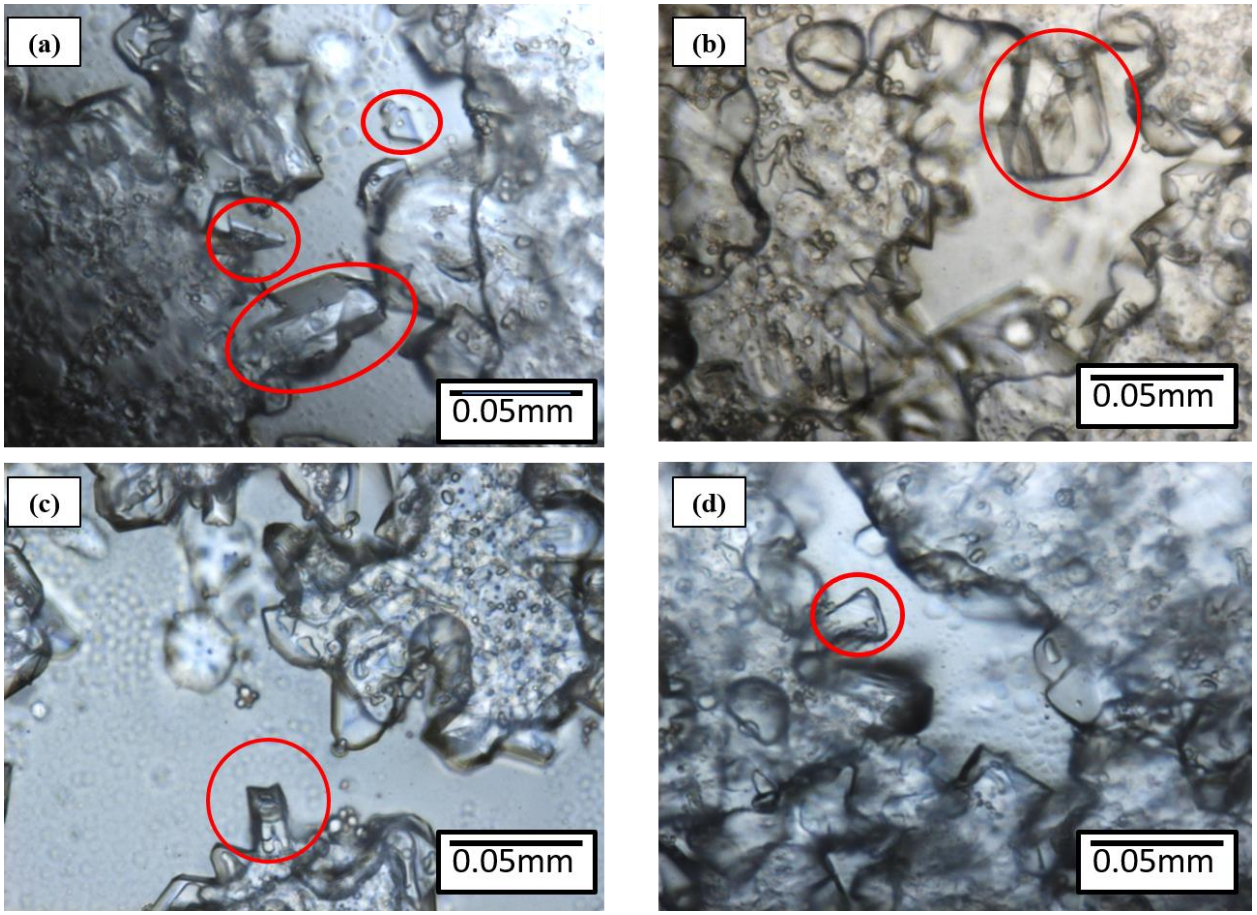

Figure 4.6: Images of hydrate crystals in surfactant stabilized 40 vol. % water emulsion captured at 50x magnification.

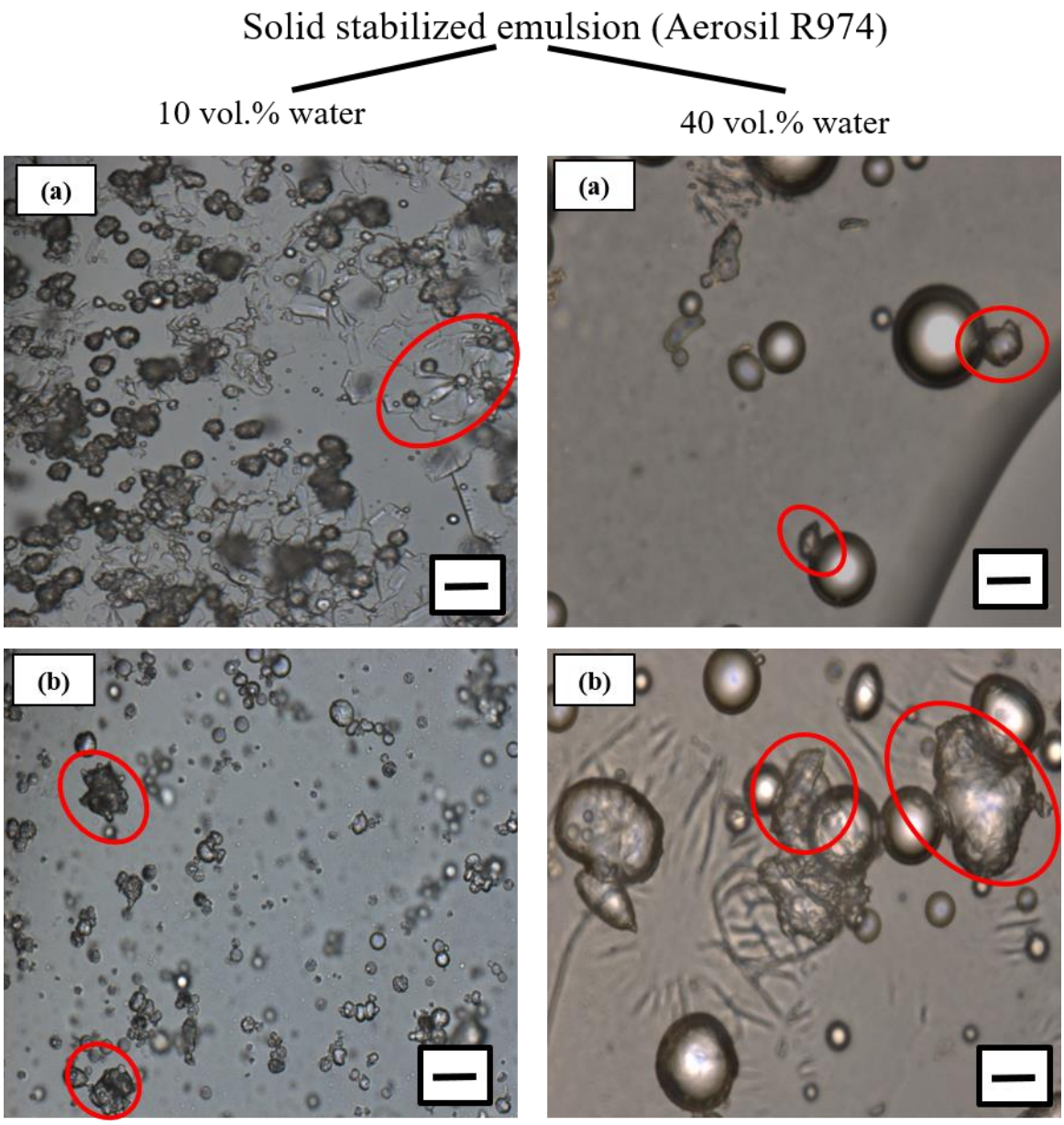

Figure 4.7: Images of hydrate crystals captured in the hydrate formation zone of 0.1°C for Aerosil R974 stabilized 10 and 40 vol. % water concentration.

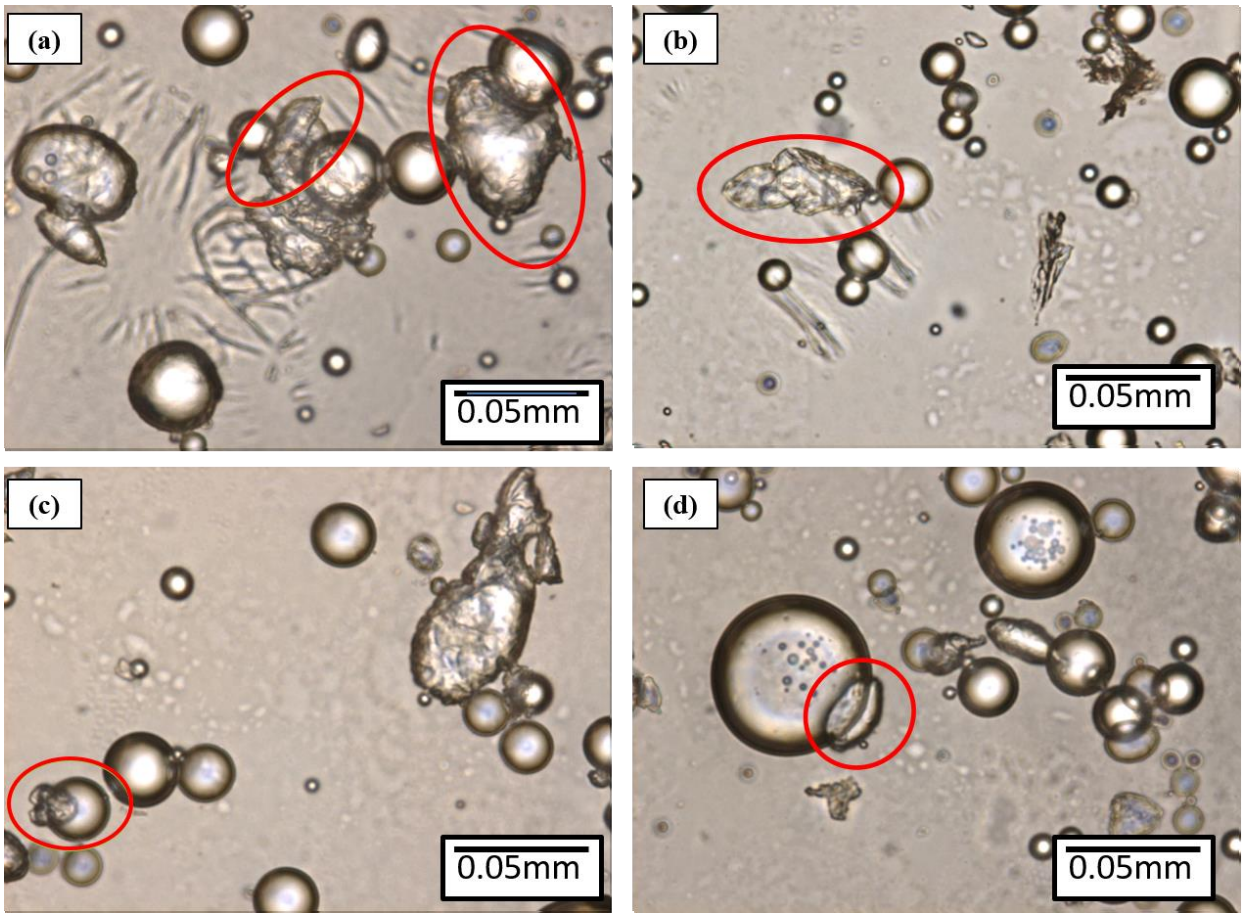

Figure 4.8: Hydrate crystals in Aerosil R974 stabilized 40 vol. % water emulsion. The regions highlighted in red indicate hydrate crystals

In solid-stabilized emulsions, hydrate formation was observed at all water fractions. However, a wide variety of hydrate crystallinity/ irregularity in the crystalline structure was observed (Figure 4.7). Figure 4.8 represents images of the hydrate crystal in Aerosil R974 stabilized 40 vol. % water emulsion. The tip of the crystals were observed to be pointing inward (Figure 4.8). Cha et al conducted a similar experiment on a cyclopentane hydrate slurry system with either span 80 or silica particles in the presence of fixed span 80 concentration [89]. They observed that at low particle concentration (<= 1 wt. %), hydrate morphology was similar to that of a surfactant stabilized system. They

also observed that at high solid concentrations, the rate of hydrate formation and agglomeration was slow.

The irregularity and random growth of hydrate crystals in solid stabilized emulsions could be attributed to the effect of solid particles on the oil-water interfacial tension. Since solid particles have minimal effect on oil-water interfacial tension (Table 4.1), it is hypothesized that during hydrate nucleation, the initial hydrate crystal doesn't experience enough excess surface/Laplace pressure, thereby retarding the compression and lateral overgrowth of conical hydrate crystals into a hairy/ mushy structure. Karanjkar [93] observed that for surfactant free systems, a faceted plate like hydrate structure was observed where the lateral growth of hydrate leads to thin shell formation. The faceted shell formed by joining hydrate facets slows the radial growth of hydrate. At the experimental conditions studied in this paper, solid particles were shown to not significantly reduce the interfacial tension, unlike the surfactant laden system (Table 4.1). The possible reason could be that the solid particles at the interface form a physical barrier around the water droplets which slow down the diffusion of hydrate forming cyclopentane molecules from the oil phase to water droplets.

Table 4.2: Summary of average drop size of emulsions before hydrate formation and after hydrate dissociation.

Emulsion		Mean droplet size (μm) ± Standard deviation	
		Before hydrate formation	Upon hydrate dissociation
Water content (vol. %)	**Stabilizer**		
10	Span 80	14.7 ± 1.8	18.3 ± 2.6
	Aerosil R974	7.7 ± 0.5	8.3 ± 0.8
	Aerosil R816	13.7 ± 7.4	13.1± 3.8
40	Span 80	13.1 ± 4.6	16.2 ± 5.9
	Aerosil R974	24.6 ± 10.6	28.2 ± 9.0
	Aerosil R816	15.4 ± 4.4	15.0 ± 6.7

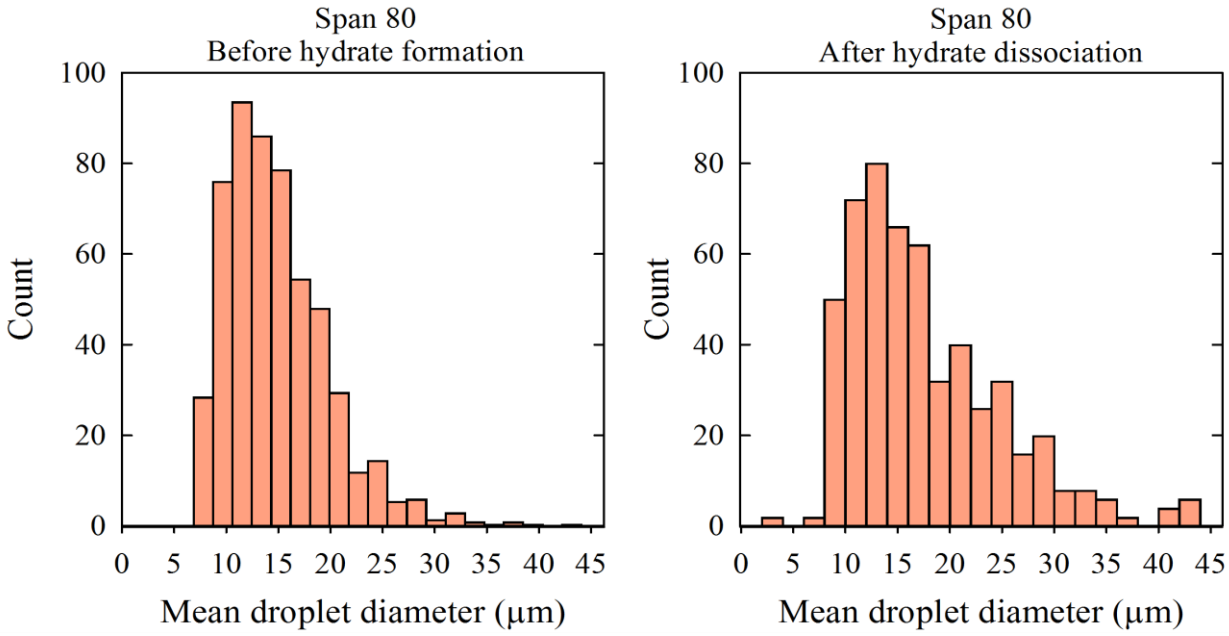

Figure 4.9: Comparison of the emulsion droplet size distribution before hydrate formation and upon hydrate dissociation for 0.1 vol. % Span 80 (surfactant) stabilized 40 vol. % water-in-oil emulsion.

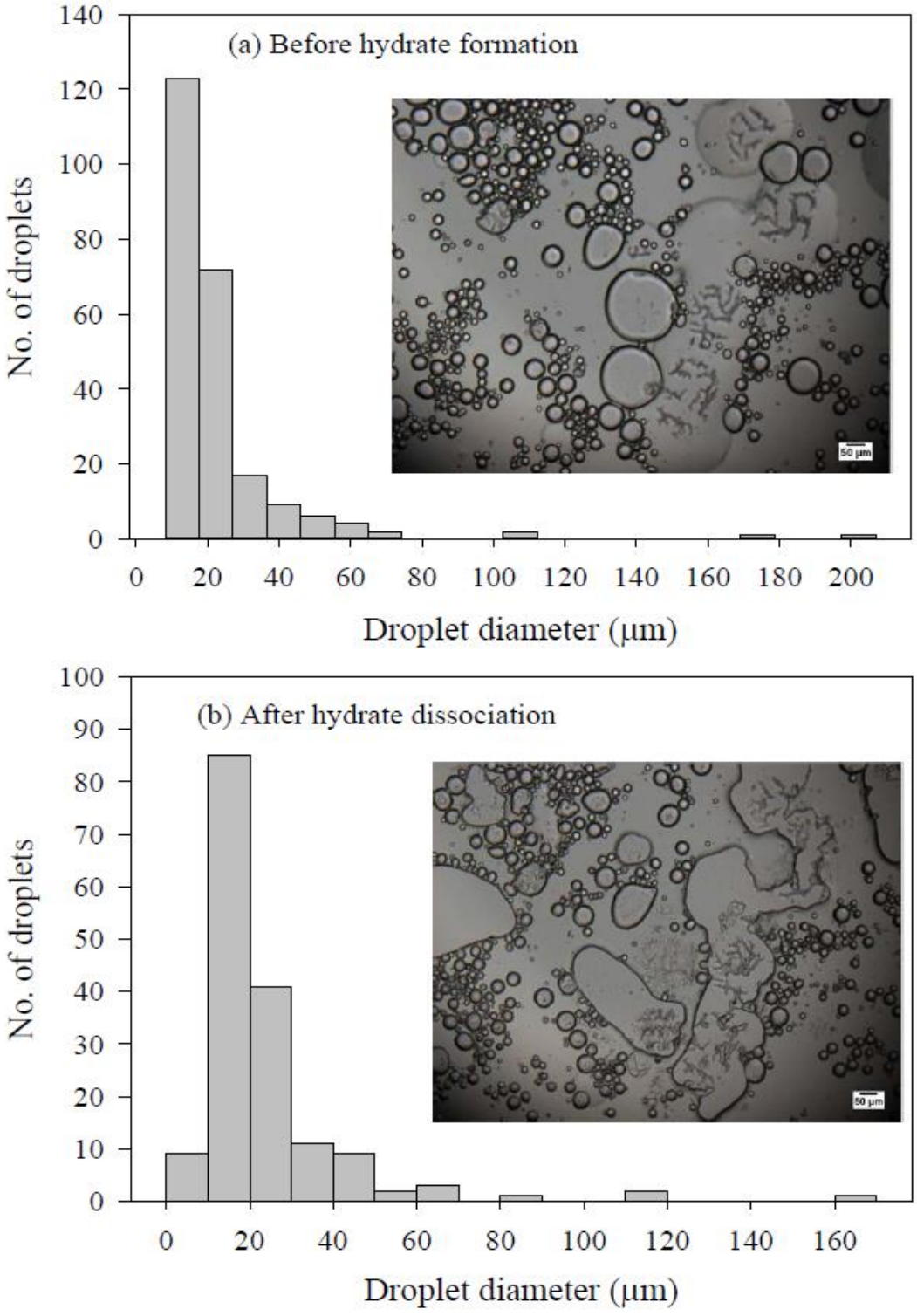

Figure 4.10: Comparison of the emulsion droplet size distribution before hydrate formation and upon hydrate dissociation for 0.1 vol. % Aerosil R974 (solid particle) stabilized 40 vol. % water emulsion. The distribution was obtained by counting the number of droplets from the inset.

Comparing the drop size distribution of the emulsions before and after hydrate formation, as seen in Figures 4.9 and 4.10, it is evident that the emulsion droplet size increases upon hydrate dissociation in surfactant stabilized 40 vol. % water emulsion. Similar observations were seen in surfactant stabilized 10 vol. % water emulsion. These observations were not evident in solid stabilized emulsions. Table 4.2 summarizes the effect of stabilizer type on emulsion mean droplet size before hydrate formation and upon hydrate dissociation. Based on results shown in Table 4.2, upon hydrate dissociation, a significant difference in the mean droplet size was observed in surfactant stabilized emulsions. A significant difference in the mean droplet size was observed in surfactant stabilized emulsions at both 10 and 40 vol. % water concentration. However, this trend was not seen on solid stabilized emulsions.

Emulsion droplet deformation, which is a characteristic feature of surfactant stabilized emulsions, has a critical influence on changes in emulsion droplet size after hydrate dissociation. Changes in the structure of the surfactant layer at the interface occur due to variations in the sample temperature [56, 94]. During hydrate formation, the hydrate particles agglomerate, thereby promoting droplet coalescence upon dissociation. The combined effect of changes in surfactant properties at the interface and flocculation leads to an increase in the mean droplet size. Conversely, solid particles are identified to impart mechanical rigidity to the oil-water interface by forming a network around water droplets and irreversibly adsorbing at the interface [22, 57]. The mechanical rigidity imparted by solid particles at the interface reduces flocculation and hydrate agglomeration. To this end, Venkataramani and Aichele conducted flow loop experiments on surfactant and on solid stabilized emulsions [95]. These experiments identified that for surfactant stabilized

emulsions, flow rate, and temperature has a significant impact on the emulsion droplet size. Solid stabilized emulsions did not exhibit changes in the mean droplet size and distributions with changes in flow rate and temperature.

4.4. Conclusions

Hydrate formation was observed in surfactant and solid stabilized emulsions at both low and high water cuts. Hydrate crystals were observed at the oil-water interface in both surfactant and solid stabilized emulsions. However, a wide variety of crystallinity was present in solid stabilized emulsions. Solid particles were observed to have no effect on the pure oil-water interfacial tension thereby resulting in a lack of excess surface pressure at the oil-water interface that drives the inward growth of conical hydrate crystals. Therefore, irregularities in the hydrate crystal structure are expected in solid stabilized emulsions as supported by visual observations. Mean emulsion droplet size increased upon hydrate dissociation in surfactant stabilized emulsions. A significant difference in the mean droplet size was seen in surfactant stabilized emulsions at both water fractions (10 and 40 vol. %). Future work will focus on the impact of particle wettability and particle loading on hydrate formation in emulsions.

CHAPTER V

SINGLE WATER DROP HYDRATE FORMATION IN WAXY OIL SYSTEMS

5.1.Introduction

Waxes are long chain, high molecular weight carbon compounds present in crude oil [51]. Visintin et al hypothesized that paraffin molecules stabilize emulsions by adsorbing at the oil-water interface, forming Pickering emulsions[96]. The authors predicted that paraffin crystals which precipitate at temperatures below the wax appearance temperature (WAT), adsorb on the droplet surface, cover it, and stabilize the emulsion forming floc-like network with dispersed water droplets entrapped in the wax crystal network [96]. Bilyeu et al studied the mechanisms involved in treating a subsea bare flow line that was plugged with hydrates and waxes[97]. Bilyeu observed that it was easier to eliminate hydrates in a pipeline that is plugged with hydrates and waxes simultaneously. Waxes were difficult to eliminate due to hard gel-like network that remained in the flow line. Two sided depressurization and micro annular pressure pulse method were utilized to remove hydrates and waxes respectively. Though techniques are available to remove hydrates and wax plugs simultaneously, there is still no literature or experimental data available on hydrate formation mechanism in waxy oil systems.

Although considerable research has been conducted on emulsions, hydrates, and wax independently, there is a void left in understanding the fluid properties when these systems occur simultaneously. Multiphase flow systems with hydrates, wax, and emulsions are commonly found in the field. There is a lack of understanding of the relationship between emulsions and other types of dispersions, such as hydrates, wax, and hydrate formation in waxy oil systems under flowing conditions [98]. This has provided an impetus to conduct experimental investigations of crude oil emulsions under flowing conditions that can lead to improved understanding of the water – oil multiphase flow phenomenon, thereby paving a way to develop economically feasible flow assurance remediation strategies.

5.2. Materials and Methods

5.2.1. Materials

The objective of this work was to investigate the hydrate formation mechanism in waxy oil systems. For this purpose, a model waxy oil continuous phase was prepared using model oil (such as light mineral oil), cyclopentane, and paraffin wax. The experimental work conducted for this study was classified into two categories: first, in the absence of surfactant in the oil continuous phase, and second, containing a surfactant in the oil phase. For all the studies discussed in this work, an oil continuous phase was prepared using 3:1 ratio of cyclopentane and mineral oil-wax mixture on a weight basis.

Light Mineral Oil with a density equal to 0.838 g/cc (at 25 °C), viscosity of 14.2 cP (at 40 °C) was purchased from Sigma-Aldrich. Paraffin wax (purchased from Sigma-

Aldrich) with a melting point of 58-62 °C and viscosity of 3-6 cP at 100 °C was used in the oil phase. The composition of the wax used in this study was determined by Gas Chromatography (GC) analysis and is provided in Table 5.1. The data presented in Table 5.1 was obtained from Parthasarthi [99]

Table 5.1: Composition of wax obtained from Gas Chromatography analysis [99]

Component	**Composition (Mass %)**
nC_{20}	0.05
nC_{21}	0.29
nC_{22}	1.07
nC_{23}	2.87
nC_{24}	5.09
nC_{25}	8.16
nC_{26}	13.42
nC_{27}	14.47
nC_{28}	12.45
nC_{29}	12.22
nC_{30}	10.7
nC_{31}	8.05
nC_{32}	6.01
nC_{33}	2.17
nC_{34}	1.38
nC_{35}	0.53
nC_{36}	0.41
nC_{37}	0.21
nC_{38}	0.19
nC_{39}	0.11
nC_{40}	0.15

As discussed earlier in chapter I, since cyclopentane forms structure II hydrates at nearly atmospheric conditions, it was considered as an appropriate hydrate-forming guest

molecule for this work. Cyclopentane (purchased from Alfa Aeaser) with a purity of 95%, density equal to 0.75 g/cm^3 was used as a hydrate-forming guest molecule. For this work, two different wax concentrations: 1.25 wt.% (low wax content) and 5 wt.% (high wax content) were used to evaluate the effect of wax concentration on hydrate formation. The oil phase consisted of 75 wt. % cyclopentane, either 1.25 or 5 wt.% wax and the remaining was light mineral oil. The oil phase was prepared in small batches of 25g. Every data point shown in this work was repeated at-least three times using the same batch of sample. A high concentration of cyclopentane (75 wt.%) was used in the oil phase, although the stoichiometric ratio required for 1 mol of structure II/ cyclopentane hydrates is only 17 mol of water. A high concentration of cyclopentane was used to ensure that hydrate formation would occur in the presence of wax in the oil phase and therefore would not become a limiting factor.

For the surfactant-free 1.25 wt.% wax system, the oil phase was prepared by first heating 23.75 wt.% of light mineral oil and 1.25 wt.% wax mixture to 100 °C on a stir/ hot plate in a glass beaker covered with parafilm for 24 hours. This step was done to ensure complete dissolution of wax nanocrystals and erase any wax crystallization history. After 24 hours of heating, the temperature of the oil-wax mixture was reduced to 45 °C prior to adding cyclopentane to the oil-wax mixture. The oil-wax mixture was cooled to 45 °C, as the boiling point of cyclopentane is 49-50 °C (from MSDS). During the entire process, the sample was stirred using a 1” long stir bar on a stir/hot plate at 600 rpm. Similarly, 5 wt.% wax in mineral oil-cyclopentane mixture was prepared by heating 20 wt.% mineral oil and 5 wt.% wax mixture to 100 C for 24 hours. 75 wt.% of cyclopentane was added after cooling the sample to 45 °C.

For the surfactant-free case, two different kinds of control sample were prepared: one containing only cyclopentane as the oil phase, and the second containing 75 wt.% cyclopentane and 25 wt.% mineral oil. Deionized water with a resistivity of 18.1 MΩcm was used as the aqueous phase.

In order to correlate the experimental work discussed in this thesis to real world systems, a model waxy oil system was prepared in the presence of a stabilizing agent such as a surfactant. A stabilizer, such as a non-ionic surfactant (span 80), was added to the oil phase to evaluate the effect of hydrate formation in waxy oil systems in the presence of an emulsifier. The oil phase preparation for the surfactant laden system was identical to the surfactant-free case except that after the addition of cyclopentane to the mineral oil-wax mixture, 0.1 wt.% span 80 was added the oil phase. The mineral oil composition was either 23.65 wt.% or 19.9 wt.% depending on the wax concentration. However, cyclopentane concentration was kept constant at 75 wt.% of the oil phase, and cyclopentane to mineral oil-wax mixture composition was kept constant at 3:1 ratio on a weight basis. Surfactant-containing 1.25 wt.% wax system was composed of 75 wt.% cyclopentane, 1.25 wt.% wax, 23.65 wt.% mineral oil, and 0.1 wt.% span 80. The control sample for the surfactant containing system was prepared with 0.1 wt.% span 80, 24.9 wt.% mineral oil and 75 wt.% cyclopentane to evaluate the effect of wax on hydrate formation in the presence of an emulsifier.

5.2.2. Visual/ Microscopy Method

Single water drop hydrate formation experiments were conducted using a temperature/ shear controlled microscope stage to evaluate the effect of wax concentration

and heating/ cooling rate on hydrate formation in waxy oil systems. For this work, an Olympus BX53 polarized optical microscope (equipped with a Linkam CSS 450 temperature controlled shear stage) and a high-speed camera was used for visualization. The microscope is equipped with a Peltier stage that could operate in the temperature range of -45 °C to 450 °C and at a maximum shear rate of 10 rad/s. For this study, the samples under visualization were not subjected to shear throughout the course of the experiment. The temperature controlled stage consisted of a circular well mounted on a quartz window with a sample diameter of 30 mm and viewing diameter of 2.8 mm as shown in Figure 5.1. The stage was previously set to 25 °C before loading the sample. For single water drop hydrate experiments, approximately 100-150 µm diameter water drop (< 2 µL) was placed on the bottom stage of the shear/ temperature controlled microscope as shown in Figure 5.1. The sample cell was then filled with the oil continuous phase. The bottom stage was immediately covered with the lid of the temperature control stage as shown in Figure 5.1 to avoid vaporization of cyclopentane. The stage was then connected to a liquid nitrogen pump for operating at lower temperatures.

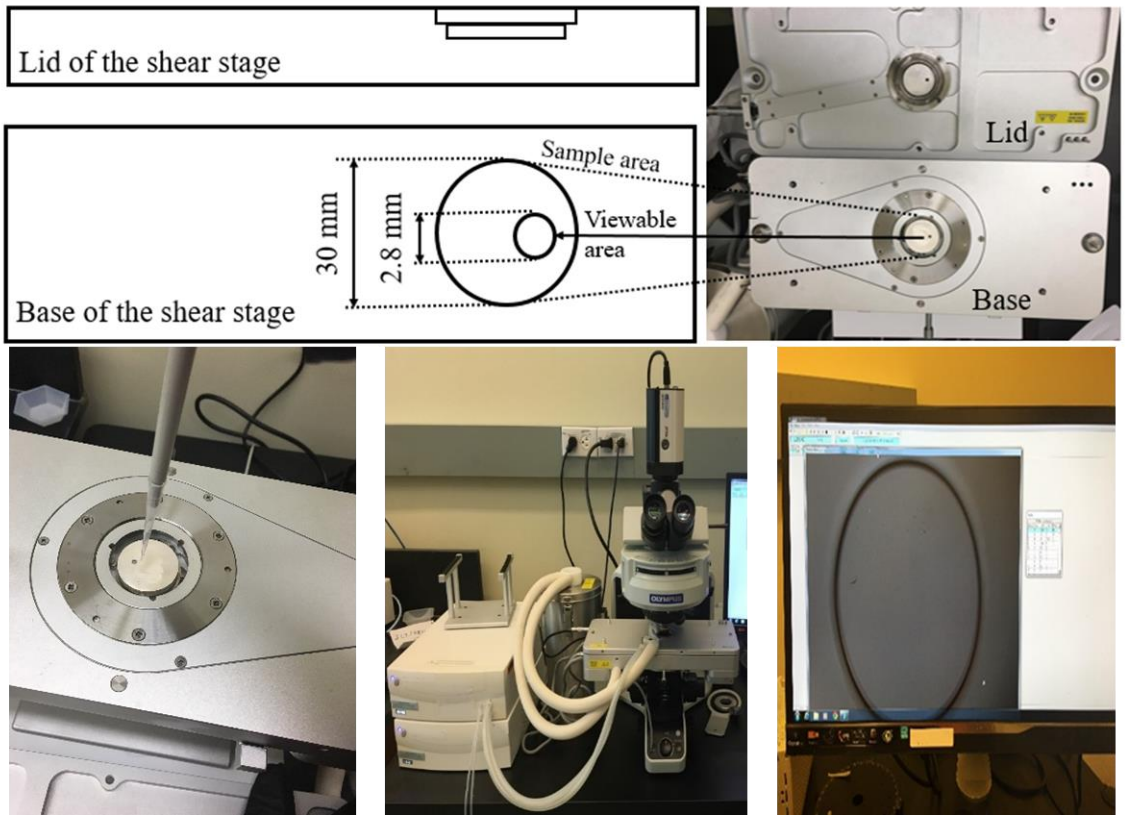

Figure 5.1: Schematic of temperature controlled and shear stage optical microscope equipped with cross polarizing lens

The temperature profile used for this study is given below:

- After loading the sample to the microscope stage that was previously set to 25 °C, the sample temperature was lowered to -25 °C at 2 °C/min rate to quench the water droplet to form ice. Quenching of water droplets to form ice was identified to reduce the stochastic hydrate induction time.

- The sample was held at -25 °C for 5 min until a visually complete conversion of the water droplet to ice was observed.

- The sample was then heated to -0.5 °C at 2 °C/min rate to melt ice into liquid water. Ice melting was observed to begin when the sample temperature was around -1.5 °C to -1.0 °C, and was completed by the time the sample temperature reached -0.5 °C. Hence, the sample was held at -0.5 °C for 5 min to ensure complete melting of ice into liquid water. The free liquid water available upon ice melting was identified to initiate hydrate nucleation by overcoming the long hydrate induction time that is otherwise associated with cyclopentane hydrate formation. Along with ice melting, hydrate nucleation and hydrate crystal growth were observed to occur simultaneously at the interface. However, hydrate crystals were easily distinguishable from ice, as these crystals were observed to form initially at the interface and subsequently grow inward.

- The sample temperature was increased to 0.1 °C at 2 °C/min rate and held at this temperature for a minimum of 30 minutes or longer until visually complete conversion of the water droplet to hydrates was observed. If complete conversion was not observed by the end of 30 minutes, the hold time was increased by another 30 minutes. This step was repeated until visually the entire water droplet was converted to hydrates and no further changes to the sample was observed through visualization. For this work, hydrate conversion time was calculated as the time taken at which the sample temperature reaches -0.5 °C to the time taken for the water droplet to completely convert into hydrates by means of visual observation (at 0.1 °C).

- After visually complete conversion was observed, the sample was heated back to 25 °C at 2 °C/min rate and held at this temperature for 5 min to evaluate changes in the hydrate-wax system upon hydrate dissociation.

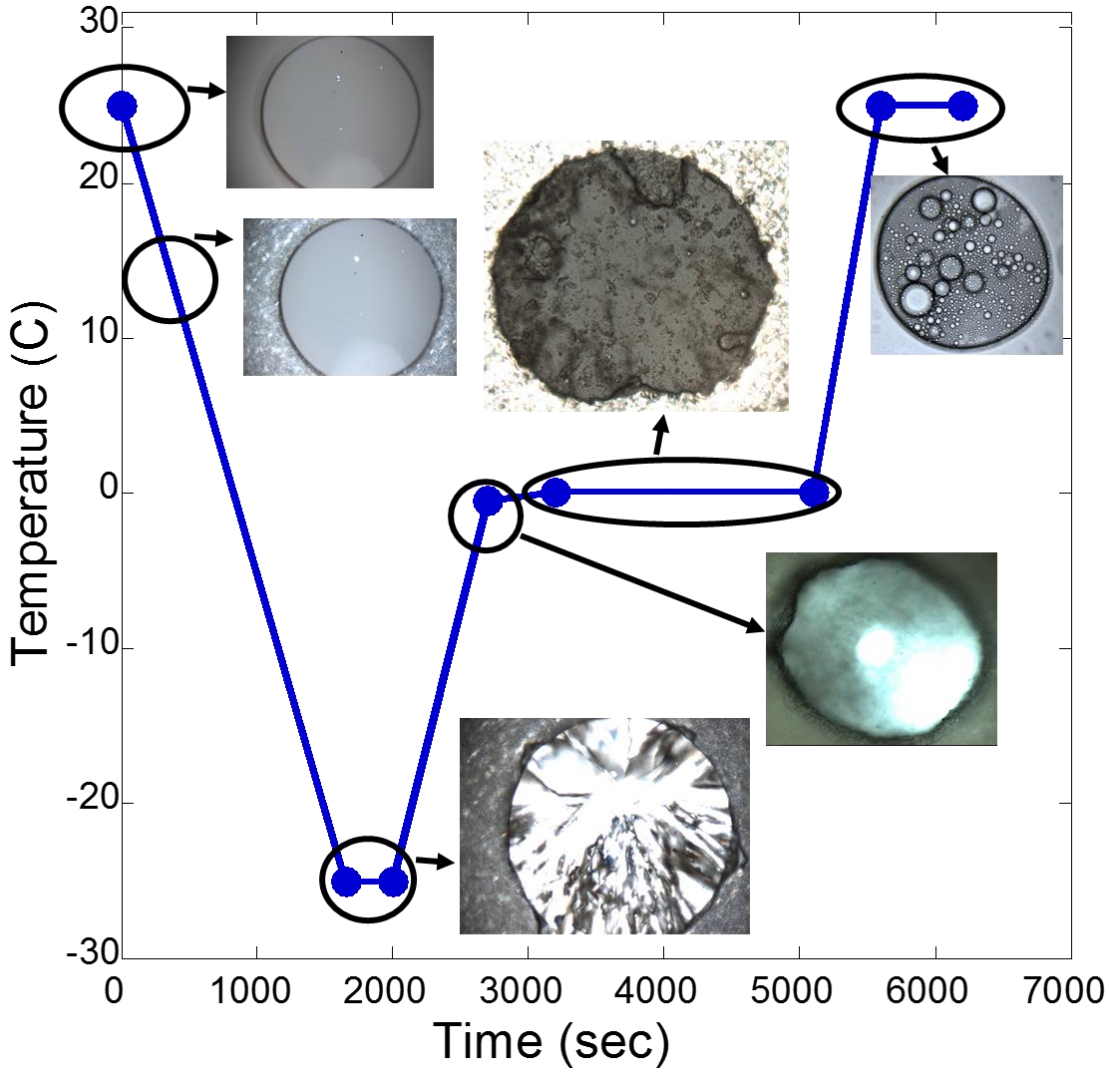

Figure 5.2: Temperature profile used for hydrate formation in waxy oil systems. The figure illustrates physical changes to the sample captured at different operating conditions

Figures 5.2 and 5.3 illustrates the temperature profile used for this work and the physical changes to the sample captured using the visualization technique. Throughout

the course of the experiment, the heating and cooling rate was kept constant. The above experimental procedure was repeated at 1 °C/min and 0.5 °C/min rates to evaluate the effect of heating and cooling rate on hydrate formation in waxy oil systems. This experiment was conducted to interrogate the effect of wax growth rate and crystal size on hydrate formation, and to validate the hypothesis that in waxy oil systems, slower cooling rate delays hydrate formation and hence, delays complete conversion.

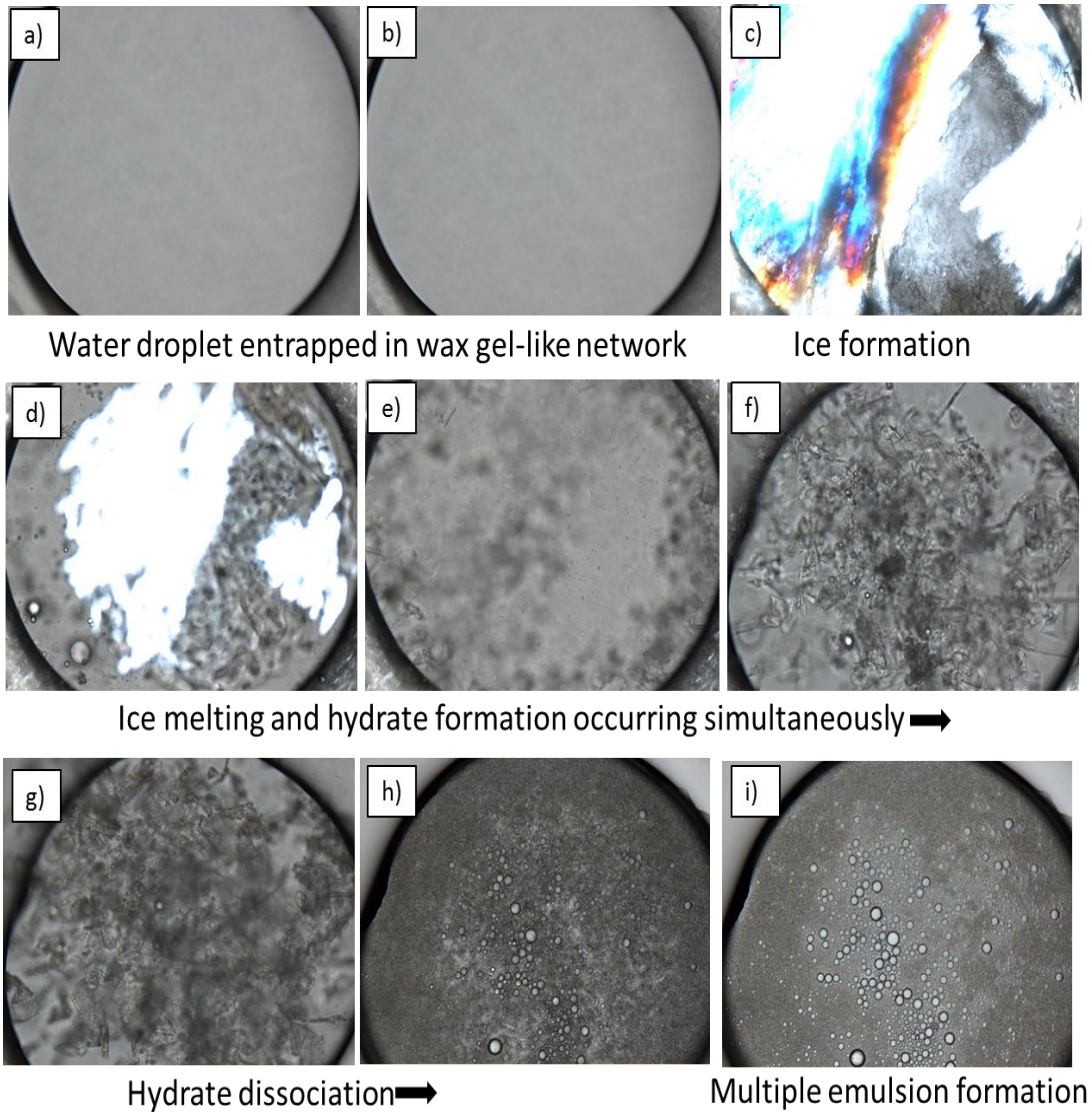

Figure 5.3: Images captured (10x magnification) at various temperatures during hydrate characterization in waxy oil system containing 1.25 wt.% wax in the mineral oil-

cyclopentane mixture. The experiment was conducted at heating and cooling rate of 2 °C/min.

The previously described experimental procedure was repeated even for surfactant containing oil phase where the wax concentration and heating/ cooling rates were varied to evaluate their effect on hydrate formation. For all the control samples used in this study, the heating and cooling rate were kept constant at 2 °C/min as the control samples did not contain any wax. Moreover, it was observed through this work, as well as several others, that heating or cooling rate didn't have a significant effect on hydrate formation or hydrate conversion time in systems containing either pure cyclopentane or cyclopentane-oil mixture [44]. However, in affected systems containing wax, the wax appearance temperature (WAT) was found to be dependent on the cooling rate. The hydrate formation experimental procedure was also repeated without quenching the water droplet to form ice. The sample was held at 0.1 °C instead of quenching to -25 °C for several hours (6 hours). No hydrate formation was observed, thereby validating the long induction time associated with cyclopentane hydrates.

5.3. Results and Discussion

5.3.1. Effect of cooling rate, wax concentration, oil phase composition on wax appearance temperature (WAT)

Wax appearance temperature (WAT), also known as cloud point, is the highest temperature below which wax crystals are precipitated. It is also known as the temperature at which visible crystallization of wax occurs. WAT depends on the concentration of wax, crude oil properties, and the molecular weight of the waxes. Measuring WAT is critical

due to its ability to cause deferred production. In addition to this, WAT acts like a guideline for the operators above which the flow lines need to be operated for easy transportation of fluids. For this study, the WAT of wax-mineral oil, wax-mineral oil-cyclopentane, and wax-mineral oil-cyclopentane-span 80 systems were measured at two wax concentrations (1.25 wt.%, and 5 wt.%) and three different cooling rates (0.5, 1, and 2 °C/min). WAT measurements were conducted on six different continuous phases: 1.25 wt.% wax in mineral oil, 1.25 wt.% wax in 23.75 wt.% mineral oil-75 wt.% cyclopentane, 1.25 wt.% wax in 23.65 wt.% mineral oil-0.1 wt.% span 80-75 wt.% cyclopentane, 5 wt.% wax in mineral oil, 5 wt.% wax in 20 wt.% mineral oil-75 wt.% cyclopentane, 5 wt.% wax in 19.9 wt.% mineral oil-0.1 wt.% span 80-75 wt.% cyclopentane. 1 mL of the sample was placed in the sample chamber and WAT was measured by cooling the sample from 40 °C to 1 °C. The microscope stage was preheated to 40 °C prior to loading the sample and was held at this temperature for at-least 10 min and sheared at 0.1 rad/s prior to cooling the sample to ensure dissolution of wax crystals. However, the sample was not sheared during the course of the experiment and shearing of the sample was observed to have no overall effect on either the WAT or wax crystal size. The oil phase was heated no higher than 40 °C, as the boiling point of cyclopentane is 45-50 °C. This step also ensured that the sample was above the cloud point, and erased any wax history due to nano-wax crystals.

The WAT of the system containing 5 wt.% wax in pure mineral oil was higher than WAT of 1.25 wt.% wax system at all three cooling rates (Table 5.2). As expected, 5 wt.% wax-mineral oil system exhibited higher WAT when compared to 1.25 wt.% wax system due to a high concentration of wax in the system (5 wt.% wax system contains four times higher wax concentration than 1.25 wt.% wax system). Several studies have

established that wax concentration has a direct influence on the WAT, and WAT increases with an increase in wax concentration using solid-liquid equilibrium [100, 101]. The amount of wax available in the 5 wt.% system was four times the concentration in the 1.25 wt.% system and hence, the density of nanometer-sized wax crystals is higher in the 5 wt.% wax system. In these systems, as temperature decreases, greater precipitation and therefore faster aggregation of nanometer-sized wax crystals occurs at a comparatively higher temperature, resulting in higher WAT. Table 5.2 illustrates a difference of at-least 10° C in WAT between the 5 wt.% wax and 1.25 wt.% wax systems in pure mineral oil at all cooling rates, thereby demonstrating the influencing of wax concentration on WAT.

Table 5.2: Wax appearance temperature (WAT) of the oil phase containing either 1.25 wt.% or 5 wt.% wax at different cooling rates using cross-polarized microscopy

Sample	**Cooling Rate (C/min)**		
	0.5	**1**	**2**
1.25wt.% Wax+Mineral Oil	15.6	14.8	13
1.25wt.%Wax+23.75wt.% Mineral Oil+75wt.% Cyclopentane	14.6	13.8	13.5
1.25wt.% Wax+0.1wt.% Span 80+23.75wt.% Mineral Oil+ 75wt.% Cyclopentane	14.2	13.6	13.3
5wt.% Wax+Mineral Oil	26.8	25.5	23.9
5wt.% Wax+20wt.% Mineral Oil+ 75wt.% Cyclopentane	18.4	17.8	17.5
5wt.% Wax+0.1wt.% Span 80+20wt.% Mineral Oil+75 wt.% Cyclopentane	17.5	17.5	17.2

Table 5.2 indicates that the WAT was observed to be higher at a slower cooling rate and lower at a faster cooling rate. Since WAT is a kinetic process, cooling rate is

determined to have a strong influence on the WAT. At slower cooling rates, due to prolonged time for wax crystallization and aggregation, the WAT appears at much higher temperatures when compared to faster cooling rates. Prolonged aggregation time causes wax molecules to acquire a more ordered arrangement and increases the ability of wax crystals to align or fit together with adjacent crystals, thereby promoting nucleation and aggregation/ growth of wax crystals [102, 103]. Similarly, the length of the wax crystals appeared to be longer in slower cooling rates and smaller in faster cooling rates, as seen in Figure 5.3. Figure 5.3 illustrates the length of the wax crystals captured at 5 °C at three different cooling rates in wax-mineral oil mixture. The wax crystals appeared to be longer at slower cooling rates due to prolonged nucleation time. At slower cooling rates, prolonged nucleation time allows the precipitated nano wax crystals to act as a nucleation site for further crystal growth due to attractive forces between the wax crystals [102]. Hence a slower cooling rate promotes longer wax crystals and higher crystal growth rate. The average length of the wax crystals at 0.5 °C /min, 1 °C /min, and 2 °C/min rate were 50, 30, and 25 µm respectively.

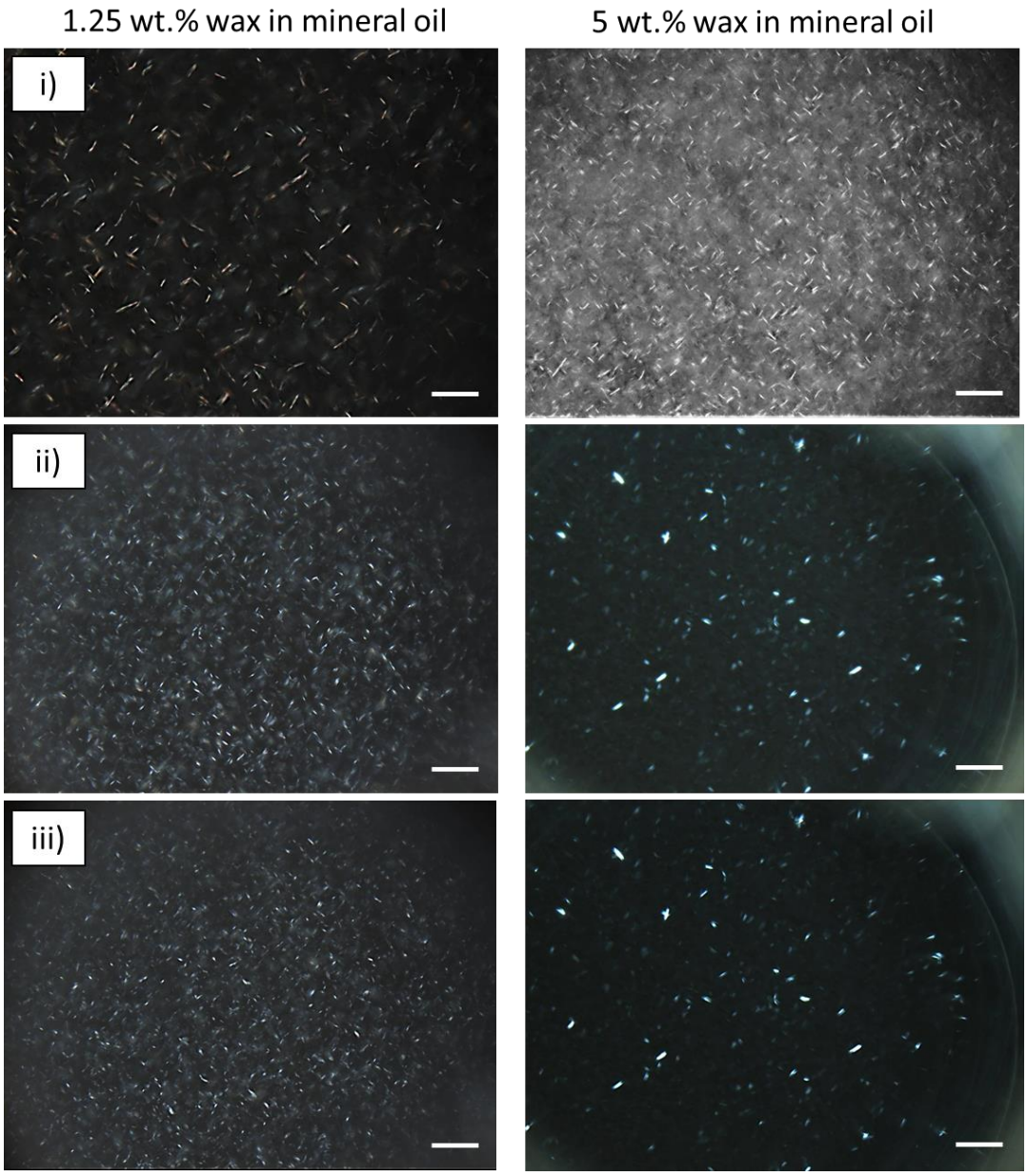

Figure 5.4: Wax crystal morphology of 1.25 wt.% wax and 5 wt.% wax in mineral oil system captured using cross-polarized optical microscope at 5 °C at three different cooling rates i) 0.5 °C/min ii) 1 °C/min iii) 2 °C/min. The scale bar indicates 100 µm.

WAT was also measured for the oil phase containing mineral oil-wax-cyclopentane mixture at different cooling rates. As seen in Table 5.2, the addition of

cyclopentane to the oil phase was observed to lower the WAT (when compared to the pure mineral oil-wax system) by 1 °C in 1.25 wt.% wax system, and by 7-8 °C in 5 wt.% wax system at all cooling rates. Since the wax molecule primarily consists of long chain hydrocarbon molecules (n-paraffin's), the presence of cyclic compounds and any associated side branches is known to build into the wax crystals, thereby solubilizing some of the hydrocarbon chains in the wax molecules and lowering the WAT. The presence of cyclopentane in the waxy oil phase showed efficiency in reducing the WAT and presented a synergistic effect with a wax inhibitor (primary role of a wax inhibitor is to cause depression of WAT thereby delaying wax precipitation and plugging). Several studies have also shown that high concentrations of cyclic compounds introduce significant structural disorientation by solubilizing some of the carbon chains in the wax structure and lowering the cloud point [55, 104, 105]. As seen in this work, the addition of cyclopentane was observed to delay the aggregation of wax crystals, thereby resulting in smaller wax crystals and lower WAT irrespective of the cooling rate and wax concentration. Similar observations were seen in other studies in which the presence of asphaltene and other aromatic compounds had a strong impact on the WAT and crystal size [106]. The addition of a stabilizing agent such as a surfactant (Span 80) to the wax-oil-cyclopentane mixture was observed to have minimal impact on WAT when compared to WAT of wax-oil-cyclopentane mixture at all cooling rates and wax concentrations except for 0.5 °C/min (Table 5.2). At the slowest rate, the WAT appeared to be lowered by 1 °C in the presence of a surfactant. Similar observations on the wax crystal size were seen in the oil-wax-cyclopentane mixture when compared to the wax-mineral oil mixture.

However, no noticeable difference in the wax crystal size was seen in the presence of a surfactant to the wax-oil-cyclopentane mixture.

5.3.2. Effect of wax concentration and cooling rates on hydrate formation

5.3.2.1 Surfactant-free case

Single water drop hydrate formation experiments were conducted in an oil phase containing no surfactant. For this study, hydrate formation experiments were carried out in the oil phase containing: 1.25 wt.% wax- 23.75 wt.% oil- 75 wt.% cyclopentane, and 5 wt.% wax- 20 wt.% oil-75 wt.% cyclopentane. Along with these systems, control experiments were conducted in pure cyclopentane and 25 wt.% oil-75 wt.% cyclopentane mixture to evaluate the effect of wax and the oil continuous phase on hydrate formation. All the control sample experiments were conducted at a constant heating and cooling rate of 2 °C/min. Figure 5.5 illustrates hydrate formation in a pure cyclopentane – water system. Hydrate formation was observed to occur simultaneously upon ice melting and instantaneously on the availability of free liquid water. Figure 5.5 represents the hydrate morphology and changes occurring at the oil-water interface and the interior of the water droplet at different time intervals. The three step hydrate formation mechanism [a) hydrate nucleation b) lateral growth c) radial growth] was observed along with the time required for complete conversion of water droplet to hydrates through visual observation. For this work, what is considered as complete conversion is based on visual observation from two-dimensional image. No quantification in terms of percent mass converted to hydrates was conducted, and therefore it can't be qualitatively confirmed whether complete conversion

was achieved in a three dimensional aspect. In the presence of pure cyclopentane, the time required for complete conversion was approximately 27 minutes.

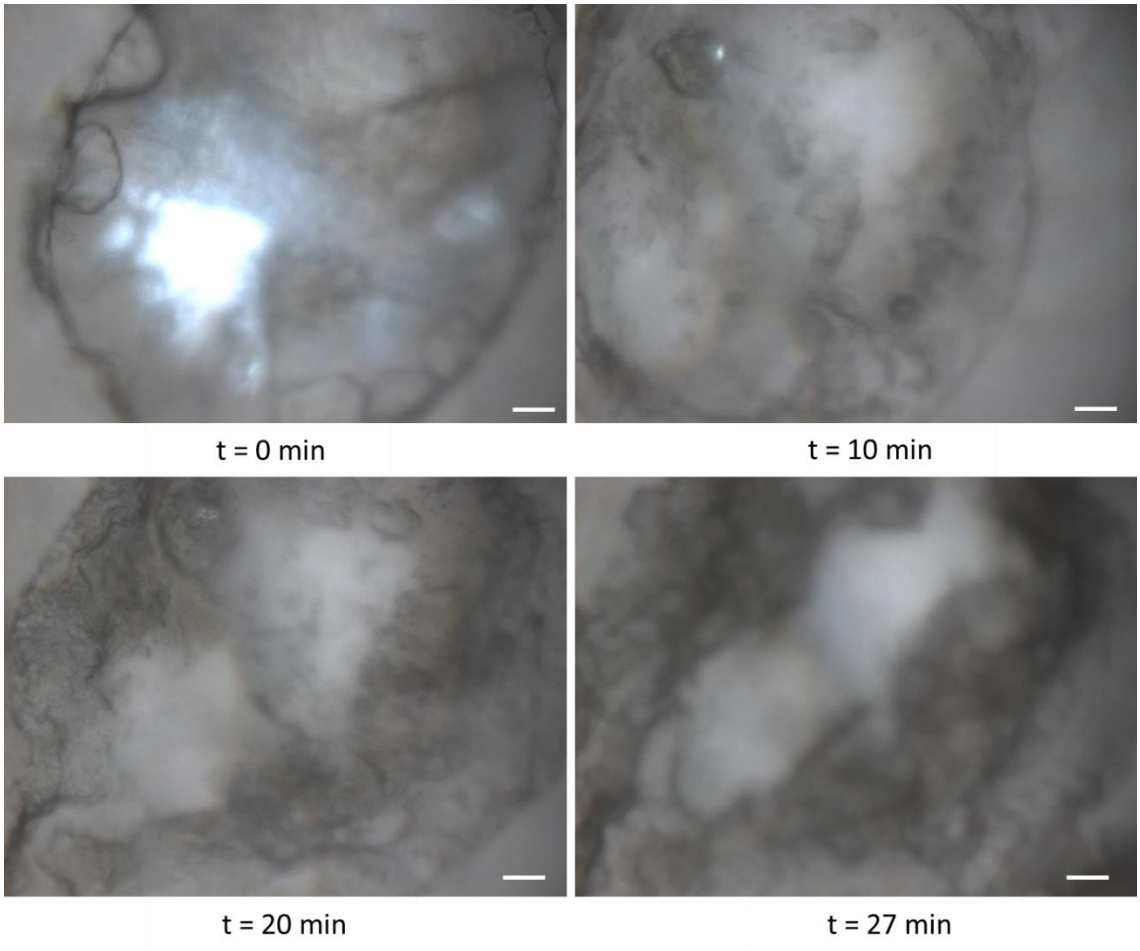

Figure 5.5: Single water drop hydrate formation in control sample containing pure cyclopentane. The scale bar represents 100 µm.

A similar experiment was conducted on the control sample with oil phase composition consisting of 25 wt.% mineral oil and 75 wt.% cyclopentane. Figure 5.6 represents the morphological changes occurring during hydrate formation and the time required for complete conversion. For mineral oil- cyclopentane mixture, the time required for hydrate conversion was 33% more than the time required in pure

cyclopentane oil phase. The three step hydrate formation mechanism was predominantly seen in these systems. Figure 5.6 illustrates the changes occurring at the oil-water interface, progression from hydrate nucleation to lateral hydrate growth, and subsequent radial growth. The time required for complete conversion was observed to increase with decrease in cyclopentane concentration. A similar study was conducted by Karanjkar in which he observed an increase in the time required for hydrate shell formation with decrease in cyclopentane concentration due to reduced sub-cooling [44]. Along with radial growth, an outward growth of hydrate crystals was observed to occur, as shown in Figure 5.6. However, the tip of the hydrate crystals was observed to be pointing inward toward the water droplet. Lateral growth of hydrate crystals occurred randomly anywhere at the interface and subsequently into the water droplet. As seen in Figure 5.6, hydrate crystals formed at the interface were observed to submerge into the water droplet and migrate inward as radial growth continued. The occurrence of radial growth of hydrate crystals was not limited to one particular point on the surface, but was in multiple locations, and even simultaneously on the water droplet surface. The initial water droplet size before and after hydrate formation was not significantly different (Figure 5.7). However, after hydrate dissociation, multiple emulsions were formed in both the control samples. The type of multiple emulsions formed in this case could be of oil-in-water-in-oil type with the cyclopentane or oil-cyclopentane mixture being the dispersed phase in the water droplet (Figure 5.7).

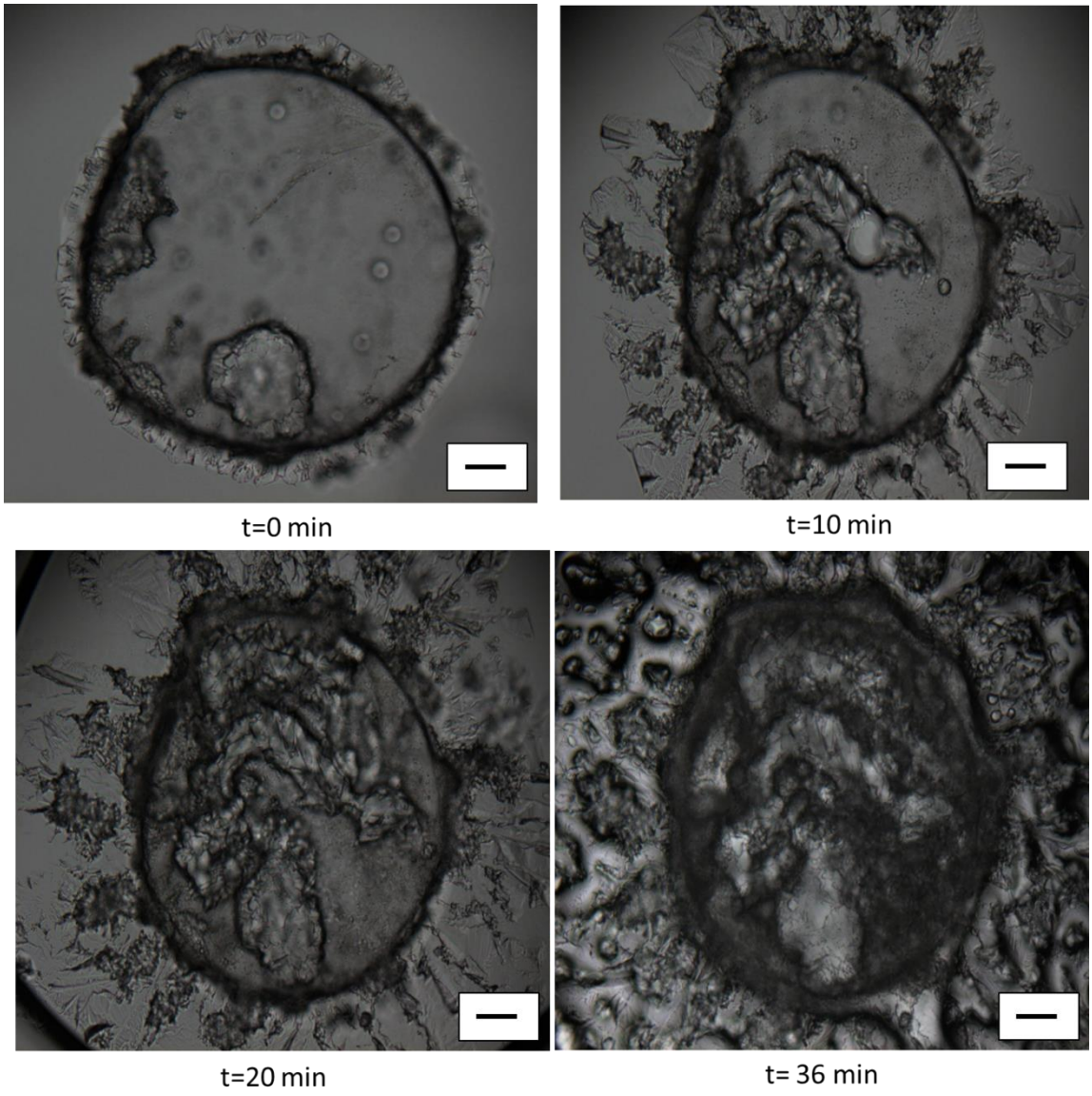

Figure 5.6: Images of control sample containing 25 wt.% mineral oil and 75 wt.% cyclopentane. The scale bar represents 100 µm.

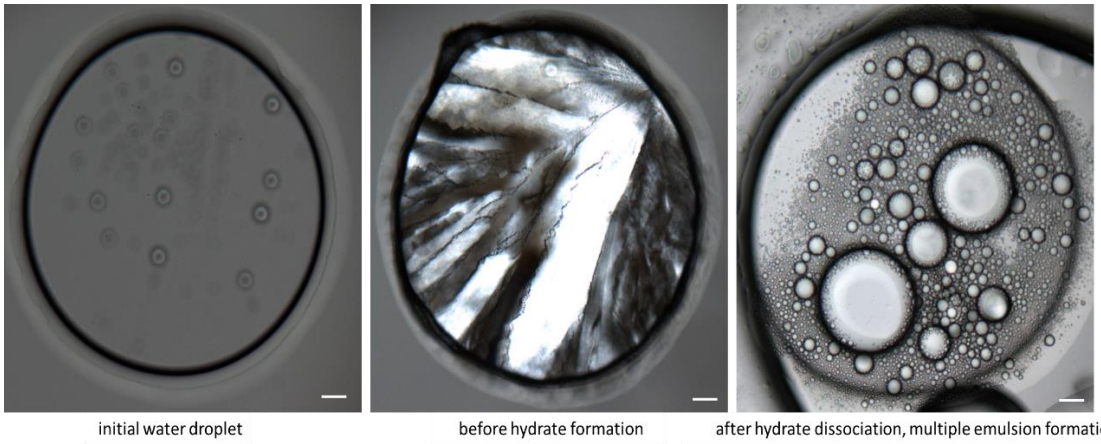

Figure 5.7: Initial emulsion droplet size, droplet size before and after hydrate formation, multiple emulsion formation upon hydrate dissociation. The scale bar represents 100 µm.

The effect of wax on hydrate formation is shown in Figure 5.8. Figure 5.8 represents hydrate formation in 1.25 wt.% wax system at constant heating and cooling rate of 2 °C/min. The hydrate formation mechanism in a waxy oil system was found to be identical to hydrate formation in a pure cyclopentane or oil-cyclopentane mixture, except that in waxy oil systems, wax precipitation and formation of a gel-like network around the water droplet occurs prior to hydrate formation. During the cooling cycle, wax precipitates out of the solution and remains suspended in the oil. With further decrease in the temperature, the precipitated wax crystals were observed to aggregate to form an ordered arrangement of wax crystals forming a gel-like network. The gel-like network was observed to entrap the water molecule and act as a barrier for cyclopentane to diffuse into the water molecule. As seen in Figure 5.8, hydrate nucleation was observed to occur simultaneously along with ice melting. However, the wax crystals around the water droplet were identified to delay the time required for complete hydrate conversion. As indicated in Figure 5.8, the time required for complete conversion was approximately 52 minutes. The time required for complete conversion in 1.25 wt.% wax system at 2 °C/min

cooling rate was observed to be 92.6%, and 31% more than the time required for hydrate formation in pure cyclopentane, and mineral oil-cyclopentane mixture respectively (Figures 5.5, 5.6, and 5.8).

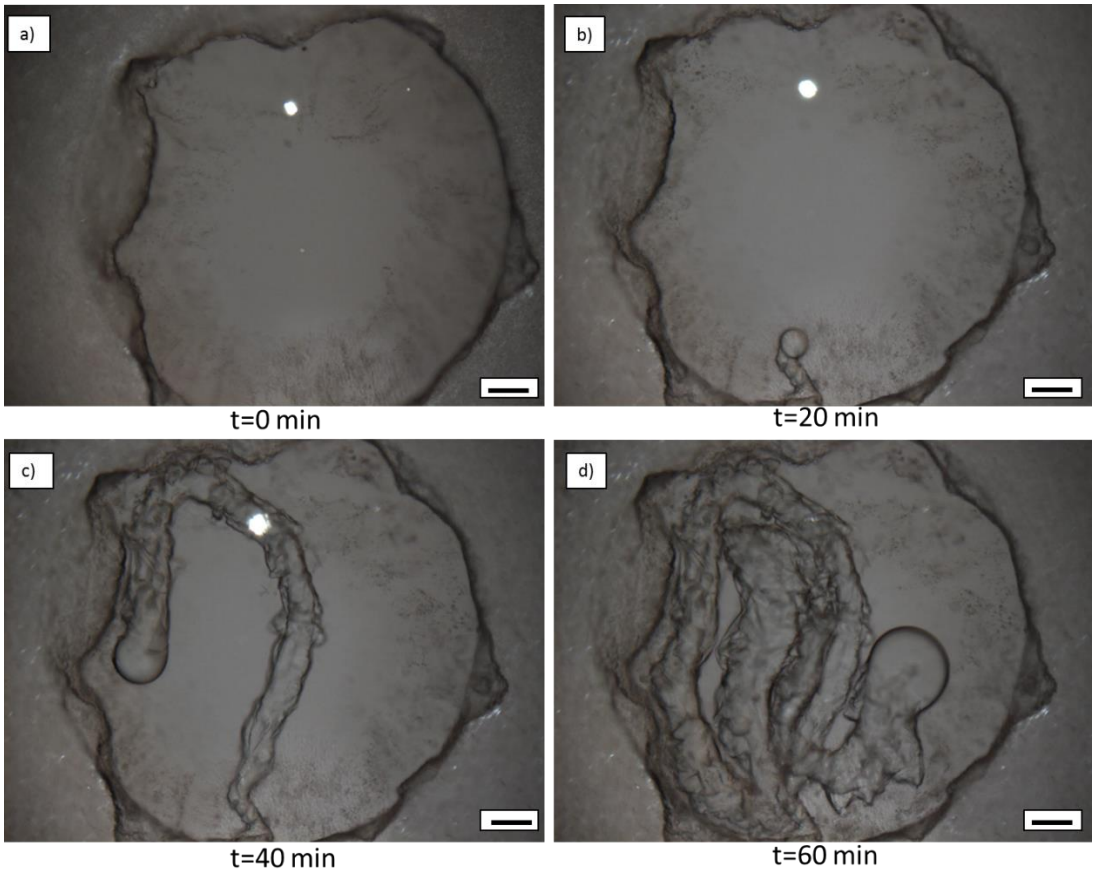

Figure 5.8: Time required for complete conversion for 1.25 wt.% wax system containing mineral oil and cyclopentane at 2 °C/min rate. The scale bar represents 100 µm.

Comparing the hydrate formation in waxy oil and non-waxy oil systems, though hydrate nucleation occurs randomly and instantaneously on the availability of free water from ice melting in both these systems, the time required for lateral growth and complete surface coverage with hydrate crystals and subsequent radial growth was further extended in the presence of wax (Figures 5.5, 5.6, and 5.8). The aggregation of wax crystals at the

interface and the presence of a network or chain-like structure around the water droplet are hypothesized to minimize the interfacial area available for transport of hydrate forming moleculue (cyclopentane) into the water droplet. Hence, wax acts as a barrier for cyclopentante transport and enhance the diffusion resistance for hydrate formation.

A similar experiment was conducted on 1.25 wt.% wax system at varying heating and cooling rates (1 °C/min and 0.5 °C/min) to evaluate its effect on hydrate formation and time required for complete conversion. Figures 5.9 and 5.10 show the evolution of hydrate formation from ice melting to complete conversion at 1 °C/min, and 0.5 °C/min cooling rates respectively. The hydrate formation mechanism was observed to be identical in all the systems (three different cooling rates), but differences exist in the time required for complete conversion. For a 1.25 wt.% wax system, the time required for complete conversion was 96 minutes, and 129 minutes at 1 °C/min, and 0.5 °C/min, respectively. The time required for complete conversion at 1 °C/min, and 0.5 °C/min cooling rate were 85%, and 148% more than the time required at 2 °C/min rate, respectively. The progression from hydrate nucleation to lateral and radial growth (in terms of time required for conversion) was found to be slower and more prolonged with a slower cooling rate due to precipitation of elongated wax crystals at the slower cooling rate (Figure 5.4). Wax crystals precipitated out of solution at slower cooling rates were observed to be longer, yielding to a strong and interconnected network of wax crystals at the oil-water and thereby reducing the interfacial area for diffusion of cyclopentane into water.

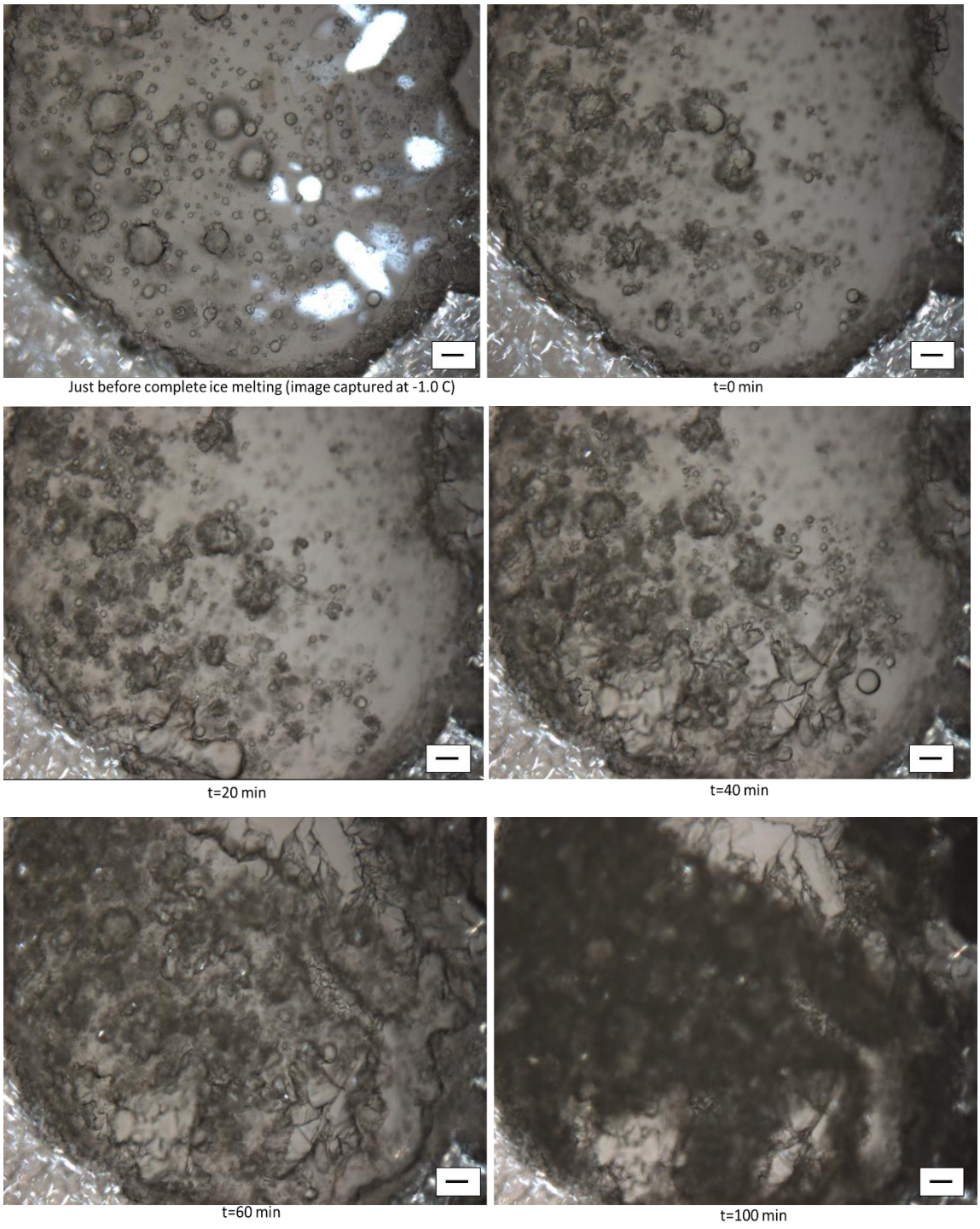

Figure 5.9: Hydrate formation in 1.25 wt.% wax system at constant heating and cooling rate of 1 °C/min at different time intervals. The scale bar represents 100 µm.

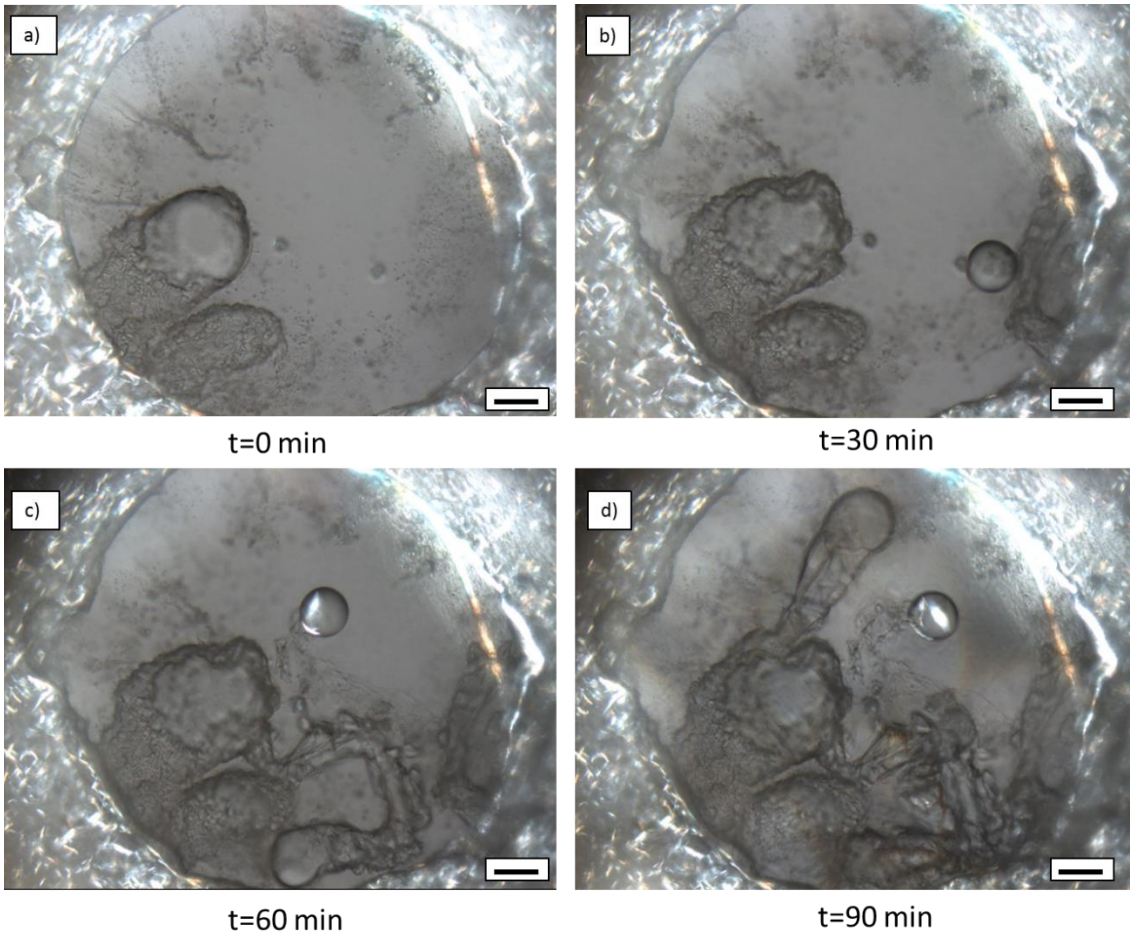

Figure 5.10: Hydrate formation in 1.25 wt.% wax system at constant heating and cooling rate of 0.5 °C/min at different time intervals.

Another hydrate formation experiment was conducted on 5 wt.% wax-20 wt.% mineral oil-75 wt.% cyclopentane mixture to evaluate the effect of wax concertation on hydrate formation. Figure 5.11 shows the evolution of water droplets toward complete conversion into hydrates at different time intervals at a constant heating and cooling rate of 2 °C/min. Comparing the 1.25 wt.% wax and 5 wt.% wax systems at 2 °C/min rate, the average time required for complete conversion was found to increase with increase in wax concentration (Figures 5.5, 5.11). The time required for completion conversion for the sample shown in Figure 5.11 was 94 minutes. The time required for complete conversion

for 5 wt.% wax system at 2 °C/min rate was 3.5 times, and 2.6 times the conversion time required in pure cyclopentane and mineral oil-cyclopentane samples, respectively (Table 5.3, and Table 5.4). For 5 wt.% wax system, a four times increase in the wax concentration yielded 57% increase in the average time for complete conversion when compared to 1.25 wt.% wax system (Table 5.4).

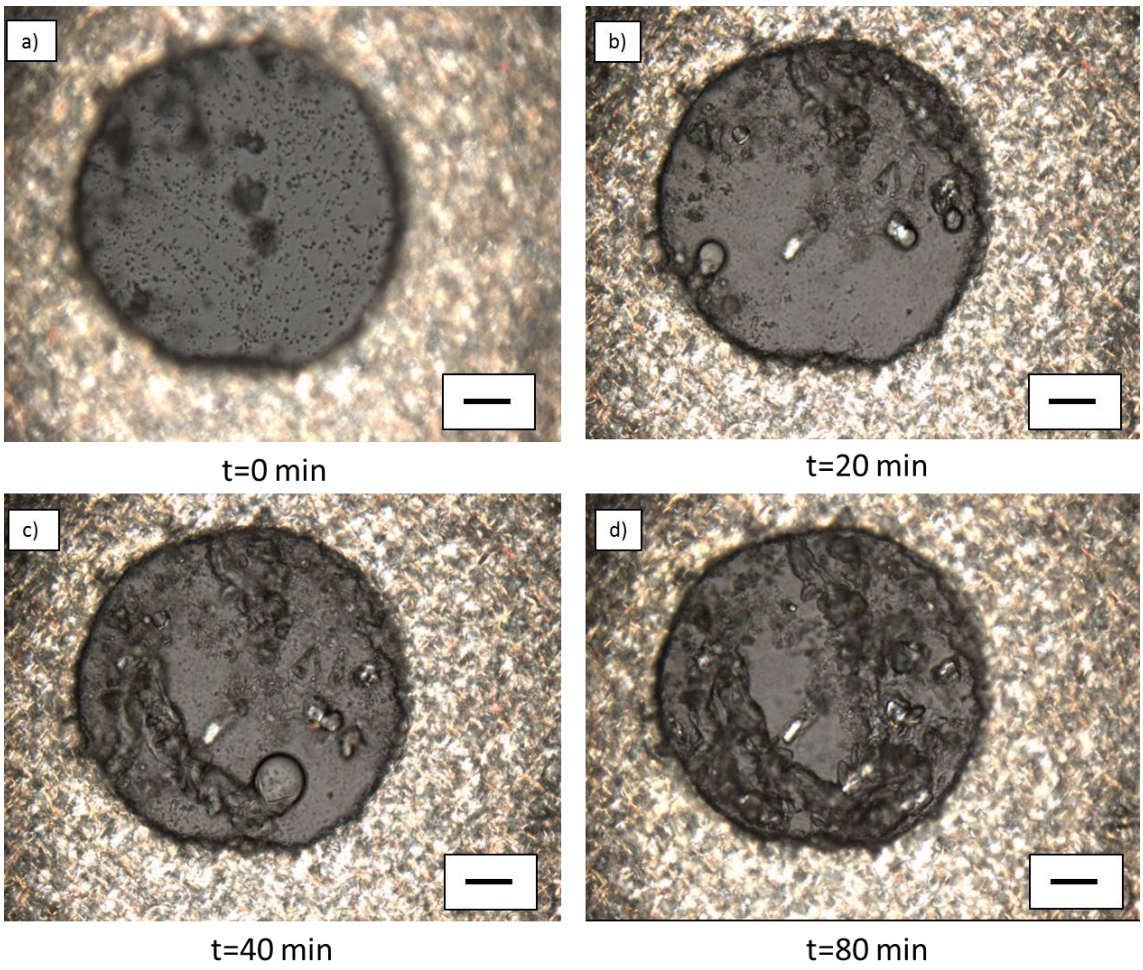

Figure 5.11: Hydrate formation in 5 wt.% wax system at constant heating and cooling rate of 2 °C/min at different time intervals. The scale bar represents 100 µm.

Table 5.3 represents the time required for complete conversion in control samples at a constant cooling rate of 2 ℃/min , whereas Table 5.4 summarizes the effect of cooling rate and wax concentration on the time required for complete conversion. The data represented in Table 5.3 and Table 5.4 are an average of three independent measurements. As seen in Table 5.4, an increase in wax concentration resulted in an increase in time required for complete conversion. However, the trend was not identical at the slowest cooling rate for the 1.25 wt.% and 5 wt.% wax systems. Comparing the hydrate conversion time between 1.25 wt.% wax and 5 wt.% wax systems, a four times increase in the wax concentration (in 5 wt.% wax system) yielded a 30-minute increase in the time required for conversion at 2 °C/min rate. A 10-minute increase was seen at 1 °C/min, and on the contrary, a 10-minute decrease was seen at 0.5 °C/min cooling rate. The addition of 1.25 wt.% wax to the mineral oil-cyclopentane mixture resulted in an increase in the hydrate conversion time by 3.5, 2.6, and 1.5 times when compared to the mineral oil-cyclopentane mixture at 2 °C/min, 1 °C/min, and 0.5 °C/min rates, respectively. A 5% increase in the wax concentration to the mineral oil-cyclopentane mixture resulted in a 3.2, 3, and 2.2 times increase in the hydrate conversion time at 2 °C/min, 1 °C/min, and 0.5 °C/min rates, respectively.

Table 5.3: Summary of the average time required for visual observation of complete conversion of water droplet into hydrates in "surfactant-free" and "with surfactant" control samples at constant heating and cooling rate of 2 °C/min

Sample	**Time for visual observation of complete conversion at 2 °C/min cooling rate (minutes)**
Pure cyclopentane (100%)	27 mins
25 wt.% mineral oil+75 wt.% cyclopentane	36 mins
0.1 wt.% Span80+24.9 wt.% mineral oil+75 wt.% cyclopentane	16 mins

Table 5.4: Summary of the average time required for visual observation of complete conversion of water droplet to hydrates at various wax concentrations and heating/ cooling rates

Sample	**Time for visual observation of complete conversion at different cooling rates (minutes)**		
	0.5 (°C/min)	**1 (°C/min)**	**2 (°C/min)**
1.25wt.%Wax+23.75wt.% Mineral Oil+75wt.% Cyclopentane	129.25	96.73	52.80
5wt.% Wax+20wt.% Mineral Oil+ 75wt.% Cyclopentane	116.53	108.76	82.25
1.25wt.% Wax+0.1wt.% Span80+23.75wt.% Mineral Oil+ 75wt.% Cyclopentane	24.53	19.53	18.25
5wt.% Wax+0.1wt.% Span80+20wt.% Mineral Oil+75 wt.% Cyclopentane	23.27	21.00	22.50

5.3.2.2 Surfactant-containing systems

To evaluate the effect of oil soluble surfactant such as Span 80 on hydrate formation, a control sample containing 0.1 wt.% Span 80, 24.9 wt.% mineral oil, and 75 wt.% cyclopentane was prepared. As shown in Table 5.3, addition of surfactant (0.1 wt.% increase in span80 concentration) to the mineral oil-cyclopentane mixture resulted in a

55% decrease in the time required for complete conversion. A reduction in the conversion time was expected, as surfactant reduces the surface tension, thereby promoting the diffusion of cyclopentane into water molecules. The process leading to hydrate formation in surfactant stabilized system was identical to the surfactant-free case and involved the three-step mechanism: hydrate nucleation, lateral growth, and radial growth. The only difference in these two systems was that the time required for complete conversion was significantly reduced in the presence of surfactant, thereby shortening the time interval between hydrate nucleation to radial growth. Figure 5.12 represents the time required for complete conversion of water droplets to hydrates at different time intervals in the presence of surfactant in a 1.25 wt.% wax system. As seen in Figure 5.12, hydrate nucleation occurred instantaneously on the availability of free water. However, the time required for progression from lateral growth to radial growth in a surfactant stabilized system was significantly reduced by at-least 65% - 80% at all cooling rates when compared to surfactant free systems. At 2 °C/min cooling rate, a 1.25 wt.% increase in the wax concentration to the surfactant-oil-cyclopentane mixture was observed to increase the hydrate conversion time by 14% when compared to the control system containing surfactant (Table 5.3, and Table 5.4). Decrease in the cooling rate was observed to have a significant increase in the time required for complete conversion from 14% to 53% when compared to the surfactant control sample. However, for the surfactant stabilized 1.25 wt.% wax system, the hydrate conversion time was 7%, and 34% higher at 1 °C/min, and 0.5 °C/min, respectively, when compared to the fastest cooling rate (2 °C/min). A minimum of 65% - 80% decrease in the hydrate conversion time was observed in the presence of surfactant in the 1.25 wt.% wax-oil-cyclopentane mixture at different cooling

rates when compared to its corresponding surfactant free system. Whereas, a 73% - 80% decrease in the hydrate conversion time was observed with the addition of 0.1 wt.% surfactant to 5 wt.% wax-oil-cyclopentane mixture. An increase in the wax concentration was shown to have minimal impact on the hydrate conversion time.

Figure 5.13 represents the trend followed by the different systems on hydrate conversion as a function of cooling rate. An increase in the hydrate conversion time was observed with a decrease in the cooling rate for all samples, but the increase in conversion time was not significant in surfactant stabilized systems when compared to a surfactant free system. Though the trend followed by surfactant stabilized systems on hydrate conversion was identical to surfactant free systems, the difference between the conversion time as a function of wax concentration was not significant as it was in the surfactant-free case.

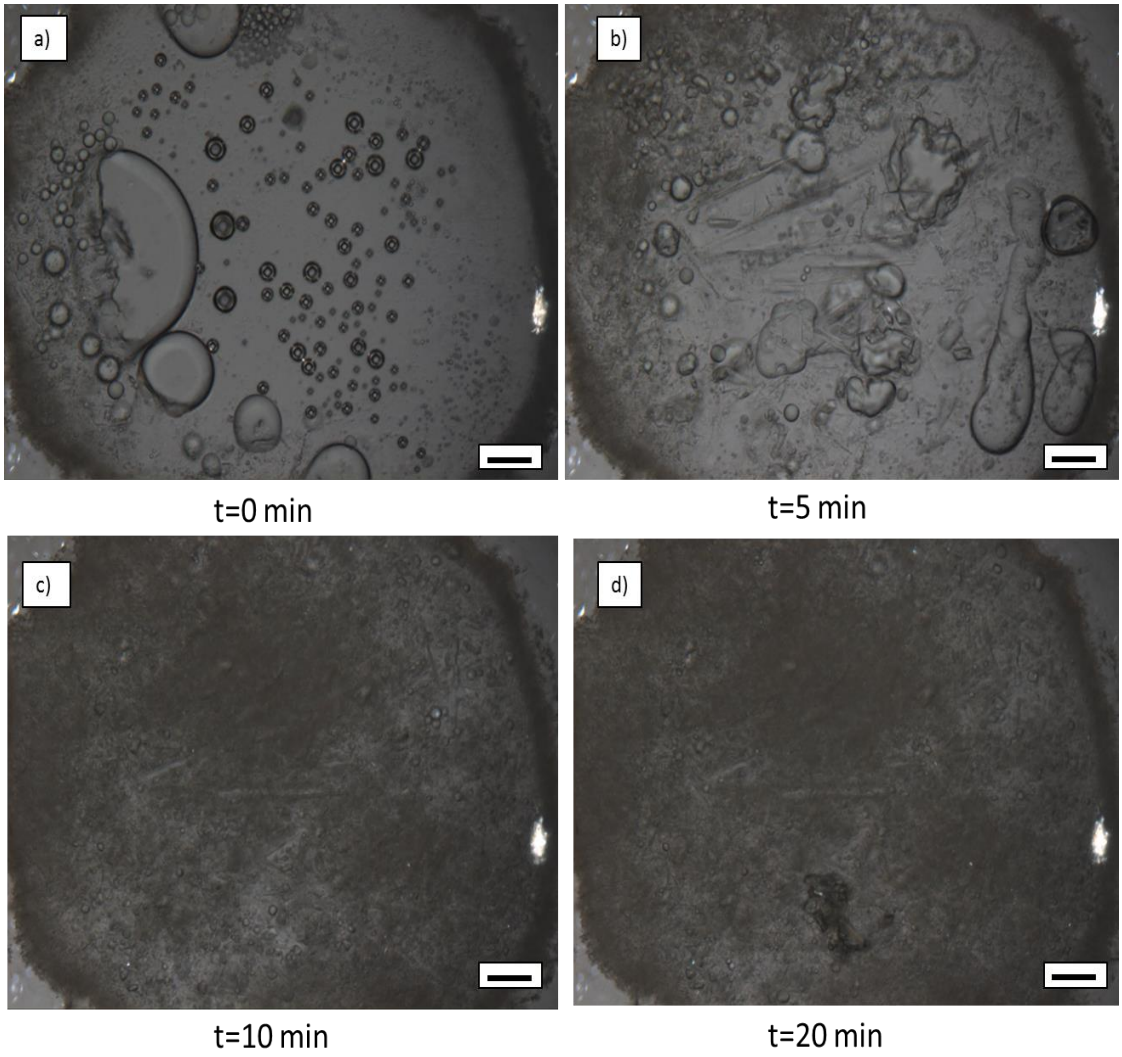

Figure 5.12: Hydrate formation in 1.25 wt.% wax system with 0.1 wt.% span 80, 23.65 wt.% mineral oil, and 75 wt.% cyclopentane at 2 °C/min heating and cooling rate

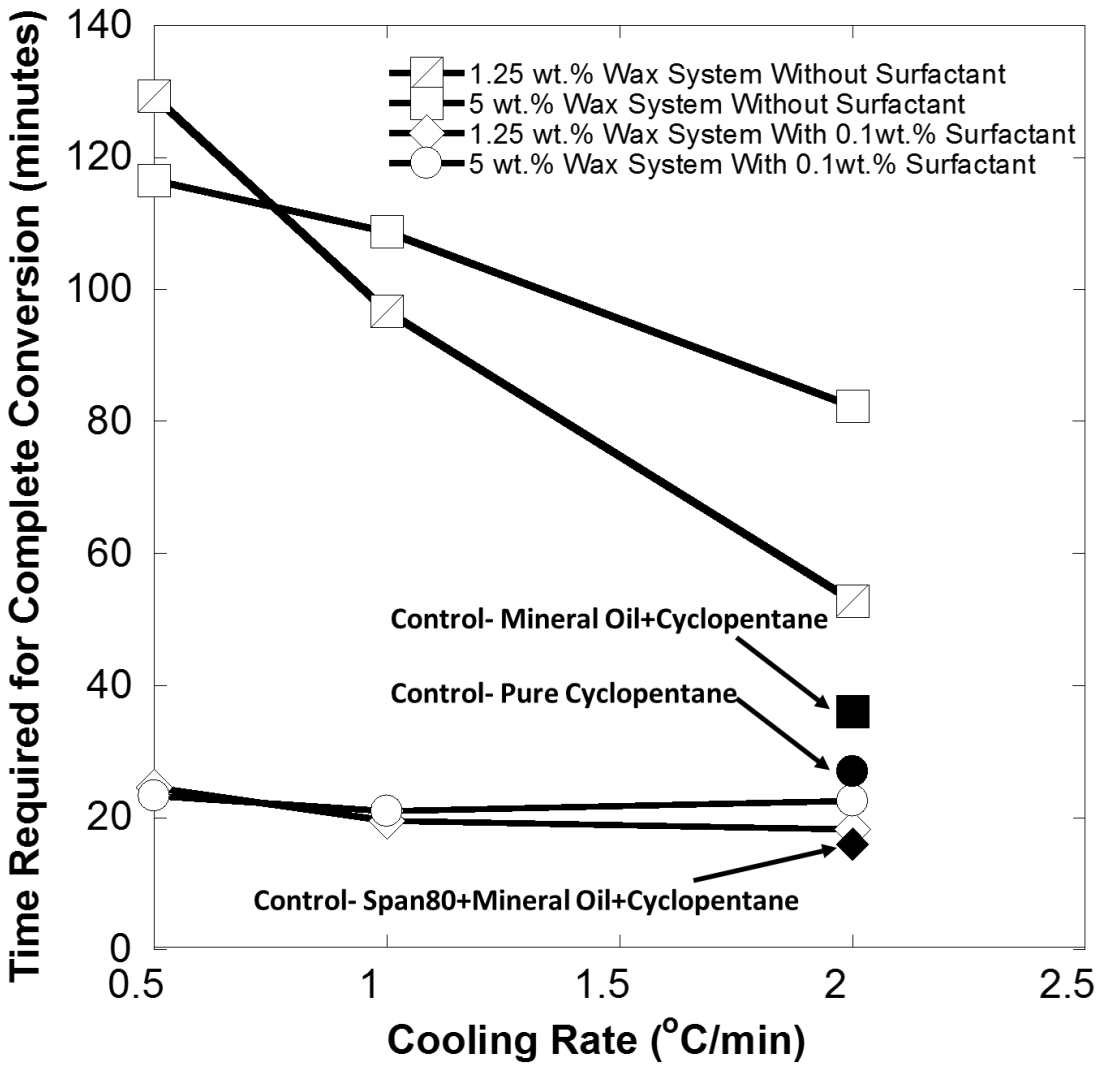

Figure 5.13: Summary of time required for complete conversion of water droplet to hydrates through visual observation as function of cooling rates and wax concentrations. The solid data points indicate control samples

5.3.2.3 Hydrate Formation Mechanism

Figure 5.15 shows the hydrate formation mechanism in waxy oil systems. In waxy oil systems, in addition to the three step mechanism associated with cyclopentane hydrates, wax precipitation and aggregation is also involved. The experimental results shown in this work demonstrated that the presence of wax greatly influenced hydrate formation and time

required for complete conversion. Moreover, the factors affecting wax appearance temperature (WAT), such as wax concentration and cooling rate, were also found to have a significant impact on hydrate formation. The hydrate formation mechanism in waxy oil systems can be described in four steps:

a) Wax precipitation around water droplet

A decrease in temperature below the wax appearance temperature (WAT) results in precipitation of nano wax crystals. The decrease in temperature results in lowering of molecular motion, and the attractive forces between the crystals increases, thereby promoting the growth of an ordered network of wax crystals [102, 103]. Wax precipitation is a two-step mechanism and involves nucleation and growth. A decrease in the solution temperature causes aggregation of nano wax crystals (also known as nucleation) until the aggregates/nuclei reach a critical size in order to be visualized and become stable. Nuclei size begins to increase and growth of wax crystals occur due to attractive forces between the molecules [102, 103].

b) Hydrate nucleation

Quenching of water drops to form ice and subsequent melting of ice to free liquid water was demonstrated to initiate hydrate nucleation rather instantaneously and randomly anywhere at the oil-water interface. The free water available from ice melting was proven to reduce the stochastic long hydrate nucleation/ induction time that is otherwise associated with cyclopentane hydrates and promotes hydrate nucleation. A similar hydrate formation experiment was conducted without quenching the water droplet to form ice. Hydrate nucleation was not observed despite holding the sample at 0.1 C for several hours.

Hence, availability of free water from ice melting due to heat transfer was determined as the rate limiting step. Though availability of free water promotes hydrate nucleation, the driving force behind the immiscible cyclopentane oil phase to diffuse into water contributes significantly towards the overall hydrate formation mechanism. The driving force behind cyclopentane diffusion into water drop is due to chemical potential difference between the phases. The driving force for cyclopentane hydrate nucleation is analogous to that of gas hydrate nucleation. For gas hydrate systems, the difference between the chemical potential for the old and the new phase acts as the driving force for hydrate formation [107]. To understand the driving force for gas hydrate formation, Kaschiev suggested a three-phase system for one component gas at constant temperature and pressure (Figure 5.14) [107].

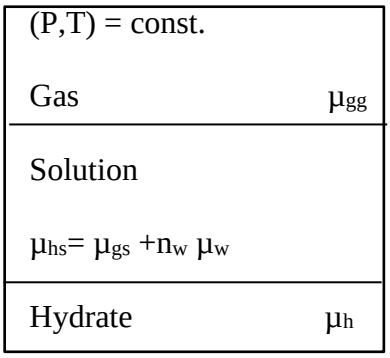

Figure 5.14: Three phase system used for describing the driving force required for hydrate formation at constant temperature (T) and pressure (P) [107].

$$\Delta\mu = \mu_{new} - \mu_{old} = \mu_{hs} - \mu_h \quad \text{Eq. 5.1}$$

$$G + n_w H_2O \Longleftrightarrow G.n_w H_2O \quad \text{Eq. 5.2}$$

$$\mu_{hs} = \mu_{gs} + n_w \mu_w \quad \text{Eq. 5.3}$$

$$\Delta\mu = \mu_{hs} - \mu_h = \mu_{gs} + n_w \mu_w - \mu_h \quad \text{Eq. 5.4}$$

At constant temperature T, and pressure P, the hydrate phase reaction occurring in solution is expressed as given in Eq. 5.2. According to the thermodynamic relation between chemical potentials in equilibria, the chemical potential of the hydrate building unit in solution (μ_{hs}) is given in Eq. 5.3. The difference in the chemical potential, $\Delta\mu$ (also known as supersaturation) is the driving force for hydrate nucleation. Supersaturation ($\Delta\mu$) is defined as chemical potential difference between the hydrate phase in solution ($\Delta\mu_{hs}$), and hydrates ($\Delta\mu_h$). Hydrate nucleation and crystal growth occurs until the system is supersaturated ($\Delta\mu > 0$), indicating that the chemical potential of the old phase is greater than the new phase. In other terms, diffusion of hydrate-forming guest molecule into water occurs rapidly as long as the chemical potential of the guest molecule in the oil phase is greater than that in the aqueous phase. Once the system reaches equilibrium, diffusion doesn't occur any further ($\Delta\mu = 0$, system is saturated). Diffusion and hydrate nucleation ceases completely, and instead hydrate dissolution starts to occur when $\Delta\mu < 0$ (undersaturated) [107].

c) Lateral growth

The nucleation of hydrate crystals at the interface further promotes the growth of hydrate crystals around the surface of the water droplet until the entire surface is covered with hydrate crystals. Figure 5.15 shows hydrate nucleation at the oil-water interface and the progression from hydrate nucleation to lateral growth where the entire surface of the water droplet is covered with hydrate crystals. In the presence of wax in the oil phase, a layer of wax crystals is formed at the interface and an interconnected or gel-like network exists around the water droplet. Wax crystals at the interface act as a barrier, thereby minimizing the interfacial area available for direct contact between the two immiscible

phases, and further elongating the time required for progression from hydrate nucleation to lateral growth. Wax crystals precipitated at the interface are dependent on the cooling rate and wax concentration. Wax enhances the diffusion resistance of cyclopentane transport to the bulk water phase and delays hydrate growth rate.

d) Radial growth

In waxy oil systems, progression from lateral growth/ complete surface coverage to radial growth is governed by mass transfer or diffusion of cyclopentane through the layer of wax crystals around the water droplet and through the hydrate shell formed during lateral growth. Thus, wax concentration, cooling rate, and diffusion determine the rate of radial growth.

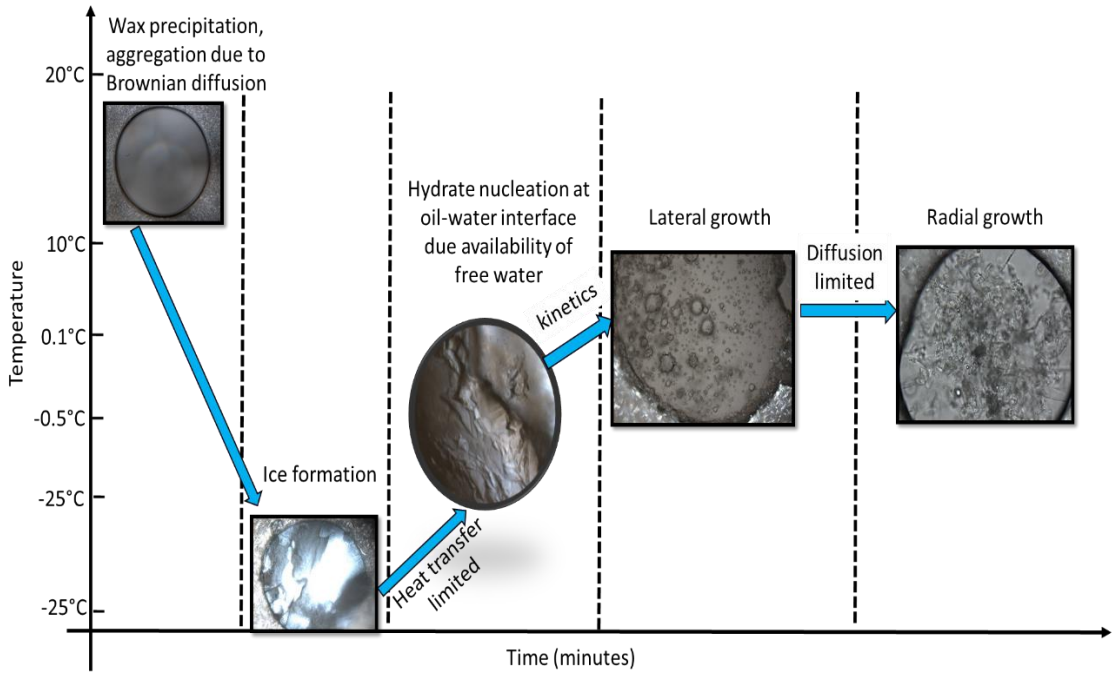

Figure 5.15: Hydrate formation mechanism in waxy oil systems. The water droplet is suspended in an oil phase containing either 1.25 or 5 wt.% wax in 1:3 ratio of mineral oil and cyclopentane on a weight basis.

The hydrate formation mechanism in waxy oil systems as described above can be primarily classified as a thermodynamically driven process until ice dissociation and hydrate nucleation occurs, following which kinetics dominates the formation mechanism. Though the formation mechanism in the presence of wax is identical to gas hydrate formation, the presence of wax was observed to enhance the diffusion resistance of hydrate formation. In the absence of a surfactant, the high interfacial tension between oil-water interface along with the diffusion barrier created by wax crystals, reduces the rate of cyclopentane transport from the oil phase to the bulk water phase thereby resulting in slower hydrate growth rate. In the presence of a surfactant, the progression from lateral growth to radial growth is much faster when compared to the surfactant-free case, owing to a reduction in the interfacial tension.

Severel studies have shown that surfactants greatly enhance the kinetics of hydrate formation by increasing the solubility of the hydrate forming guest molecule in the aqueous phase [108-113]. Increase in the solubility results in a decrease in the time required for the chemical potential difference (driving force for hydrate formation) to reach equilibrium (saturation). Surfactant molecules were observed to not only increase the solubility of hydrocarbon gas in the aqueous phase but also acts as a nucleating site, inducing the formation of hydrate crystals around the micelles [109]. However, several studies have shown that micelle formation is not responsible for faster hydrate growth rate as hydrate formation occurs at temperature below the Krafft point of the surfactant [112-114]. Studies have shown that the presence of micelles accelerate the hydrate growth rate by reducing the hydrate nucleation barrier (presence of surfactant results in lower induction time). Additionally it was observed that surfactants do not influence the

thermodynamic phase boundary as the surfactant molecules do not participate in hydrate formation. For this study, the surfactant concentration (0.1 wt.% of the oil phase) was above the critical micelle concentration (CMC) indicating the prence of micelles in the oil phase. Studies have shown that along with increase in the solubility of hydrate forming guest molecule, lower interfacial tension due to the presence of surfactants, favorably affects hydrate formation rate by enhancing the mass transfer and diffusion of hydrate forming gases to the bulk water [110-112, 115, 116]. Lowering of interfacial tension is also seen to significantly change the hydrate morphology resulting in catastrophic hydrate growth. It has been suggested that this catastrophic growth of hydrates in the presence of surfactants is probably due to continuous availability of water at the interface.

5.4. Conclusions

The presence of wax in the oil phase was observed to have a significant impact on the time required for complete conversion. For systems containing no surfactant, wax concentration, and cooling rate were observed to impact the time required for complete conversion. While in surfactant stabilized systems, cooling rate, and wax concentration didn't have a significantly strong influence on the hydrate conversion time. The addition of mineral oil to cyclopentane oil phase was found to increase the hydrate conversion time by 33%, but addition of surfactant to the oil-cyclopentane mixture was found to reduce the hydrate conversion time by > 50%. Presence of wax in the oil-cyclopentane mixture was observed to further increase the time required for complete conversion in the surfactant free case. Hydrate conversion time was identified to increase with slower

cooling rate irrespective of the wax concentration in the surfactant free system. Hydrate formation mechanism in waxy oil systems was hypothesized to be a four step process that includes: wax precipitation and aggregation, hydrate nucleation, lateral growth, and radial growth.

CHAPTER VI

CONCLUSIONS AND RECOMMENDATIONS

6.1. Significant Contributions

This thesis focuses on the characterization of emulsions and hydrates in waxy oil systems. A novel experimental method for characterizing hydrate formation with and without surfactant as a function of wax concentration (1.25 and 5 wt.% wax) and cooling rates (0.5, 1, and 2 °C/min) is presented. A direct visualization of hydrate growth in a single water drop suspended in the waxy oil phase is introduced in this thesis that can be used to visualize the changes occurring in the system when hydrates and wax occur simultaneously. The visualization experiment provided a fundamental understanding of the hydrate formation mechanism in the presence of wax and the effect of surfactant, wax concentration, and cooling rates on hydrate formation. The presence of wax in the oil phase was observed to enhance the diffusion resistance for cyclopentane transport from the oil phase to the bulk water phase. The presence of surfactant in the oil phase (waxy oil continuous phase) was observed to accelerate the hydrate formtion rate by a factor of 2.5-5.3 when compared to the surfactant free waxy oil system. In surfactant containing systems, wax concentration and cooling rates were observed to have a minimal impact on

hydrate conversion time. Similar observations were not seen in the surfactant-free systems. In surfactant free systems, the slower cooling rate was identified to increase the hydrate conversion time. However, faster cooling rates resulted in a decrease in the hydrate conversion time. Precipitation of longer/ elongated wax crystals and formation of an inter-connected network of wax crystals at slower cooling rates were considered to minimize the contact area available between oil and water thereby delaying hydrate formation. A four step hydrate formation mechanism in waxy oil systems (wax precipitation, hydrate nucleation, lateral growth, and radial growth) was postulated based on the experimental data. The presence of wax was observed to delay the rate of diffusion of cyclopentane due to the chemical potential difference between cyclopentane in the oil phase and aqueous phase (driving force for hydrate formation), high interfacial tension, and diffusion resistance. On the contrary, surfactant reduced the diffusion resistance of cyclopentane transport across the oil/water interface, thereby promoting hydrate growth. An in-situ, hydrate formation experimental method was developed using a visualization technique. The experimental method enabled direct visualization of changes occurring in the emulsion upon ice dissociation, hydrate formation, and hydrate dissociation. Ice melting and hydrate formation were observed to occur simultaneously. Hydrate crystals were observed to form at the oil-water interface and in-situ conversion of water droplets to hydrates were also captured using this method. An irreversible formation of multiple emulsions was observed upon hydrate dissociation.

This thesis provides a fundamental understanding of concentrated emulsion characterization at both quiescent and flowing conditions. Data are presented on concentrated emulsion characterization using several experimental techniques such as

inflow microscope, acoustic spectroscopy, and optical microscopy. The experimental results from each of these techniques were validated with other techniques used for emulsion characterization. A flow loop setup equipped with an inflow microscope was used for characterizing model water-in-oil emulsions. The effect of water cut (5, 10, and 20 vol.%), stabilizer type (span 80 and aerosol R972), temperature (25 °C and 15 °C), and flow rate (3.3 gpm, 6.6 gpm and 8.3 gpm) on emulsion properties and droplet size distribution were measured. This work showed that the drop size distribution was a function of temperature, water concentration, and flow rate for surfactant stabilized emulsions. The solid stabilized emulsions indicated that only water concentration had an overall impact on the drop size distributions.

Water-in-oil emulsions with a dispersed phase fraction equal to 15 wt.% were prepared using either a non-ionic surfactant or solid hydrophobic nanoparticles under identical conditions of high energy mixing. Acoustic spectroscopy measurements were carried out on these emulsions to determine the initial droplet size distributions and their evolution over a period of one week. Transient stability, solution conductivity, and surface charge measurements were conducted in parallel to compare the behavior of surfactant and solid particles at the oil-water interface. Coalescence of solid-stabilized emulsions led to broad droplet size distributions with larger droplets when compared to surfactant-stabilized emulsions. Incomplete surface coverage by solid particles resulted in the emulsions being unstable against coalescence, thereby shifting the distribution towards larger droplet size. This behavior was captured by acoustic spectroscopy in terms of change in the raw experimental attenuation, colloidal vibration current, and conductivity measurements at different time intervals. Conductivity measurements in solid stabilized

emulsions showed that with time, counter-ions from water droplets were released into the continuous oil phase, thereby increasing the conductivity of the emulsions. Complimentary bottle test and optical microscopy experiments were conducted on these emulsions to validate the droplet size distribution and transient behavior of emulsions measured using acoustic spectroscopy.

6.2. Future Work

Experimental investigations of hydrate formation in waxy oil systems were conducted in a small-scale laboratory setup. Single drop hydrate formation experiments were performed at various wax concentrations (1.25 and 5 wt.% wax) and cooling rates (0.5, 1, and 2 °C/min). The next step would be to interrogate the hydrate formation mechanism in waxy oil systems in the presence of multiple water droplets in the form of an emulsion. This work will be significant as oilfield emulsions are commonly encountered at high water concentrations, and it is imperative to develop experimental results that have direct applications for field study. Further experimental investigation on hydrate formation in waxy oil emulsions in flowing conditions would provide an insight into the flow behavior of hydrate forming emulsions in the presence of wax and stabilizing agents such as a surfactant. This work would lead to an understanding of multiphase fluid flow behavior due to hydrates, wax, and emulsions, thus paving a way to develop better economically feasible flow assurance remediation strategies for a wide variety of industrial applications.

Preliminary experimental work was conducted using optical microscopy to investigate hydrate formation in model waxy oil emulsions at various water

concentrations. For this work, hydrate-forming water-in-oil emulsions were prepared using paraffin wax, surfactant (span 80), cyclopentane, light mineral oil, and deionized water. An oil phase composition was prepared with a 50:50 mixture of light mineral oil and cyclopentane on an equal weight basis. Light mineral oil purchased from Sigma-Aldrich was used as model mineral oil. 95% purity cyclopentane purchased from Alfa Aesar was used as the hydrate forming liquid molecule. An oil soluble non-ionic surfactant such as Span 80 was used as the stabilizing agent. For all the systems, the surfactant concentration was kept constant at 0.1 wt.%. Model paraffin wax with a melting point of 58-62 °C was purchased from Sigma-Aldrich. The wax concertation was kept constant at 1.25 wt.% for all the systems. A low wax concentration was chosen for this study in order to avoid phase separation issues at low temperatures and at high water concentration systems. Hydrate forming water-in-oil emulsions were prepared at 5, 10, 20, 30, and 40 wt.% water concentrations. For 40 wt.% water-in-oil emulsion, an oil phase was prepared with 0.1 wt.% span80, 1.25 wt.% wax, and 58.65 wt.% of model mineral oil-cyclopentane mixture on 50:50 equal weight basis. For this work, 100 g basis of the sample was used. For preparing 100 g of a water-in-oil emulsion, an oil phase was prepared by heating 29.325 wt.% mineral oil and 1.25 wt.% wax mixture to 100 °C for 24 hours to ensure complete wax dissolution and erase any thermal history. The sample was heated on a stir/ hot plate using a 1” long stir bar at 600 rpm. The sample temperature was reduced to 40 °C prior to adding 29.325 wt.% cyclopentane and 0.1 wt.% span 80. The oil phase was stirred using an Ultra Turrax T25 homogenizer at 2800 rpm for one minute prior to adding the dispersed phase. 40 wt.% of water was added dropwise to the oil mixture and the sample was prepared using the homogenizer at 8000 rpm, for 20 mins. The sample was

immediately placed in the chiller previously set to 0.1 °C. Figure 6.1 illustrates the chiller setup used for this work. After placing the sample in the chiller, it was constantly stirred using a homogenizer set at 3000 rpm to ensure mixing of the sample during hydrate formation. The sample temperature was measured periodically, and once the sample temperature reached approximately 1-2 °C, the sample was seeded using ice crystals. It took about 2 hours to reach this temperature after placing it in the chiller. A small quantity (less than one spatula full) of ice crystals were added to the sample and stirred well before placing it back into the chiller. The sample was constantly stirred after seeding. Within 2-3 hours after seeding, the entire sample was converted into hydrates. Hydrate formation was confirmed, as the sample turned into a solid-like structure and didn't flow (Figure 6.2). After hydrate formation, the sample was kept at room temperature to investigate the effect of hydrate formation on emulsion droplet size distribution and its stability (Figure 6.3). Phase separation was observed in this sample upon hydrate dissociation (Figures 6.3, and 6.4). A small amount of the sample from the emulsion layer in the phase separated sample was used to measure the emulsion droplet size upon hydrate dissociation (Figure 6.4). A significant increase in the emulsion droplet size and distribution was observed after hydrate dissociation when compared to the initial emulsion droplet size. Simultaneously, an emulsion stability test was conducted to evaluate any changes in the emulsion droplet size over the course of the experiment (Figure 6.5). A transient stability test indicated no significant changes in the emulsion droplet size and distribution.

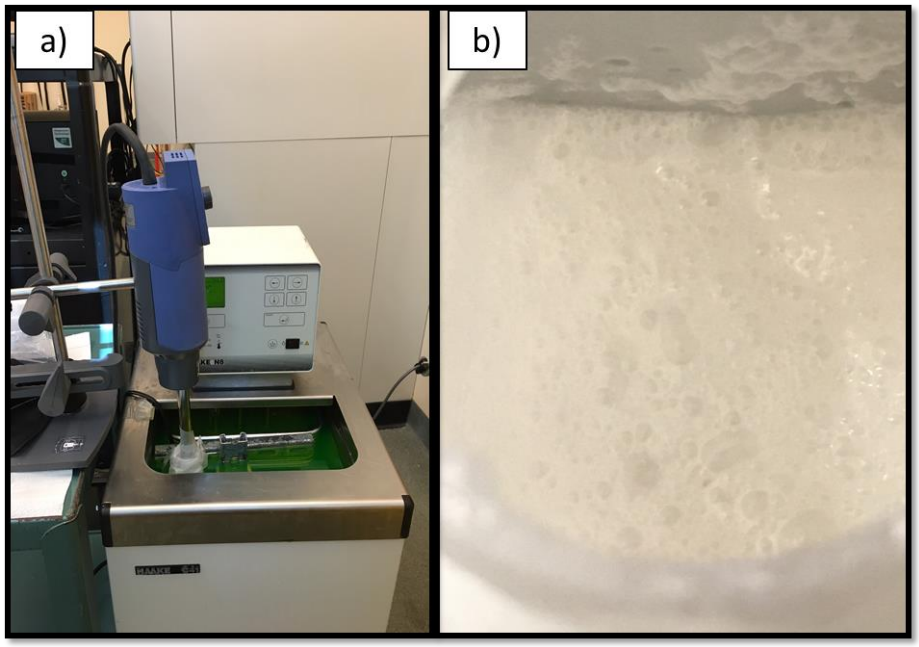

Figure 6.1: Experimental setup of the chiller used for carrying out hydrate formation experiment in waxy oil systems

Figure 6.2: Visual confirmation of hydrate formation in 40 wt.% water-in-oil emulsion containing wax and surfactant in the oil phase

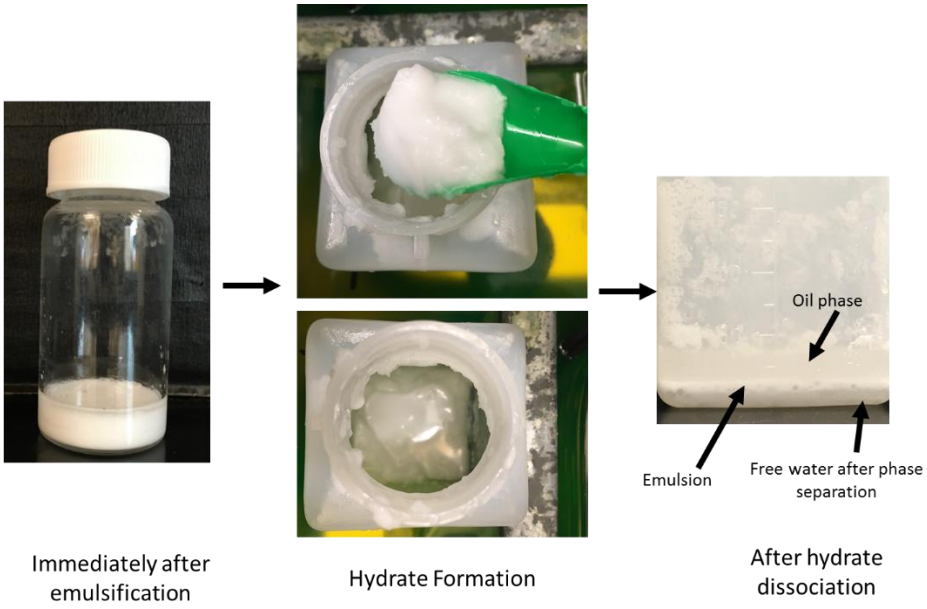

Figure 6.3: Evolution of sample from emulsification to hydrate formation, and to hydrate dissociation

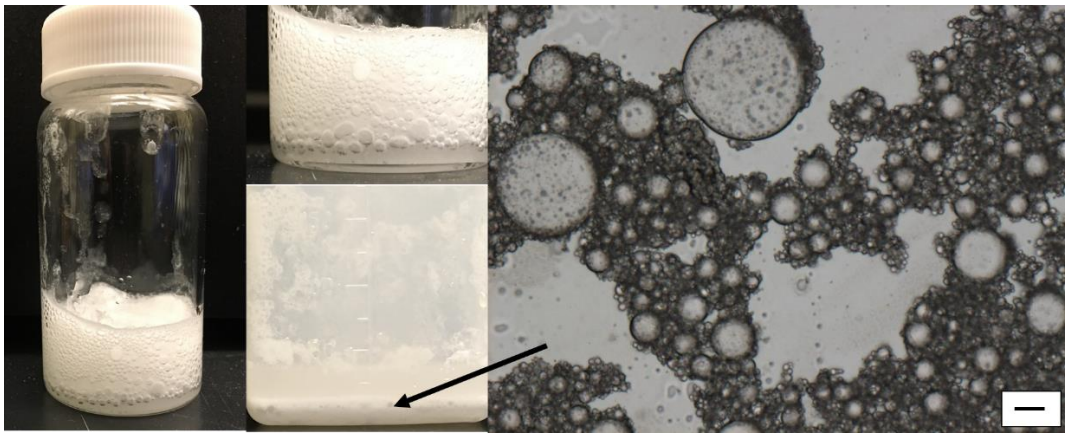

Figure 6.4: Emulsion after hydrate dissociation and microscope image of the sample taken from the emulsion layer of the sample subjected to hydrate formation. The scale bar represents 50 µm

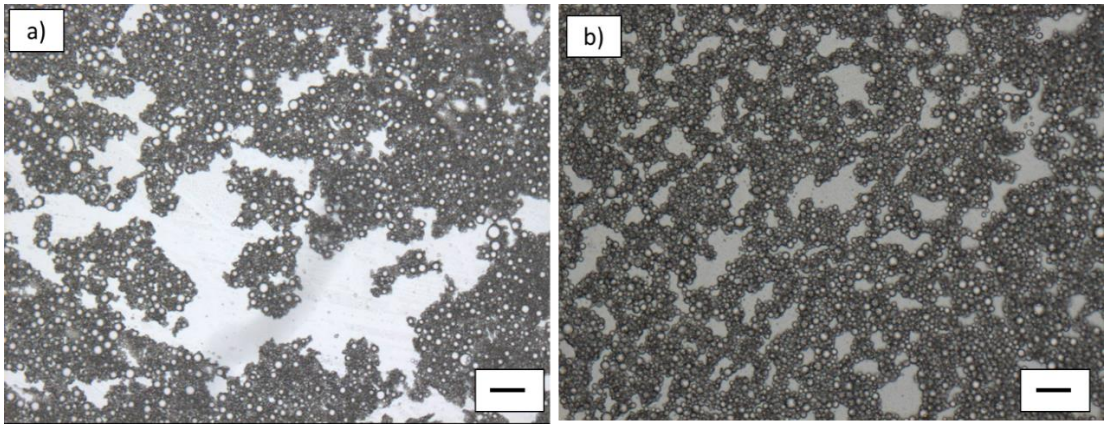

Figure 6.5: Transient stability microscope images of the 40 wt.% water-in-oil emulsion used for hydrate studied in waxy oil systems. A) image of the emulsion sample at 0^{th} hour (immediately after emulsification) b) image of the sample after 6 hours of emulsification. The scale bar represents 100 µm

A comparable experiment was conducted at 30, 20, 10, and 5 wt.% water concentrations. Hydrates were observed to form at 30 and 20 wt.% water concentrations. However, hydrate formation was not observed in 5 and 10 wt.% water concentrations, even after 12 hours of seeding. The next step forward would be to conduct in-situ hydrate formation in waxy oil emulsions using an optical microscope. A similar experimental procedure, as discussed in Chapter IV, can be used to investigate the changes in the emulsion properties and oil-water interface upon hydrate formation and dissociation. In order to correlate the experimental work discussed above to real world systems, a flow loop setup can be used to interrogate the multiphase fluid flow behavior in the presence of hydrates and wax. The flow loop setup discussed in Chapter III was redesigned and rebuilt into a horizontal setup. The modification to the experimental design was carried out in order to avoid any changes to the fluid property with change in the pipe orientation, and also to enable the use of hazardous chemicals such as crude oil and flammable materials. Consequently, the vertical flow loop setup discussed in Chapter III was

redesigned as shown in Figure 6.6. The new flow loop setup is equipped with pressure transducers at different locations in the flow loop test section to evaluate pressure changes along the length of the pipe. Any pressure fluctuations due to hydrate formation or wax build up can be easily detected using these transducers. This setup would also enable pressure drop calculation between two points in the test section associated with changes in the fluid property.

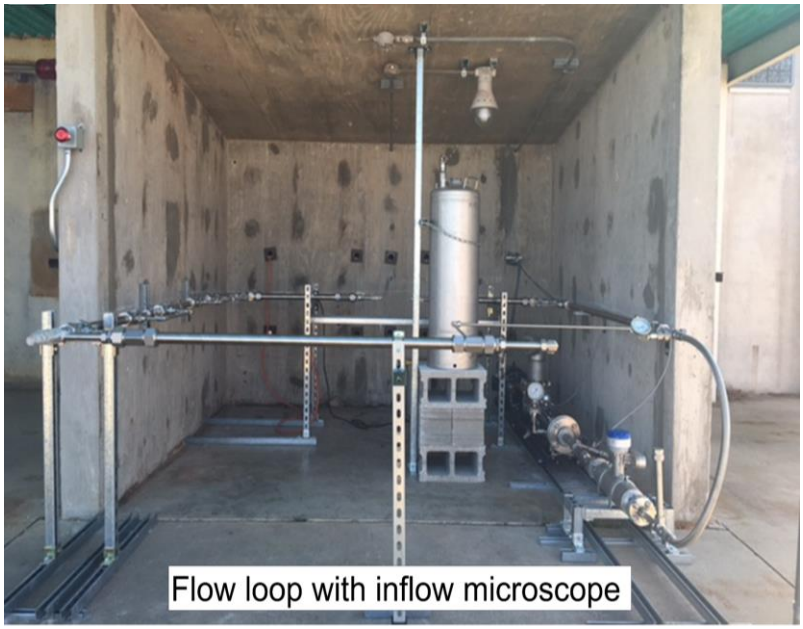

Figure 6.7: Flow loop setup used for emulsion, hydrates, and wax characterization. The flow loop setup is equipped with inflow microscope, pressure transducer for measuring properties under flowing conditions

REFERENCES

1. Sjöblom, J., *Emulsions and Emulsion Stability*. Second ed. 2005: CRC Press.
2. Laurier, L.S., *Petroleum Emulsions*, in *Emulsions*. 1992, American Chemical Society. p. 1-49.
3. Langevin, D., et al., *Crude Oil Emulsion Properties and their application to Heavy Oil Transportation.* Oil & Gas Science and Technology - Rev. IFP, 2004. **59**(5): p. 511-521.
4. Sjöblom, J., *Encyclopedic Handbook of Emulsion Technology*, ed. J. Sjöblom. Vol. 1. 2001, New York: Marcel Decker.
5. Hudson, J.D., et al., *Flow Assurance for Subsea Wells*. 2000, Offshore Technology Conference.
6. Kokal, S.L., *Crude Oil Emulsions: A State-Of-The-Art Review.* Society of Petroleum Engineers 2004.
7. Dendy Sloan, E.J. *Hydrate Engineering*. in *Society of PEtroleum Engineering*. 2000. Richardson, Texas: Society of Petroleum Emgineering.
8. Zerpa, L.E., et al., *Surface Chemistry and Gas Hydrates in Flow Assurance.* Industrial & Engineering Chemistry Research, 2010. **50**(1): p. 188-197.
9. Sloan, E.D. and C.A. Koh, *Clathrate Hydrates of Natural Gases*. 2008. 643.
10. Høiland, S., et al., *Wettability of Freon hydrates in crude oil/brine emulsions.* Journal of Colloid and Interface Science, 2005. **287**(1): p. 217-225.

11. Sum, A.K., C.A. Koh, and E.D. Sloan, *Clathrate Hydrates: From Laboratory Science to Engineering Practice.* Industrial & Engineering Chemistry Research, 2009. **48**(16): p. 7457-7465.

12. Sjöblom, J., et al., *Investigation of the Hydrate Plugging and Non-Plugging Properties of Oils.* Journal of Dispersion Science and Technology, 2010. **31**(8): p. 1100-1119.

13. Binks, B.P., ed. *Modern Aspects Of Emulsion Science*. 1998, The Royal Society of Chemistry: Cambridge, UK.

14. Bancroft, W.D., *The Theory of Emulsification, I.* The Journal of Physical Chemistry, 1911. **16**(3): p. 177-233.

15. Bancroft, W.D., *The Theory of Emulsification, II.* The Journal of Physical Chemistry, 1911. **16**(5): p. 345-372.

16. Bancroft, W.D., *The Theory of Emulsification, III.* The Journal of Physical Chemistry, 1911. **16**(6): p. 475-512.

17. Bancroft, W.D., *The Theory of Emulsification, IV.* The Journal of Physical Chemistry, 1911. **16**(9): p. 739-758.

18. Bancroft, W.D., *The Theory of Emulsification, V.* The Journal of Physical Chemistry, 1912. **17**(6): p. 501-519.

19. Becher, P., *Encyclopedia Of Emulsion Technology*. Vol. 1. 1983, New York: Marcel Dekker.

20. Becher, P., *Emulsions: Theory And Practice*. 2001, Washington D.C: Oxford University Press.

21. Ramsden, W., *"Separation of solids in the surface-layers of solutions and 'Suspensions' (Observations on surface-membranes, bubbles, emulsions, and mechanical coagulation). Preliminary Account."*. Proceedings of the Royal Society of London, 1903. **72**(479): p. 156-164.

22. Pickering, S.U., *Pickering Emulsions.* Journal of Chemical Society, 1907. **91**.

23. Binks, B.P. and J.H. Clint, *Solid Wettability from Surface Energy Components: Relevance to Pickering Emulsions.* Langmuir, 2002. **18**: p. 1270-1273.

24. Finkle, P., H.D. Draper, and J.H. Hildebrand, *The Theory of Emulsification I.* Journal of the American Chemical Society, 1923. **45**(12): p. 2780-2788.

25. Aveyard, R., B.P. Binks, and J.H. Clint, *Emulsions stabilised solely by colloidal particles.* Advances in Colloid and Interface Science, 2003. **100-102**: p. 503-546.

26. Binks, B.P. and S.O. Lumsdon, *Catastrophic inversion of w/o emuslion stabilized by hydrophobic silica.* Langmuir, 2000. **16**: p. 2539-2547.

27. Tambe, D.E. and M.M. Sharma, *Factors Controlling the Stability of Colloid-Stabilized Emulsions: I. An Experimental Investigation.* Journal of Colloid and Interface Science, 1993. **157**(1): p. 244-253.

28. Menon, V.B. and D.T. Wasan, *Characterization of Oil-Water Interfaces Containing Finely Divided Solids with Applications to the Coalescence of Water-in-Oil Emulsion: A review.* Colloid and Surfaces, 1988. **29**: p. 7-27.

29. Tambe, D.E. and M.M. Sharma, *Factors Controlling the Stability of Colloid-Stabilized Emulsions: II. A Model for the Rheological Properties of Colloid-Laden Interfaces.* Journal of Colloid and Interface Science, 1994. **162**(1): p. 1-10.

30. Binks, B.P. and M. Kirkland, *Interfacial structure of solid-stabilised emulsions studied by scanning electron microscopy.* Physical Chemistry Chemical Physics, 2002. **4**(15): p. 3727-3733.

31. Simon, S., et al., *Rheological Properties of Particle-Stabilized Emulsions.* Journal of Dispersion Science and Technology, 2010. **31**(5): p. 632-640.

32. Vignati, E., R. Piazza, and T.P. Lockhart, *Pickering Emulsions: Interfacial Tension, Colloidal Layer Morphology, and Trapped-Particle Motion.* Langmuir, 2003. **19**(17): p. 6650-6656.

33. Fan, H. and A. Striolo, *Nanoparticle effects on the water-oil interfacial tension.* Physical Review E, 2012. **86**(5).

34. Sullivan, A.P. and P.K. Kilpatrick, *The Effects of Inorganic Solid Particles on Water and Crude Oil Emulsion Stability.* Industrial & Engineering Chemistry Research, 2002. **41**(14): p. 3389-3404.

35. Hannisdal, A., et al., *Particle-stabilized emulsions: Effect of heavy crude oil components pre-adsorbed onto stabilizing solids.* Colloids and Surfaces A: Physicochemical and Engineering Aspects, 2006. **276**(1–3): p. 45-58.

36. Englezos, P., *Clathrate hydrates.* Industrial & Engineering Chemistry Research, 1993. **32**(7): p. 1251-1274.

37. Sloan Jr, E.D. and C. Koh, *Clathrate hydrates of natural gases*. 2007: CRC press.

38. Li, X., L. Negadi, and A. Firoozabadi, *Anti-agglomeration in Cyclopentane Hydrates from Bio- and Co-surfactants.* Energy & Fuels, 2010. **24**(9): p. 4937-4943.

39. Aman, Z.M., et al., *Interfacial mechanisms governing cyclopentane clathrate hydrate adhesion/cohesion.* Physical Chemistry Chemical Physics, 2011. **13**(44): p. 19796-19806.

40. Dieker, L.E., *Cyclopentane hydrate interparticle adhesion force measurements*. 2009, Colorado School of Mines.

41. Mitarai, M., et al., *Surfactant Effects on the Crystal Growth of Clathrate Hydrate at the Interface of Water and Hydrophobic-Guest Liquid.* Crystal Growth & Design, 2015. **15**(2): p. 812-821.

42. Ahuja, A., G. Zylyftari, and J.F. Morris, *Calorimetric and Rheological Studies on Cyclopentane Hydrate-Forming Water-in-Kerosene Emulsions.* Journal of Chemical & Engineering Data, 2015. **60**(2): p. 362-368.

43. Karanjkar, P.U., J.W. Lee, and J.F. Morris, *Calorimetric investigation of cyclopentane hydrate formation in an emulsion.* Chemical Engineering Science, 2012. **68**(1): p. 481-491.

44. Karanjkar, P.U., *Evolving morphology and rheological properties of an emulsion undergoing clathrate hydrate formation*, in *Chemical Enginnering* 2012, City University of New York: New York.

45. Ahuja, A., G. Zylyftari, and J.F. Morris, *Yield stress measurements of cyclopentane hydrate slurry.* Journal of Non-Newtonian Fluid Mechanics, 2015. **220**: p. 116-125.

46. Zylyftari, G., A. Ahuja, and J.F. Morris, *Nucleation of cyclopentane hydrate by ice studied by morphology and rheology.* Chemical Engineering Science, 2014. **116**: p. 497-507.

47. Zylyftari, G., A. Ahuja, and J.F. Morris, *Modeling Oilfield Emulsions: Comparison of Cyclopentane Hydrate and Ice.* Energy & Fuels, 2015.

48. Dirdal, E.G., et al., *Can cyclopentane hydrate formation be used to rank the performance of kinetic hydrate inhibitors?* Chemical Engineering Science, 2012. **82**: p. 177-184.

49. Nicholas, J.W., et al., *Assessing the feasibility of hydrate deposition on pipeline walls—Adhesion force measurements of clathrate hydrate particles on carbon steel.* Journal of Colloid and Interface Science, 2009. **331**(2): p. 322-328.

50. Nakajima, M., R. Ohmura, and Y.H. Mori, *Clathrate Hydrate Formation from Cyclopentane-in-Water Emulsions.* Industrial & Engineering Chemistry Research, 2008. **47**(22): p. 8933-8939.

51. Wardhaugh, L. and D. Boger, *Flow characteristics of waxy crude oils: application to pipeline design.* AIChE Journal, 1991. **37**(6): p. 871-885.

52. Aiyejina, A., et al., *Wax formation in oil pipelines: A critical review.* International Journal of Multiphase Flow, 2011. **37**(7): p. 671-694.

53. B.T. Ellison, C.T.G., L.M. Frostman, and S.E. Lorimer, *The Physical Chemistry of Wax, Hydrates, and Asphaltene*, in *Offshore Technology Conference*. 2000, Offshore Technology Conference: Houston, TX.

54. Roenningsen, H.P., et al., *Wax precipitation from North Sea crude oils: 1. Crystallization and dissolution temperatures, and Newtonian and non-Newtonian flow properties.* Energy & Fuels, 1991. **5**(6): p. 895-908.

55. Pedersen, K.S. and H.P. Rønningsen, *Influence of Wax Inhibitors on Wax Appearance Temperature, Pour Point, and Viscosity of Waxy Crude Oils.* Energy & Fuels, 2003. **17**(2): p. 321-328.

56. Drelich, A., et al., *Evolution of water-in-oil emulsions stabilized with solid particles-Influence of added emulsifier.* Colloids and Surfaces A: Physicochemical and Engineering Aspects, 2010. **365**(1-3): p. 171-177.

57. Binks, B.P., *Particles as surfactants similarities and differences.* Colloid and Interface Science, 2002. **7**: p. 21-41.

58. Leal-Calderon, F. and V. Schmitt, *Solid-stabilized emulsions.* Current Opinion in Colloid & Interface Science, 2008. **13**(4): p. 217-227.

59. Binks, B.P. and S.O. Lumsdon, *Influence of Particle Wettability on the Type and Stability of Surfactant-Free Emulsions.* Langmuir, 2000. **16**: p. 8622-8631.

60. Frelichowska, J., M.-A. Bolzinger, and Y. Chevalier, *Effects of solid particle content on properties of o/w Pickering emulsions.* Journal of Colloid and Interface Science, 2010. **351**(2): p. 348-356.

61. Dukhin, A.S. and P.J. Goetz, *Acoustic and electroacoustic spectroscopy.* Langmuir, 1996. **12**(18): p. 4336-4344.

62. Dukhin, A.S., *Ultrasound for Characterizing Colloids Particle Sizing, Zeta Potential Rheology*. 2002: Elsevier.

63. M. Chatterjee, M.K.N., B. Siladitya, and D. Ganguli, *Role of organic solvents and surface-active agents in the sol-emulsion-gel synthesis of spherical alumina powders.* Journal of Materials Research, 1999. **15**(1): p. 176-185.

64. Dukhin, A.S. and P.J. Goetz, *Characterization of Liquids, Nano- and Microparticulates, and Porous Bodies using Ultrasound* 2ed. 2010: Elsevier. 503.

65. Dukhin, A.S. and P.J. Goetz, *Acoustic and electroacoustic spectroscopy for characterizing concentrated dispersions and emulsions.* Advances in Colloid and Interface Science, 2001. **92**(1–3): p. 73-132.

66. Drelich, A., et al., *Evolution of water-in-oil emulsions stabilized with solid particles.* Colloids and Surfaces A: Physicochemical and Engineering Aspects, 2010. **365**(1-3): p. 171-177.

67. Dukhin, A. and P. Goetz, *Evolution of water-in-oil emulsion controlled by droplet-bulk ion exchange: acoustic, electroacoustic, conductivity and image analysis.* Colloids and Surfaces A: Physicochemical and Engineering Aspects, 2005. **253**(1-3): p. 51-64.

68. Horozov, T.S. and B.P. Binks, *Particle-Stabilized Emulsions: A Bilayer or a Bridging Monolayer?* Angewandte Chemie International Edition, 2006. **45**(5): p. 773-776.

69. Yan, Y. and J.H. Masliyah, *Solids-stabilized oil-in-water emulsions: Scavenging of emulsion droplets by fresh oil addition.* Colloids and Surfaces A: Physicochemical and Engineering Aspects, 1993. **75**(0): p. 123-132.

70. Arditty, S., et al., *Some general features of limited coalescence in solid-stabilized emulsions.* Eur. Phys. J. E, 2003. **11**(3): p. 273-281.

71. Wiley, R.M., *Limited coalescence of oil droplets in coarse oil-in-water emulsions.* Journal of Colloid Science, 1954. **9**(5): p. 427-437.

72. Binks, B.P. and C.P. Whitby, *Silica Particle-Stabilized Emulsions of Silicone Oil and Water: Aspects of Emulsification.* Langmuir, 2004. **20**(4): p. 1130-1137.

73. Destribats, M., et al., *Outstanding Stability of Poorly-protected Pickering Emulsions*, in *Trends in Colloid and Interface Science XXIII*. 2010, Springer Berlin Heidelberg. p. 13-18.

74. Levine, S., B.D. Bowen, and S.J. Partridge, *Stabilization of emulsions by fine particles I. Partitioning of particles between continuous phase and oil/water interface.* Colloids and Surfaces, 1989. **38**(2): p. 325-343.

75. Binks, B.P. and S.O. Lumsdon, *Pickering Emulsions Stabilized by Monodispersed Latex Particles: Effects of Particle Size.* Langmuir, 2001. **17**: p. 4540-4547.

76. Sjoblom, J., et al., *Investigation of the Hydrate Plugging and Non-Plugging Properties of Oils.* Journal of Dispersion Science and Technology, 2010. **31**(8): p. 1100-1119.

77. Pichot, R., F. Spyropoulos, and I.T. Norton, *Competitive adsorption of surfactants and hydrophilic silica particles at the oil–water interface: Interfacial tension and contact angle studies.* Journal of Colloid and Interface Science, 2012. **377**(1): p. 396-405.

78. Masalova, I. and E. Kharatyan, *Effect of silica particles on stability of highly concentrated water-in-oil emulsions with non-ionic surfactant.* Colloid Journal, 2013. **75**(1): p. 95-102.

79. Palermo, T.A., D; Borregales, M.; Dalmazzone, C.; Rousseau, L. *Study of the agglomeration between hydrate particles in oil using differential scanning*

calorimetry (DSC). in *5th International Conference on Gas Hydrates*. 2005. Trondheim, Norway.

80. Turner, D.J., *Clathrate hydrate formation in water-in-oil dispersions*, in *Department of Chemical and Petroleum Refining Engineering*. 2005, Colorado School of Mines: Golden, Colorado.

81. Delgado-Linares, J.G., et al., *Model Water-in-Oil Emulsions for Gas Hydrate Studies in Oil Continuous Systems.* Energy & Fuels, 2013. **27**(8): p. 4564-4573.

82. Lachance, J.W., et al., *Formation of Hydrate Slurries in a Once-Through Operation.* Energy & Fuels, 2012. **26**(7): p. 4059-4066.

83. Peixinho, J., et al., *Rheology of hydrate forming emulsions.* Langmuir, 2010. **26**(14): p. 11699-11704.

84. Zylyftari, G., J.W. Lee, and J.F. Morris, *Salt effects on thermodynamic and rheological properties of hydrate forming emulsions.* Chemical Engineering Science, 2013. **95**: p. 148-160.

85. Ahuja, A., *Hydrate Forming Emulsion: Rheology and Morphology Analysis for Flow Assurance*, in *Department of Chemical Engineering*. 2015, The City University of New York: New York.

86. Patrick J. Rensing, M.L., Amadeu K. Sum, Carolyn A. Koh, Dendy E. Sloan, *Viscosity and yield stress of ice slurries formed in water-in-oil emulsions.* Non-Newtonian Fluid Mechanics 2011. **166**: p. 859-866.

87. Boxall, J.A., et al. *Hydrate blockage potential in an oil-dominated system studied using a four inch flow loop*. in *Proceedings of the Sixth Internantional Conference on Gas Hydrates*. 2008. Vancouver, Canada.

88. Turner, D.J., K.T. Miller, and E. Dendy Sloan, *Methane hydrate formation and an inward growing shell model in water-in-oil dispersions.* Chemical Engineering Science, 2009. **64**(18): p. 3996-4004.

89. Cha, M., et al., *Hydrophobic Particle Effects on Hydrate Crystal Growth at the Water–Oil Interface.* Chemistry – An Asian Journal, 2014. **9**(1): p. 261-267.

90. Webb, E.B., et al., *High-pressure rheology of hydrate slurries formed from water-in-oil emulsions.* Energy & Fuels, 2012. **26**(6): p. 3504-3509.

91. Fidel-Dufour, A., F. Gruy, and J.-M. Herri, *Rheology of methane hydrate slurries during their crystallization in a water in dodecane emulsion under flowing.* Chemical Engineering Science, 2006. **61**(2): p. 505-515.

92. Joshi, S.V., et al., *Experimental flowloop investigations of gas hydrate formation in high water cut systems.* Chemical Engineering Science, 2013. **97**: p. 198-209.

93. Karanjkar, P.U., *Evolving morphology and rheological properties of an emulsion undergoing clathrate hydrate formation*. 2012: City University of New York.

94. Sjöblom, J., et al., *Our current understanding of water-in-crude oil emulsions.* Advances in Colloid and Interface Science, 2003. **100-102**: p. 399-473.

95. Venkataramani, D. and C.P. Aichele, *Concentrated Emulsion Characterization in Flowing Conditions.* Energy & Fuels, 2015. **29**(5): p. 2801-2807.

96. Visintin, R.F.G., et al., *Structure of waxy crude oil emulsion gels.* Journal of Non-Newtonian Fluid Mechanics, 2008. **149**(1-3): p. 34-39.

97. Bilyeu, D.J. and T.X. Chen, *Clearing Hydrate and Wax Blockages in a Subsea Flowline*. Offshore Technology Conference.

98. Moradpour, H., A. Chapoy, and B. Tohidi, *Phase Inversion in Water-Oil Emulsions with and without Gas Hydrates.* Energy and Fuels, 2011. **25**: p. 5736-5745.

99. Parthasarathi, P., *Deposition and Aging of Waxy Solids from Paraffinic Mixtures*, in *Department of Chemical and Petroleum Engineering*. 2004, The University of Calgary: Calgary, Alberta.

100. Dantas Neto, A.A.G., E. A. S.; Barros Neto, E. L.; Dantas, T. N. C.; Moura, C. P. A. M, *Determination Of Wax Appearance Temperature (Wat) In Paraffin/Solvent Systems By Photoelectric Signal And Viscosimetry.* Brazilian Journal Of Petroleum And Gas, 2009. **3**(4): p. 149-157.

101. Zhao, Y., et al., *Utilization of DSC, NIR, and NMR for wax appearance temperature and chemical additive performance characterization.* Journal of Thermal Analysis and Calorimetry, 2015. **120**(2): p. 1427-1433.

102. Turner, W.R., *Normal Alkanes, Technical Review.* Ind. Eng. Chem. Prod. Res. Dev., , 1971. **10**(3): p. 238-260.

103. Hammami, A., *Thermal Behaviour and Non-isothermal Crystallization kinetics of normal-Alkanes and their Waxy Mixtures under Quiescent Conditions*. 1994, University of Calgary: Calgary, Alberta.

104. Oliveira, G.E., et al., *The Effect of Asphaltenes, Naphthenic Acids, and Polymeric Inhibitors on the Pour Point of Paraffins Solutions.* Journal of Dispersion Science and Technology, 2007. **28**(3): p. 349-356.

105. García, M.d.C., et al., *The influence of alkane class-types on crude oil wax crystallization and inhibitors efficiency.* Journal of Petroleum Science and Engineering, 2000. **25**(3–4): p. 99-105.

106. Venkatesan, R., et al., *The strength of paraffin gels formed under static and flow conditions.* Chemical Engineering Science, 2005. **60**(13): p. 3587-3598.

107. Kashchiev, D. and A. Firoozabadi, *Driving force for crystallization of gas hydrates.* Journal of Crystal Growth, 2002. **241**(1–2): p. 220-230.

108. Zhang, J.S., S. Lee, and J.W. Lee, *Kinetics of Methane Hydrate Formation from SDS Solution.* Industrial & Engineering Chemistry Research, 2007. **46**(19): p. 6353-6359.

109. Zhong, Y. and R.E. Rogers, *Surfactant effects on gas hydrate formation.* Chemical Engineering Science, 2000. **55**(19): p. 4175-4187.

110. Kumar, A., et al., *Influence of contact medium and surfactants on carbon dioxide clathrate hydrate kinetics.* Fuel, 2013. **105**: p. 664-671.

111. Watanabe, K., S. Imai, and Y.H. Mori, *Surfactant effects on hydrate formation in an unstirred gas/liquid system: An experimental study using HFC-32 and sodium dodecyl sulfate.* Chemical Engineering Science, 2005. **60**(17): p. 4846-4857.

112. Kumar, A., et al., *Role of Surfactants in Promoting Gas Hydrate Formation.* Industrial & Engineering Chemistry Research, 2015. **54**(49): p. 12217-12232.

113. Kalogerakis, N., et al., *Effect of Surfactants on Hydrate Formation Kinetics.* Society of Petroleum Engineers.

114. Di Profio, P., et al., *Surfactant promoting effects on clathrate hydrate formation: Are micelles really involved?* Chemical Engineering Science, 2005. **60**(15): p. 4141-4145.

115. Zhang, B.-y., Q. Wu, and D.-l. Sun, *Effect of surfactant Tween on induction time of gas hydrate formation.* Journal of China University of Mining and Technology, 2008. **18**(1): p. 18-21.

116. Rogers, R., et al., *Investigations into surfactant/gas hydrate relationship.* Journal of Petroleum Science and Engineering, 2007. **56**(1–3): p. 82-88.

APPENDICES

APPENDIX A- IMAGES CAPTURED USING CROSS POLARIZED OPTICAL MICROSCOPY FOR HYDRATE FORMATION STUDIES IN WAXY OIL SYSTEMS

Images at the oil-water interface captured at 20x magnification in surfactant free 1.25 wt.% wax in mineral oil-cyclopentane mixture

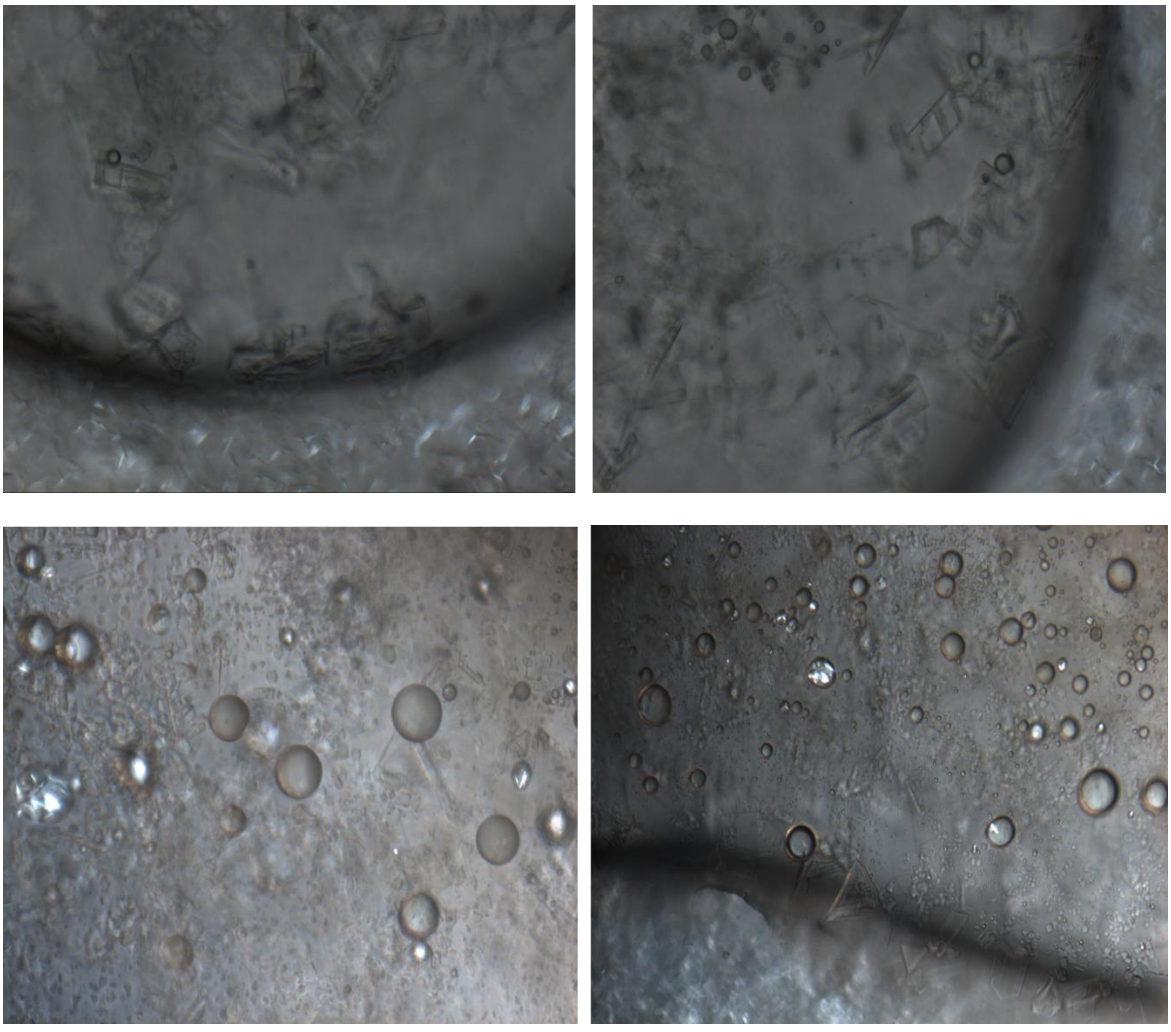

APPENDIX B- DROP SIZE DISTRIBUTION OF REFERENCE SYSTEMS USED FOR CALIBRATION

Particle size distribution of 10 wt.% colloidal silica solution captured using acoustic spectroscopy. The inset image was captured using transmission electron microscopy (TEM)

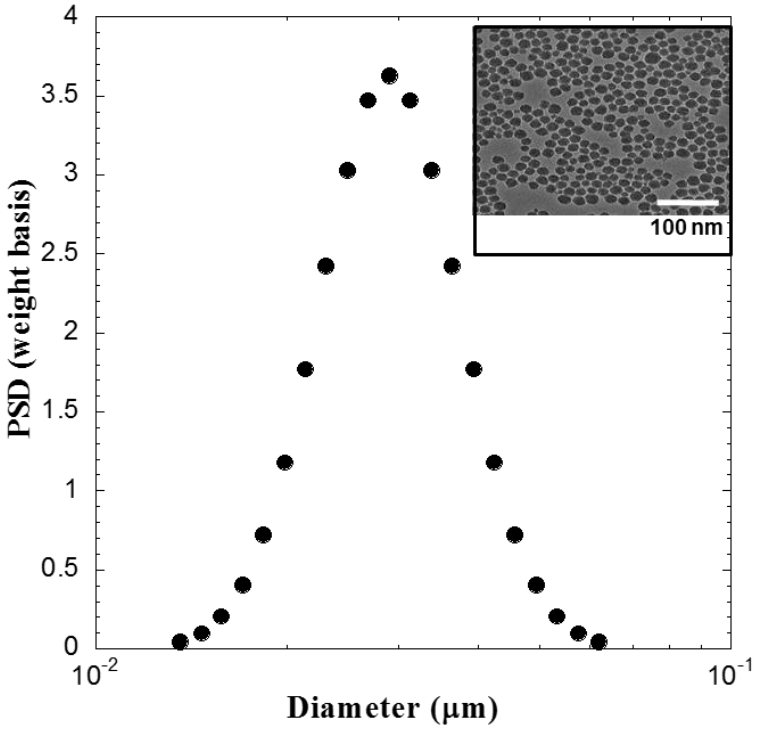

Particle size distribution of 0.1 wt.% Aerosil R972 in crystal plus 70T mineral oil in captured using acoustic spectroscopy. The inset image was captured using transmission electron microscopy (TEM)

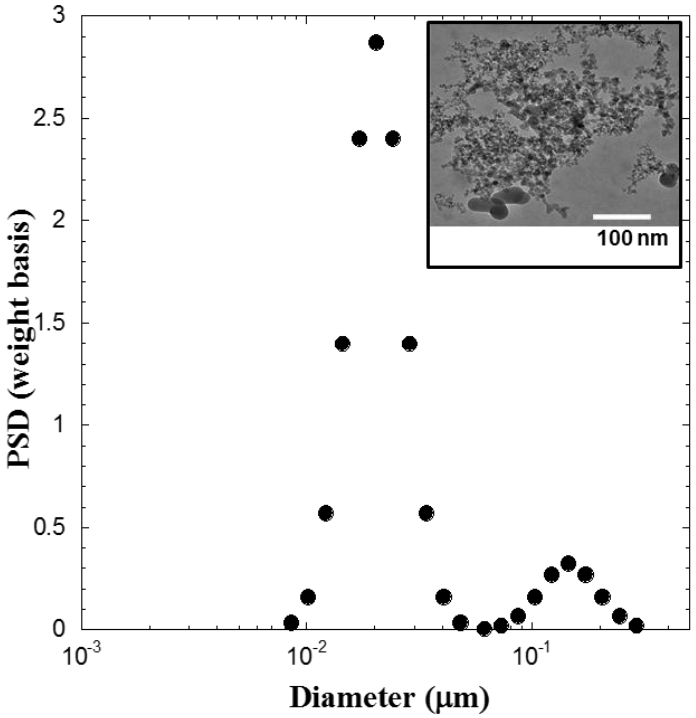

Nonaqueous conductivity measurement of water-in-oil emulsion stabilized using solid particle and surfactant discussed in Chapter II

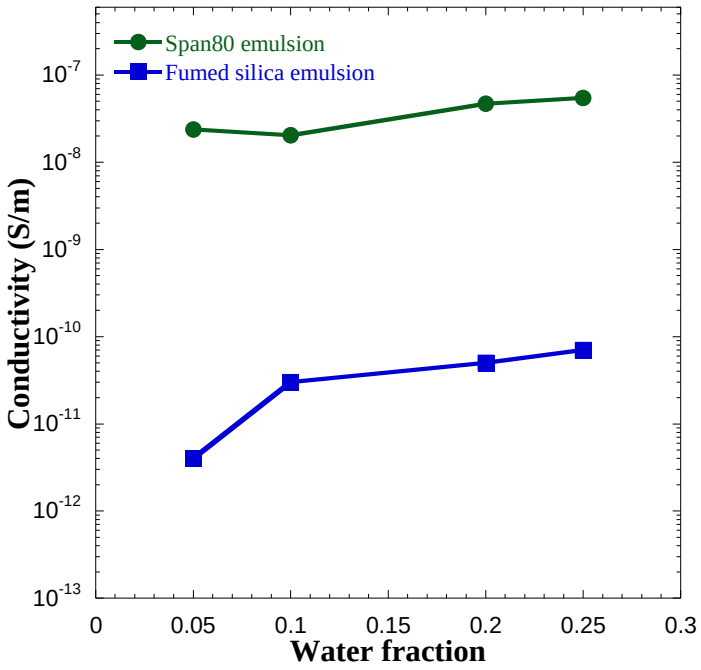

APPENDIX C- FLOW LOOP SETUP USED FOR EMULSION AND HYDRATE CHARACTERIZATION DESCRIBED IN CHAPTER III

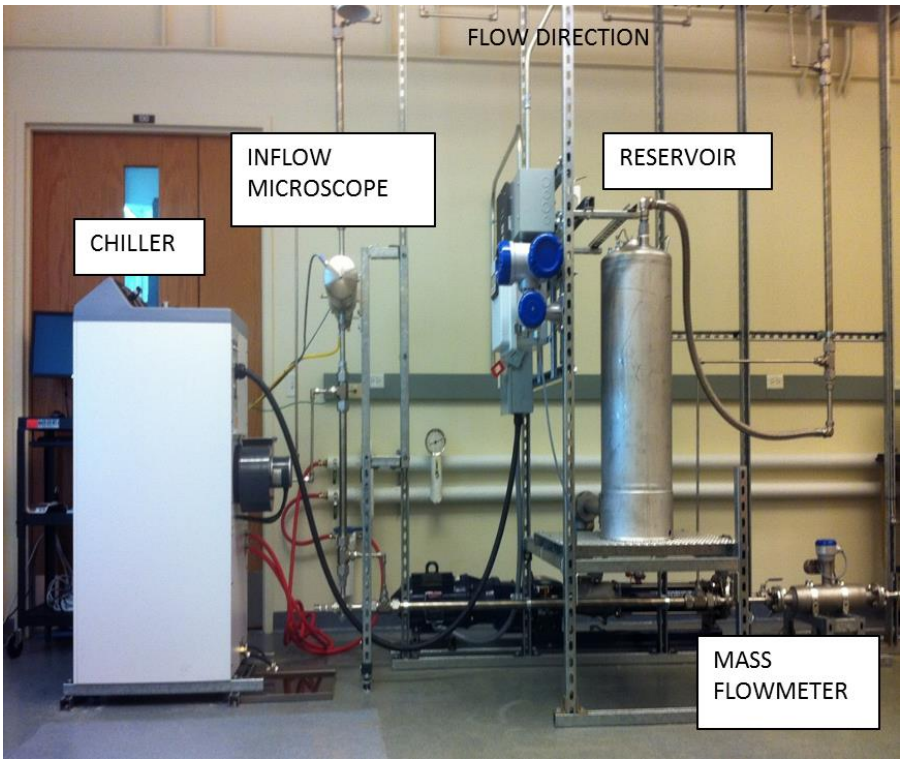

Reservoir

Top view of the reservoir

VITA

Deepika Venkataramani

Candidate for the Degree of

Doctor of Philosophy

Thesis: HYDRATE FORMATION IN WAXY OIL SYSTEMS

Major Field: Chemical Engineering

Biographical:

Education:
Completed the requirements for the Doctor of Philosophy in Chemical Engineering at Oklahoma State University, Stillwater, Oklahoma in December, 2016.

Completed the requirements for the Master of Science in Environmental Engineering at Syracuse University, Syracuse, New York in December, 2010.

Completed the requirements for the Bachelor of Engineering in Chemical Engineering at University of Pune, Pune, Maharashtra, India in May, 2006.

Experience:
Graduate Intern (Research and Development), Shell Global Solutions, Houston, Texas: May 2015- August 2015

Research Assistant, School of Chemical Engineering, Oklahoma State University, Stillwater, Oklahoma: August 2012 – December 2016

Teaching Assistant, School of Chemical Engineering, Oklahoma State University, Stillwater, Oklahoma: August 2008 – May 2010

Professional Memberships:

American Institute of Chemical Engineers, American Chemical Society, Society of Petroleum Engineers, Sustainable Remediation Forum, American Academy of Environmental Engineers, Indian Institute of Chemical Engineers

Honor Societies:
Omega Chi Epsilon